Radar Imaging with a Network of
Digital Noise Radar Systems

THESIS

Ashley L. Schmitt, Captain, USAF

AFIT/GE/ENG/09-39

AFIT/GE/ENG/09-39

# Radar Imaging with a Network of Digital Noise Radar Systems

THESIS

Presented to the Faculty

Department of Electrical and Computer Engineering

Graduate School of Engineering and Management

Air Force Institute of Technology

Air University

Air Education and Training Command

In Partial Fulfillment of the Requirements for the

Degree of Master of Science in Electrical Engineering

Ashley L. Schmitt, B.S.E.E.

Captain, USAF

March 2009

AFIT/GE/ENG/09-39

# Radar Imaging with a Network of Digital Noise Radar Systems

Ashley L. Schmitt, B.S.E.E.

Captain, USAF

Approved:

| | |
|---|---|
| /signed/ | 9 March 2009 |
| Dr. Peter J. Collins, PhD (Chairman) | date |
| /signed/ | 9 March 2009 |
| Dr. Andrew J. Terzuoli (Member) | date |
| /signed/ | 9 March 2009 |
| Dr. Steven K. Rogers (Member) | date |

AFIT/GE/ENG/09-39

## *Abstract*

Today's battlefield consists of a blend of humans and machines working together to locate and monitor the enemy. Due to the threat of terrorism, today's enemy can be anyone and they can exist anywhere even in populated cities. Monitoring human activities in an urban environment is a difficult problem due to walls, clutter, and other obstructions. This thesis focused on developing a network of digital noise radar sensors that could operate simultaneously to track humans and non-human targets inside rooms and through walls. The theory, application, and results are discussed throughout this thesis. A noise radar works by cross correlating the received signal with a time delayed replica of the transmit signal. A high correlation indicates a target. A digital noise radar digitizes the transmit and receive signals and accomplishes the correlation in software. A network of three digital noise radars was constructed to triangulate the (x, y) position of a target within a room. The results were presented in two-dimensional graphs. In nine out of ten cases the stationary targets were clearly identified. In eight out of ten cases the stationary targets were located within the range solution of the system, 0.375 m. In the one miss case, the results image indicated the presence of the human target, but the detection was faint and possible to miss. Tests were also accomplished with moving human targets. In these tests the network of radar systems tracked the human target in an empty and cluttered room until the target was out of range. The test results prove that a network of simultaneously operating noise radars can locate and track human and non-human targets within rooms.

## *Acknowledgements*

First and foremost, I owe a large debt of gratitude to my husband and two daughters who put up with crazy mommy. Maybe dinner wasn't perfect and I was a little scatterbrained, but throughout it all you loved me and made me laugh at myself. Secondly, I owe a thank you to my thesis advisor for suggesting such a wonderful topic and guiding me along the way. Third, I owe much to my thesis committee and sponsor for trusting me to actually build a working radar and supporting my efforts. Last, I want to thank Dr. Narayanan and the PhD students at Pennsylvania State University for meeting with me and bestowing upon me so much information and knowledge.

Ashley L. Schmitt

## *Table of Contents*

## List of Figures

x

## List of Tables

Radar Imaging with a Network of

Digital Noise Radar Systems

## I.  Introduction

Today's battlefield consists of a blend of humans and machines working together to
anticipate, interact, find, fix, track, target, and engage the enemy. Our systems of
sensors are good at finding, fixing, tracking, and targeting the enemy. But what if
our systems could anticipate and interact with the enemy with a reduced dependency
on human input? A belief exists that humans are the only beings that can anticipate,
interact, and in essence think. This may not be the most advantageous operating
environment in today's battlefield. New ideas and concepts need to be explored so
that our sensors can advance and provide the best possible overview of the battlefield.
A new theory is on the horizon called exploitation driven sensing. Instead of humans
telling the sensor what to do, the sensor will be connected to an in-development
processing kernel based on concepts collectively termed QUalia Exploitation of Sensor
Technology (QUEST).

Traditional pattern recognition programs look at the physical properties (i.e.
height, weight, size, etc.) of a situation and are limited to well defined areas with a
single application. Variations in application require re-engineering of the recognition
program [33]. Pattern recognition programs do not learn or have the capability of
adapting as the situation changes. Humans can adapt, learn, and form conclusions
from familiar items though the situation may be unfamiliar. Traditional pattern
recognition programs cannot do this and do not take the context (subjective repre-
sentation of the situation) of a situation into account. With humans, the context of a
situation can offer additional information that help with recognition of the new object
or unfamiliar situation. QUEST seeks to create a general purpose pattern recognition
machine that has the ability to fuse both memory and knowledge to hierarchically rep-
resent instances. This hierarchical model takes relative concepts (qualia), maps them

into plausible narratives (in context), and manipulates (reason) its representation of the situation to create, a consistent world model [35]. The QUEST program consists of a quale generating kernel and a set of processes that manipulate the representation of the situation. The representation is characterized by links between the qualia [35].

With exploitation driven sensing, the sensor and its QUEST processor will observe the situation, acquire enough information to anticipate the enemy, and then it can change focus of its interrogation to highlight the most informative aspects of the situation. This thesis focuses on creating a sensor with a digital interface that will allow for seamless connection to a QUEST processor. The sensor developed in this thesis is a through-the-wall ultra-wideband digital noise radar.

## 1.1   Problem Statement

Due to the threat of terrorism, today's enemy can be anyone and can exist anywhere from barren wastelands to populated cities. Monitoring human activities with sensors in an urban environment is a difficult problem due to walls, clutter, and other obstructions. Development of sensors that can monitor the enemy through walls and other obstructions will bring more knowledge to our warfighters.

## 1.2   Research Goals

The overall goal of this research is to build a network of noise radar systems that can operate simultaneously without interference, locate multiple human or non-human targets, and track human movement through a room. Another goal is to design this network of sensors in a manner that will allow for integration with the QUEST processing kernel.

## 1.3   Research Contributions

Individuals, governments, and researchers have become interested in discovering methods to monitor suspicious human activities through walls. Monitoring human activities through walls is also of interest to rescue workers and fire fighters. Discovering

2

the location of humans within a crumbling or on-fire building would allow lifesaving activities to be directed appropriately. Noise radars with ultra-wideband (UWB) signals have shown great promise at locating human and non-human targets through walls. Recently, Dr. Narayanan from Pennsylvania State University has developed a digital noise radar system that was capable of locating humans through-the-wall within 0.375 m of the target's location [25]. Digitization of the transmit and receive signals allow for the use of signal processing techniques that can improve radar performance. Also, digitization offers an opportunity for the QUEST processing kernel to manipulate the digital performance parameters of the radar system. This thesis proposes to use Dr. Narayanan's digital radar concept as a basis and build upon that foundation.

This research establishes the initial digital noise radar test bed at the Air Force Institute of Technology (AFIT). This research seeks to go beyond what was accomplished by Dr. Narayanan by developing three separate digital noise radar systems and networking them together. The three systems will operate simultaneously, consolidate received data, and two-dimensionally locate human (stationary and mobile) and non-human targets. Simultaneous operation of noise radars has been proven in simulation, but real world demonstration of this was not apparent in any literature on noise radars [38]. This thesis seeks to prove that digital noise radars can be networked and operate simultaneously to locate multiple human or non-human targets within a room.

Once complete, the QUEST processor will be integrated with this noise radar test bed, tested, and baselined. The baseline results can then be compared to the results of current methods to establish if there is a measurable improvement in effectiveness. AFIT's QUEST sensor test bed enables the development of the exploitation driven sensing concept which can ultimately increase our battlefield awareness.

## 1.4  Thesis Organization

This thesis is divided into seven chapters and has three appendices.

- Chapter 1: This chapter gives an introduction to the general problem, the purpose and importance of researching noise radars, and an overview of the organization of this thesis.

- Chapter 2: This chapter provides an introduction to the QUEST development project, background information on noise radars, and a review of the research already accomplished in the field of noise radars.

- Chapter 3: This chapter develops the theoretical foundations of noise radar technology. Comprehensive theoretical models are developed for UWB noise radar, digital noise radar, and wall attenuation.

- Chapter 4: This chapter describes the overall hardware design for the radar system, each individual component, the network of desktop computers, and the software algorithm used for correlation and imaging.

- Chapter 5: This chapter highlights the research methodology and procedures used during the experiments. Sections include the purpose and objective of the experiments, methods and procedures, analysis of targets used, and explanation of each test scenario and its purpose.

- Chapter 6: This chapter reports and analyzes the results of all tests accomplished with the noise radar system.

- Chapter 7: This last chapter discusses the implications of this research and offers suggestions for future research.

- Appendix A: This appendix section contains the `Matlab`® signal processing code used to correlate the transmit and receive signals. The code also plots the two-dimensional images.

- Appendix B: This appendix section lists of all of the tests conducted while accomplishing this thesis.

- Appendix C: This appendix section shows additional test scenarios, photos of the test scene, and two-dimensional image results not shown in the main body of the thesis.

- Appendix D: This appendix section details a project that created a realistic simulation model of a noise radar in the Matlab® Simulink application that detects a human target through a concrete wall. The simulation model was validated with data obtained by a actual noise radar measuring human targets through a concrete wall.

## II. Introduction to QUEST, History of Noise Radar, and Current Developments in Noise Radar Technology

Due to the state of the world and the threat of terrorism, individuals, governments, and researchers have become interested in discovering methods to monitor human activities. Development of sensors that can monitor, anticipate, and interact with the enemy will bring more knowledge to the operating environment and require less manpower. Noise radars with ultra-wideband (UWB) signals integrated with the QUEST processing kernel are well suited for this problem. This chapter begins with an introduction to QUEST to enable a better understanding of the concept. Next, the history of UWB technology is discussed and its applications in traditional and noise radar systems. Last, there is a discussion of the current developments in noise radar technology.

### 2.1 QUalia Exploitation of Sensor Technology (QUEST)

Dr. Rogers, assisted by several other researchers, at Air Force Research Laboratories (AFRL) and the Air Force Institute of Technology (AFIT) are working to develop the QUEST concept. In an article on sensors they discuss QUEST's unique approach that seeks to incorporate the concept of qualia into future sensor systems [34]. They feel that in over half a century of creating computer recognition programs no one has developed a general purpose recognition machine. The QUEST developers contend that many problems exist that require a new approach. Example problems include detection of cyber intruders or malicious code on a computer network, detection of a suicide bomber, and detection of vehicle-based improvised explosive devices. Currently, computers cannot recognize the signs or possible patterns that surround these events. QUEST seeks to provide a continued sensing of the battle space from multiple sensors and multiple platforms. It makes use of high speed computing power to peel back the information layers generating an increased situational awareness. Improved situational awareness increases our overall capabilities and allows for detection of events not easily detectable today.

The QUEST program seeks to accomplish these goals through the use of a qualia approach rather than the standard pattern recognition approach. Qualia provides the representation through which all life forms generate a useful and consistent world model. Qualia are the sensory experiences of an individual as she senses the world. Qualia is the red she 'sees' or the pain she 'feels'. Qualia are the internal subjective representations that allow for exploitation of sensory data. A qualia approach is different from the standard pattern recognition approach in that it seeks to use the more abstract and subjective qualities of an object for recognition. Standard pattern recognition seeks to identify objects with very clear parameters such as height, weight, length, shape, color, etc. A qualia approach will utilize this information, but will attempt to go beyond this information and form a concept of the object in reference to what data it has and what data is in the surrounding environment. With this concept it will try to identify the object and probe for more information and/or make a prediction about the object.

For example, in the distance there is the profile of an object that has the size and shape of a tank. The standard recognition processor would identify the object as a tank based on size and shape. The qualia processor would take the information in and guess that it was a tank. Then, it could make the prediction that if its sensor moved in a certain direction it would find the front dimensions of the tank. When the sensor moved and probed the area it would find the dimensions did not match its predictions. It now knows the object was not a tank and it seeks to find more information out to determine the identity of the object. In actuality, the object was a one-dimensional fake tank the enemy had erected to confuse his enemy. Traditional pattern recognition would not have known a fake tank from a real tank. A qualia processor would say the object looks like a tank at one angle, but it was not a tank. Quickly knowing the location of the real tanks in a battlefield would be of great importance. Then, efforts to neutralize the threat could be placed in the proper direction.

When development of QUEST is complete it will need to be integrated with a sensor to see if a qualia approach does provide a measurable increase over standard

pattern recognition in situational awareness on the battlefield. The first sensor to be connected to the QUEST processing kernel will be the network of UWB noise radar systems developed in this thesis.

## 2.2    UWB Technology History

The beginning seeds of UWB are seen in the nanosecond range technology which was an effort to discriminate between two close flying aircraft. The work really accelerated when a man by the name of Dr. Ross became interested in describing the transient response of a type of microwave network through its characteristic impulse response. Ross developed his theories on impulse responses and applied them to an array of wideband antennas. Once this proved successful, he realized these techniques could be applied to radar and communication arenas. The landmark of UWB history came in 1973 when Gerald F. Ross was awarded the first patent for UWB communications. Though the term UWB was not applied at the time, instead the research was known as baseband, carrier-free or impulse. UWB technology began to find applications in communications, radar, automobiles, positioning systems, and altimetry. UWB had over 30 years of research and applications by the time the Department of Defense coined the phrase UWB [9].

Due to UWB's ability to be used in communication systems with a low probability of intercept (LPI) the U.S. government began to fund research for UWB under classified programs, focusing on impulse communications. This continued until 1994 when much of the work moved into the unclassified realm [9]. As the work became unclassified the research in the area exploded. Also, the FCC has now permitted the marketing and operation of ultra-wideband antennas for short distance communications at low power. The FCC in the United States allocated 3.1 GHz to 10.6 GHz for UWB use [5]. This act accelerated the development of UWB technology into innumerable military and commercial applications.

### 2.3 UWB Radar Systems

In 1989, the United States Department of Defense coined the term UWB, but the theory and beginning applications reach as far back as the 1950's [9]. UWB held an allure for scientists and engineers because of its excellent range resolution qualities and its quantity of information content [3]. A bandwidth of a few hundred megahertz provides a range resolution and range position accuracy within a few tens of centimeters. With such a high bandwidth, UWB signals are not considered to have a carrier frequency and are labeled as baseband or carrier free signals. The official definition of a UWB signal is a signal having a fractional bandwidth $\triangle f > 25\%$. The fractional bandwidth is given by [2]

$$FractionalBandwidth(FBW) = \frac{2(f_H - f_L)}{f_H + f_L} = \frac{f_H - f_L}{f_o} \qquad (2.1)$$

where $f_H$ and $f_L$ are the upper and lower band edges of the signal and $f_o$ is the average of $f_H$ and $f_L$. Fig. 2.1 shows the spectral density function for an UWB signal. The large frequency bandwidth means that in a radar application a target is interrogated over a wide range of frequencies. Among other things, a target's response to a signal is based on its geometric size, $a$, and the signal's wavelength, $\lambda$. There are three types of responses; optical $\lambda \ll a$, resonant $\lambda \approx a$, and Rayleigh $\lambda \gg a$. A signal with a wide enough bandwidth and the proper center frequency is capable of extracting information from each of the target response regimes [3].

Also, since the energy is spread across a large frequency range it is less affected by clutter and multipath effects. This effect is of great advantage when the UWB radar is meant for an application of through the wall sensing or ground penetration. Radars that are highly sensitive to multipath effects and clutter would not be effective in those applications. Researchers dealing with through the wall sensing, ground penetration and penetration through foliage began to gravitate towards the use of white Gaussian noise as a waveform for the UWB radar [3]. These researchers broke off the main branch of the UWB radars and began to specialize in radars labeled
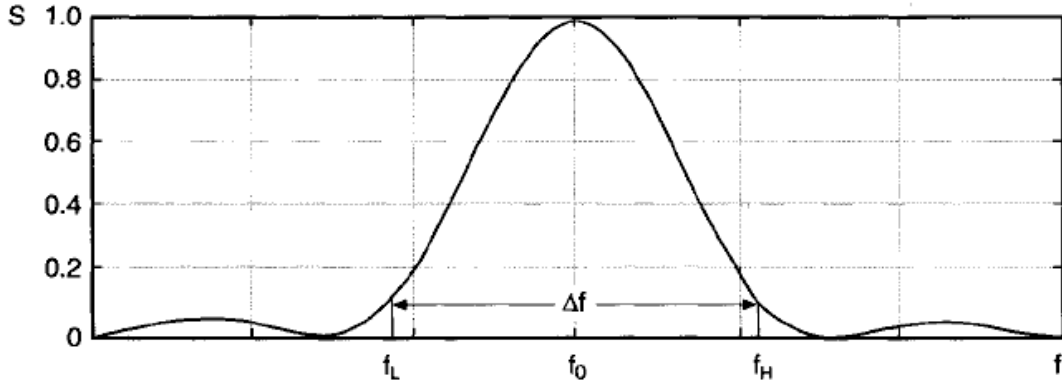
Figure 2.1:    UWB Signal Spectral Density Function [2]

UWB noise radars or noise radars. Noise radars are UWB radars that use a noise waveform. Recent research and advancements in the area of UWB have been in the field of UWB noise radars and will be discussed next.

## 2.4    UWB Noise Radar Systems

Use of a random noise signal in radar systems has many advantages and these advantages propelled the research of UWB noise radars. Dr. Narayanan of Pennsylvania State University detailed several of these advantages in a journal article on noise radars [25]. The article stated that a noise signal has an ideal 'thumbtack' ambiguity function, low probability of intercept (LPI), difficulty to jam, the ability of several radars to operate in the same area simultaneously, and cost effectiveness. This section will discuss the advantages in detail and the basic operation of a noise radar.

Noise has an ideal 'thumbtack' ambiguity function. The ambiguity function expresses the time response of a filter matched to a finite energy signal when the signal has a delay of $\tau$ and a Doppler shift $\nu$ relative the values expected by the filter. Skolnik defines the ambiguity function as [36]

$$|\chi(\tau,\nu)| = |\int_{-\infty}^{\infty} u(t)u^*(t+\tau)exp(j2\pi\nu t)dt| \qquad (2.2)$$

10

where $u$ is the complex envelope of the signal. A 'thumbtack' ambiguity function means that an ideally narrow peak exists at $\tau$ and $\nu$ equal to zero. This peak means that the range resolution and the doppler resolution are both very high. This is not true with other waveforms. Some waveforms have excellent range resolution and fair to poor Doppler resolution. With others the opposite is true, but no other waveform has equally excellent range and Doppler resolution. High accuracy in both range and Doppler space is a highly desirable trait in a radar system. Noise radars capitalize on the thumbtack ambiguity function of noise [36].

Noise signals inherently have LPI. Noise is all around in the environment and is expected. With a noise radar the only way to detect or make use of the noise signal is through the use of the original signal. Currently, no equipment exists that can detect random noise radars. Research and simulations accomplished by a graduate student at the Naval Post Graduate school offer a possible detection method [16]. The research focused on a method termed time-frequency, bi-frequency detection analysis. This method used two modes of analysis. The first mode looked at the signal from a time-frequency perspective. The time-frequency mode analyzed the tradeoff in time and frequency resolution that occurs as the signal propagates. The second mode used cyclostationary analysis. This analysis was accomplished through correlation of the noise signal using the cyclic spectral density, that was represented on the two-dimensional bi-frequency plane with frequency and cycle frequency. The spectral correlation properties of the noise signal can be seen in cyclic autocorrelation function and the spectral correlation density function. The appearance of spectral correlation properties means that the noise signal analyzed was intentional and not part of the random noise in the environment. This method has promise but currently has not been put to use in hardware.

Another feature is that a noise radar is very difficult to jam. The random frequencies of a noise radar make traditional jamming methods useless. The only possible jamming method is to blanket an area with a powerful noise source. Then the noise radar's signal to noise ratio decreases, causing all targets to get lost in the

noise [38]. While effective, it also is not particularly feasible for an adversary. Also, if the adversary is unaware he is being watched, this tactic would not be employed.

Noise radars also have the ability to occupy the same spectral frequency band without interfering with one another due to the unique transmit signal which decorrelates with neighboring noise radar transmissions [25]. Each radar's received signal will only correlate with its own unique replica signal. Thus several noise radars can operate near one another, interrogating different parts of the scene, providing more information quickly and not interfere with one another. Additional advantages can be gained if the radars are networked and are able to create a consolidated picture. Radar systems not making use of a noise waveform could not operate in this manner due cross-interference [38]. The ability to network and operate several noise radars in the same area is of interest for this thesis. Since the goal of this thesis is to create a network of noise radars that can locate the two-dimensional (x, y) position of a target, then the ability to operate simultaneously is important.

Simulations accomplished by government researchers in Canada showed that noise radars could operate simultaneously and still accurately locate their target [25]. The specific goal of the simulations was to see if noise radars operating in near proximity and in the same frequency band would experience mutual interference. The simulation considered three noise radars with a carrier frequency of 10 GHz and with a 25 MHz bandwidth. The first and second radars were located at the same position. The third radar was located 75 m horizontally to the right of radars one and two. The pulse repetition frequency (PRF) was 97.7 kHz for radars one and three. The PRF for radar two was 116 kHz. In the simulation, a target moved away with a constant velocity of 200 m/s in the direct line of sight of radars one and two. Fig. 2.2 shows the locations of the radars and the target. The researchers simulated five cases altering the power output of the first and second radars. As long as no radar's power was 30 dB higher than that of the other radars the target was accurately located in range and Doppler. Fig. 2.3 shows the range-Doppler profile results from the simulation with radar one's power 30 dB higher and radar two's power 3 dB higher than radar
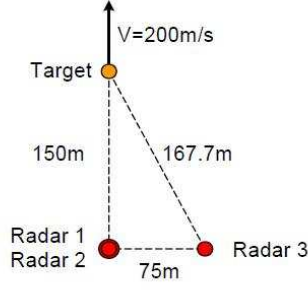
Figure 2.2:    Location of the Three Radars and the Target [25]
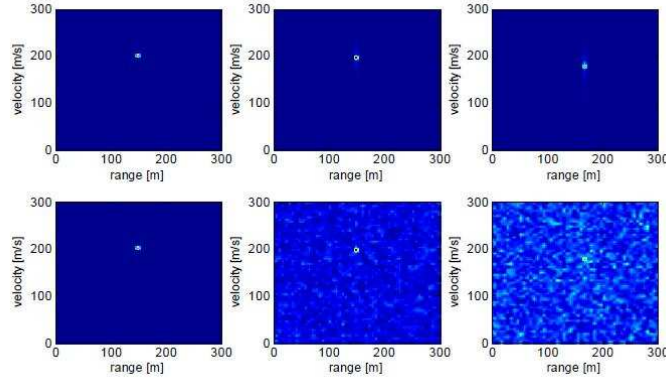


Figure 2.3:    Range-Doppler profiles. Upper Row: Radar returns of the first, second, and third radars without any of the other radars in operation. Lower Row: Radar returns of first radar (+30 dB), second radar (+3 dB), and third radar (0dB). [25]

three's power. Though the results for radar three show clutter the target is still visible. The research of this thesis seeks to go beyond simulation and built actual noise radar systems that will operate simultaneously, without interference, at approximately the same power levels.

Another benefit of noise radars is that noise radars can be cost effective. Noise source technology is well developed, reliable, and manufactures of noise sources are plentiful. Noise sources have been used for the past 40 years in broadband communication receiver testing and they are generally low power solid-state devices. The noise source technology is not new, and with many manufactures, excellent quality noise source can be easily found for a modest cost. Generally, noise sources are much lower

in cost than the high quality, expensive modulators with excellent linearity that are necessary components in traditional radars.

Qualities such as an ideal thumbtack ambiguity function, low probability of intercept (LPI), difficulty to jam, the ability of several radars to operate in the same area simultaneously, and cost effectiveness make the noise radar of great interest to researchers. The next part of this section discusses the basics of how a noise radar works.

The basic working premise of a digital or analog noise radar is straight forward. A noise signal is produced by a noise source. The signal is split and one part is transmitted into the environment at a target. The other part is an exact duplicate and is put through delay lines or stored digitally and is considered the time delayed replica [2]. The backscatter from the target is then cross-correlated with the a time delayed replica of the original transmitted signal. Where the round trip time delay to the target matches the time delayed replica a peak occurs in the correlator [25]. A correlator is a hardware or software device that combines sampled voltage time series from one or more antennas to produce sets of complex vectors [6]. In doing this it compares how closely the signals resemble one another. The more the signals resemble each other the more they are correlated and the stronger the correlation peak [3]. Fig. 2.4 shows a very generalized block diagram of a UWB radar. Many researchers have taken this same basic premise and created different noise radar systems. The next section looks at recent noise radar research, its goals, and what has been achieved.

## 2.5  Recent Noise Radar Research

Researchers from several areas of interest and universities have become involved in furthering this technology. Researchers from Ohio State University, Dr. Eric Walton, and from Pennsylvania State University, Dr. Narayanan, are top experts in noise radar technology. The following information looks at these researchers, their goals, and their accomplishments to provide a solid background on the variations in hardware implementation and proven applications of noise radars.

14
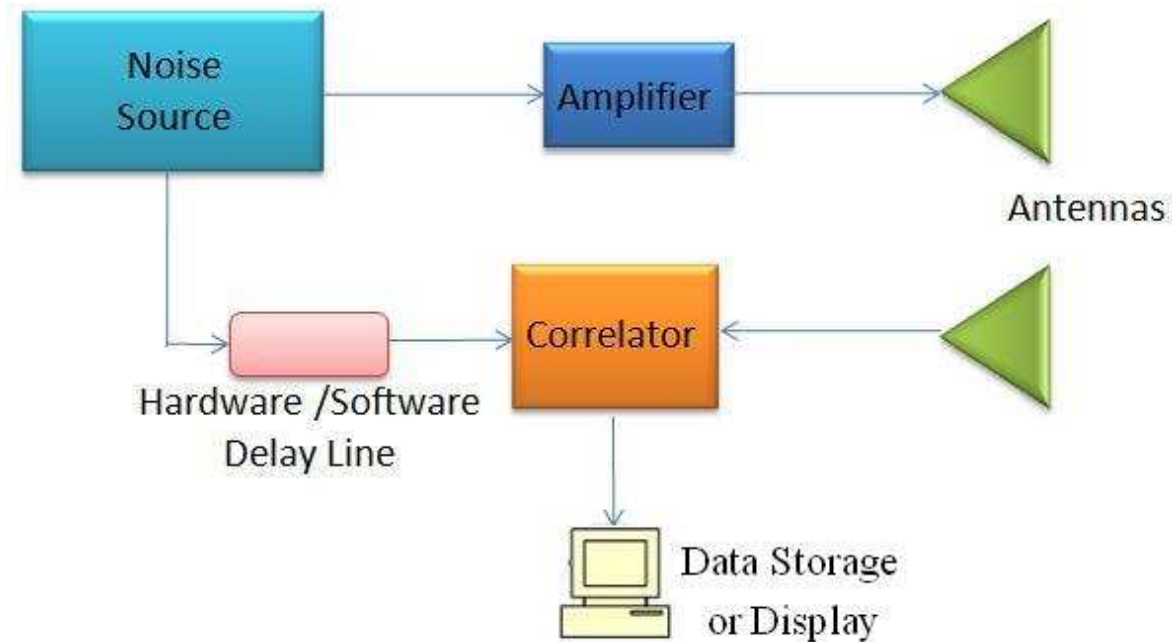
**Figure 2.4:** Generalized UWB Radar Block Diagram [2]

Dr. Eric Walton from Ohio State accomplished many experiments using noise radar technology. In fact, he was the first to receive a patent in March of 2005 for his noise radar designs [45]. Initially, he developed and worked with noise radars that had applications in through-the-wall imaging [46], ground penetration [46] [41] [47], finding moving and non-moving objects [42] [44], and RCS measurements [39]. Dr. Walton's first implementations used a noise source and cable delay lines to find a target through foliage, walls, and other obscuring devices. Fig. 2.5 shows a basic design for this type of noise radar.

An exemplary experiment performed with this type of noise radar design is with the radar using an UWB noise signal ranging from 50 MHz to 600 MHz [42]. Transverse electromagnetic (TEM) traveling wave antennas were used, because of their wideband characteristics and well-defined phase centers. A TEM traveling wave antenna is an antenna whose current and voltage distribution can be represented as a TEM plane wave traveling through air [4]. This assumes air is the medium of interest. The antennas and system were placed out in a grassy, non-cluttered field. The system

15
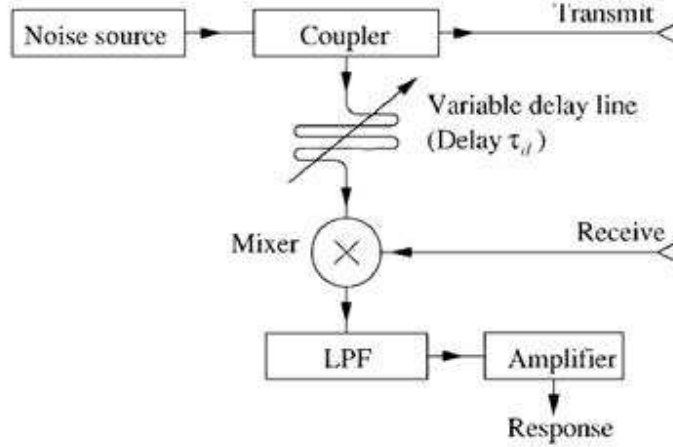
Figure 2.5:    Block Diagram of Analog Noise Radar that was Implemented by Dr. Walton of Ohio State University [42]

had a coaxial cable delay system that gave a 85 ns delay. This translates into a range gate of 12.8 m. A trihedral, 2.37 m long measured along the sides, is slowly moved by a pulley system of strings from 9 m to 14 m. The range gate is 12.8 m so a high response is expected at this approximate location. Fig. 2.6 shows the results of this experiment. The results show high positive and negative correlation peaks between 12 m and 13 m [42].

Dr. Walton's accomplishments with noise radars are worthy of note since locating a target is of interest in this thesis. The concept is good, but the design is not ideal. Dr. Walton's design was hardware oriented with cumbersome cable delay lines and would not be easily integrated well with a QUEST processor. So, another design concept is necessary to meet the goal of this thesis.

As Dr. Walton's research in the area continued, he began to work with noise radars that used an arbitrary waveform generator (AWG) to generate the noise waveform. The random sequence generated by the AWG was loaded into a first-in-first-out (FIFO) device. A FIFO is a memory device that stores data in a queue order so that the first input is the first element out. The system was named a FIFO noise radar.
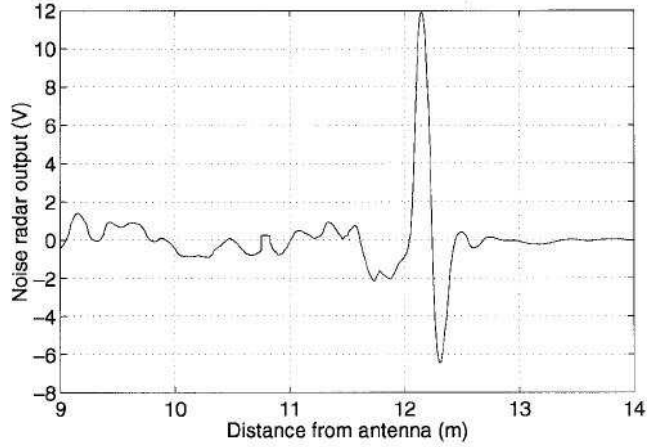
Figure 2.6:    Results from Dr. Walton's Experiment with a Trihedral Moved from 9 m to 14 m. The Range Gate was at 12.8 m. [42]

The FIFO generated the waveform digitally and then a digital to analog converter (DAC) changed the signal to analog. The signal was then upconverted to a higher carrier frequency, and then broadcast into the environment. The received signal was brought into the correlator and combined with a time delayed version of the digitized transmit signal. The correlator then correlates the signal and locates the target. Fig. 2.7 shows a block diagram of the FIFO noise radar system. This particular application tracked a corner reflector that moved from a range of 40 ft to 185 ft from the radar while using an operating power of less than 0.25 watts [44] [46].

This implementation of the noise radar would allow the QUEST processor to generate the noise waveform. This tighter integration between processor and sensor could offer some advantages. Unfortunately, the correlator in this implementation still exists in hardware rather than software. Software signal processing techniques can be very powerful. When working to seamlessly integrate into a QUEST processor it would seem prudent to make use of a digital correlator that accomplishes correlation in software. Though another noise radar design seems necessary for this thesis, each of Dr. Walton's noise radar implementations proved that noise radar technology in

17
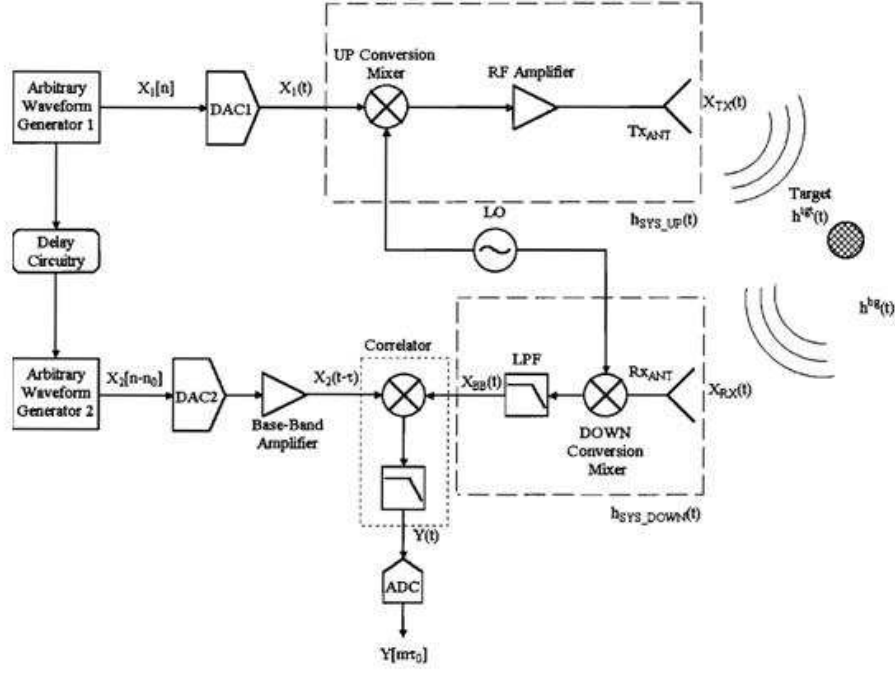
Figure 2.7: Block Diagram of a FIFO Noise Radar [44]

various forms could track targets with accuracy and over a distance using low power methods.

Other researchers have worked extensively with UWB noise radar systems. One researcher in particular, Dr. Narayanan of Pennsylvania State University, has been working with noise radars for many years and made great strides in furthering the technology. Dr. Narayanan's initial research worked with Doppler visibility and estimations with coherent noise radar systems [26] [28] [27]. Phase coherence was obtained with a heterodyne receiver. The replica of the 1-2 GHz noise transmit signal was mixed with a coherent 160 MHz oscillator. A time delay was applied. Then, the signal was sent to a mixer to be correlated with the received waveform. The correlated signal was then flowed through an In-phase/Quadrature (I/Q) detector. The I/Q detector created I and Q channels by mixing the correlated signal with the oscillator signal and a 90° phase shifted oscillator signal. Both mixed signals were sent through a lowpass filter to isolate the phase information provided by the

oscillator. The I and Q channels provided the phase information and the correlated signal provided the amplitude information [26]. The results of the I and Q channels and the correlated signal were then stored to memory for analysis. Fig. 2.8 shows a block diagram of a phase coherent noise radar.

Dr. Narayanan and researchers at Pennsylvania State University performed a field test of this system [26]. The system operated at 1-2 GHz and had a down-range resolution of 15 cm. The maximum range was about 200 m. The experiment included an array of triangular trihedrals with 45.7 cm sides mounted on at 3 m height on top of a van. The radar system was mounted on top of another van with the antennas on a 10 m high telescopic boom. Fig. 2.9 shows a picture of the two vans with the equipment on top. The radar van stayed stationary while the target van moved away in the boresight direction at the uniform speeds of 4.5 m/s, 6.7 m/s, and 9 m/s. Ten trials were conducted at each speed and the data was collected. In order to compare the noise radar's result to that of a constant frequency waveform the three test speeds were repeated with a radar with a 1.5 GHz fixed frequency. Results from Dr. Narayanan experiments at 4.5 m/s are shown in Fig. 2.10. The figure shows the individual trials and the extracted mean Doppler at each frequency. The researchers determined that the system was successful at measuring the Doppler frequency of a target moving in a linear motion.

Dr. Narayanan and his researchers wanted expand the usefulness of the noise radar and decided to apply Synthetic Aperture Radar (SAR) techniques to the noise radar. SAR is well described by Skolnik's text [36]. SAR produces a high-resolution image of the target or scene by synthesizing in software the equivalent of a large antenna. The larger the antenna the better the resolution in the cross-range direction. A SAR can achieve good resolution in the range direction by either short pulses or pulse compression. A good SAR can have resolution in cross-range and range of one meter that produce high resolution images.
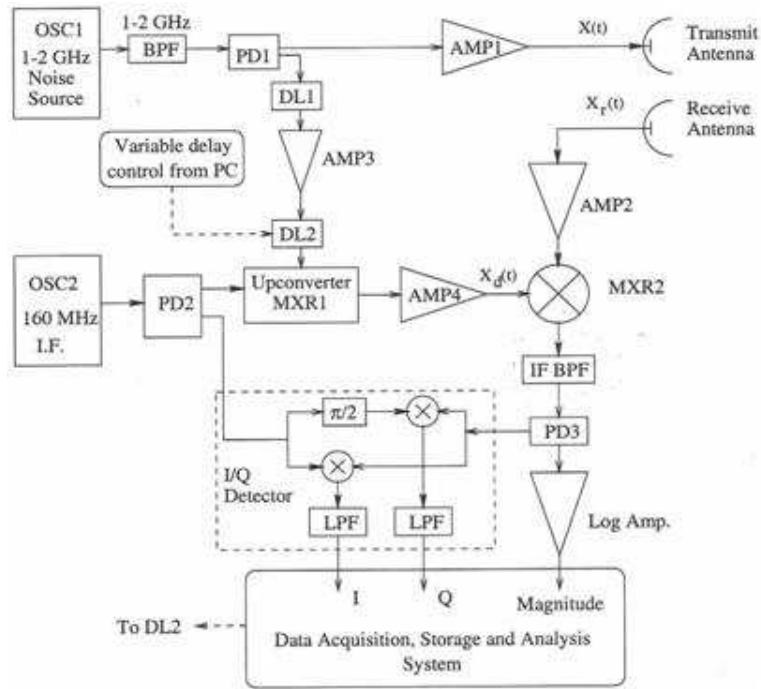
Figure 2.8:    Block Diagram of a Phase Coherent Noise Radar [26]



Figure 2.9:    Picture of Radar and Target Van [26]
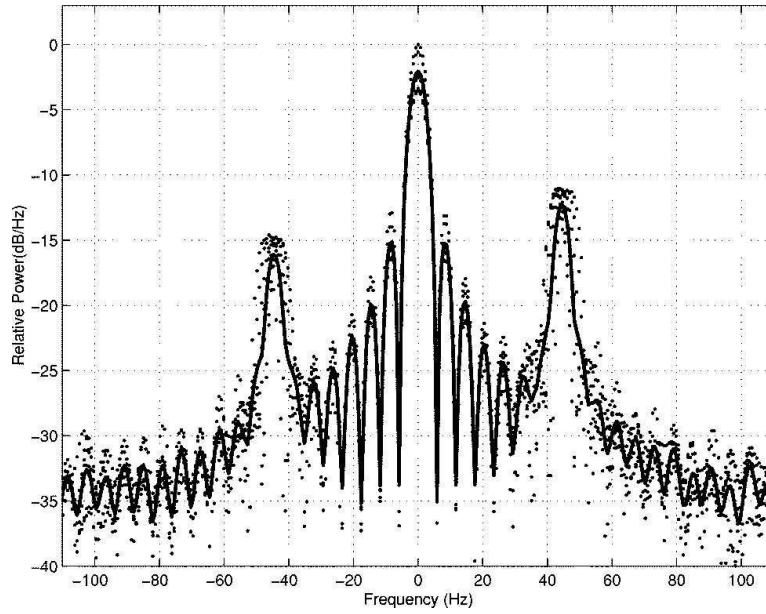
(a) Results with the Radar Using 1.5 GHz Fixed Frequency
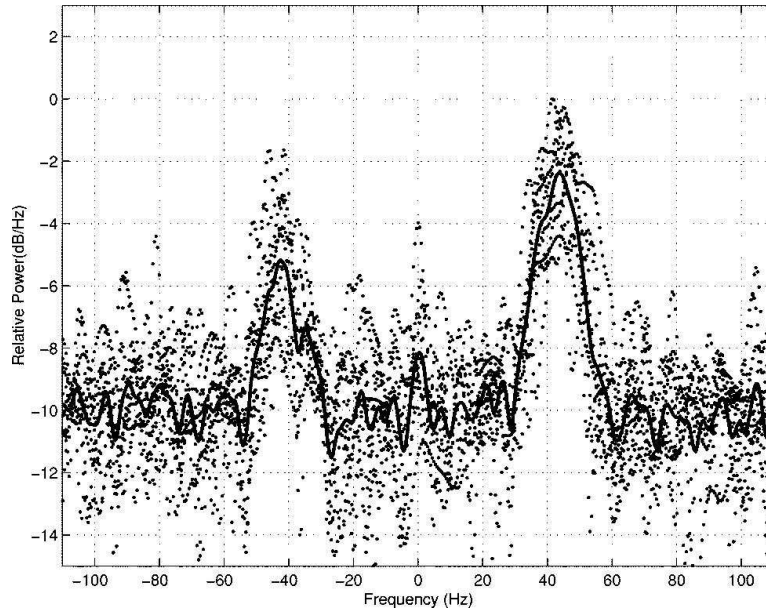


(b) Results with the Radar Using 1-2 GHz Noise Waveform

Figure 2.10:    Measured Doppler Spectra of of a Target Moving at 4.5 m/s [26]

Researchers applied these SAR imaging techniques to a 250-500 MHz noise radar system. Fig. 2.11 shows the target scenario and the resulting SAR image. In this test, a radar was placed outside a room with a trihedral reflector placed on the other side of the room's wall. To obtain the synthetic aperture, the radar was moved in a path parallel to the wall as shown in Fig. 11(a). The results highlight areas where the trihedral, power boxes, and door were located in the room. These results show that a noise radar system using SAR techniques can accurately locate a target through walls. The current focus of research at Pennsylvania State University includes increasing the noise radar SAR capability. In addition, they would like to increase the portability of the system and increase range resolution.

As experimentation with noise radar technology continued, Dr. Narayanan and fellow researchers started looking at streamlining the noise radar system and using it for applications in through-the-wall imaging. These two efforts generated a new generation of noise radar system based on the software defined radio (SDR) concept. This SDR concept is of great interest for this thesis because it does away with much of the cumbersome hardware of delay lines and mixers and utilizes a more digital approach. Digital signals enable better integration with the QUEST processor, an inherently digital device.

The through-the-wall system developed by Dr. Narayanan, shown in Fig. 2.12, uses the SDR design concept. The biggest difference in this noise radar system from other radar systems is that physical delay lines are not necessary and the correlator is digital. Dr. Narayanan's radar system operated in the 350-750 MHz range and yielded a 37.5 cm range resolution. The replica of the transmitted signal and the received signal are digitized at $1.5 \times 10^9$ samples per second. The delay and cross correlation are performed digitally in software [25]. Table 2.1 shows a summary of the radar characteristics of Pennsylvania State University's Noise Radar [18]

The frequency range of 350 MHz to 750 MHz was choose after Dr. Narayanan's PhD student, C. Lai, performed tests measuring the microwave through wall loss
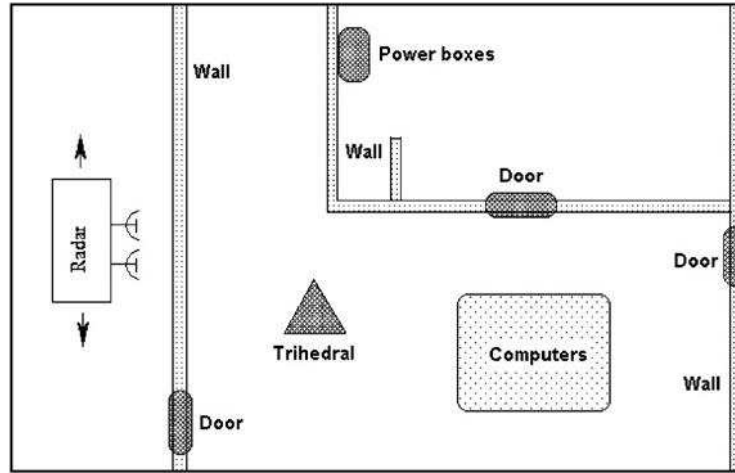
(a) Target Scenario
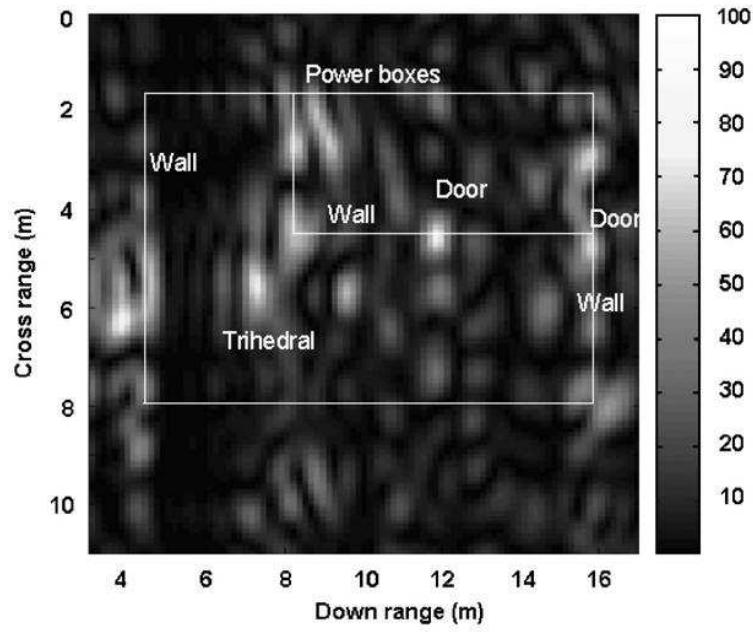


(b) SAR Image

Figure 2.11:     Target Scenario and Resulting SAR Image [25]

23
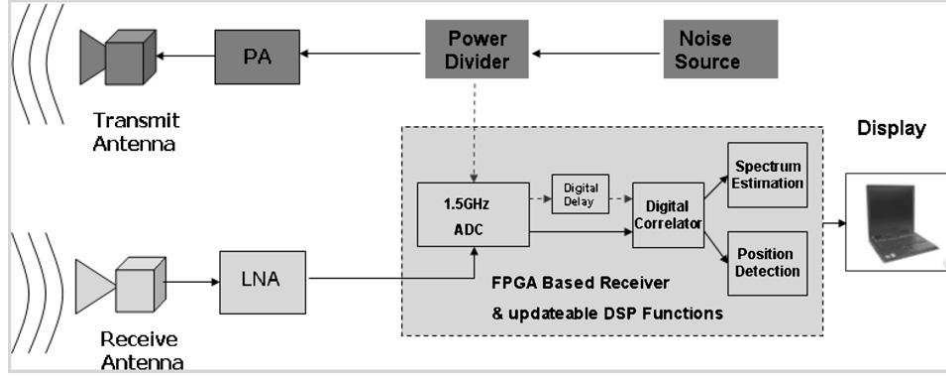
Figure 2.12: Block Diagram of Pennsylvania State University's SDR Noise Radar [18]

Table 2.1: Summary of Radar Characteristics of Pennsylvania State University's Noise Radar [18]

| Parameter | Value |
|---|---|
| Frequency | 350 MHz-750 MHz |
| Transmit PSD at Noise Source | -22 dBM/MHz |
| Input Power at Power Amplifier | -30 dBM/MHz |
| Gain a Power Amplifier | 27 dB |
| Total Transmit Power to the Antenna | +23 dBm |
| Polarization | HH |
| Antenna Gain | 6 dB |
| ADC | 8 Bits |
| Sampling Rate | 1.5 GHz/per channel |
| Dynamic Range (0.8 $P_d$, 0.2 $P_f$) | 20 dB |
| Range Resolution | 37.5 cm |
| Maximum Receive Power | +30 dBm |

at frequencies of 400 MHz to 2600 MHz [18]. The thickness of the wall was 10 cm and its dielectric constant was unknown. The microwave loss was measures with two antennas and a network analyzer. The lowest loss region was from 450 MHz to 750 MHz. Based on these measurement the frequency range of 350 MHz to 750 MHz was chosen. Table 2.2 summarizes Pennsylvania State University's wall loss constants at different frequency bands.

Pennsylvania State University and Dr. Narayanan was most interested in detecting humans through walls. In real world testing, this system detected a human's

Table 2.2:    Summary of Pennsylvania State University's Wall Loss Constants at Different Frequency Bands [18]

| Frequency (MHz) | 450-750 | 750-1000 | 400-1000 | 900-1500 | 1500-2600 | 900-2600 |
|---|---|---|---|---|---|---|
| Loss (dB/cm) | 0.0052 | 0.27 | 0.136 | 0.5 | 0.27 | 0.35 |
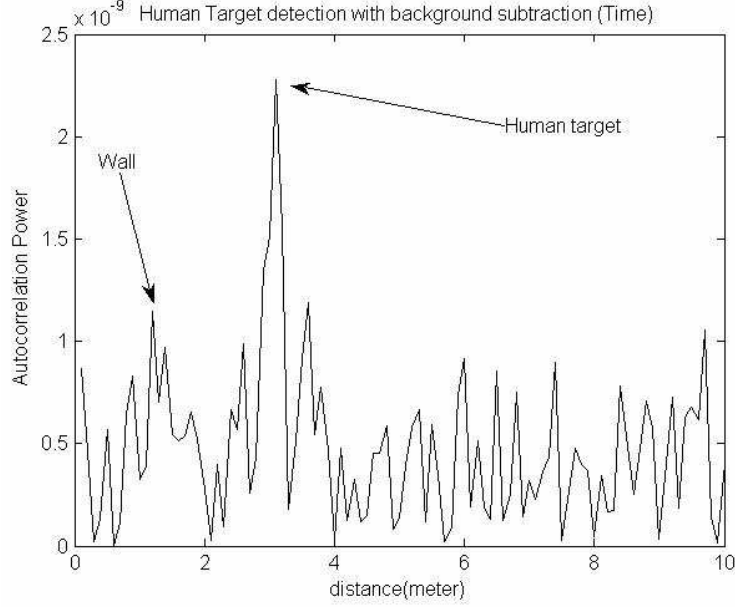


Figure 2.13:    Noise Radar Target Detection of Human Target with Background Subtraction [25]

presence and motion through a 30 cm thick concrete wall [25]. Fig. 2.13 shows the detection of a human target behind a concrete wall with the human at a distance 3 m from the radar. The wall was approximately 1 m from the radar. To improve human target detection results, background subtraction of the wall scene was accomplished in post processing. Fig. 2.13 clearly shows a peak at 3 m for the human target, but a peak at 1 m, from the wall, can still be seen.

Matlab® scripted computer simulations of this system showed that it would be able to achieve a probability of false alarm ($P_f$) of 20 percent with a probability of detection ($P_d$) of 95 percent [18]. These performance statistics are based on assuming a known radar cross section (RCS) for the average human based on laboratory experiments using a suitable threshold received signal strength. A false alarm is said
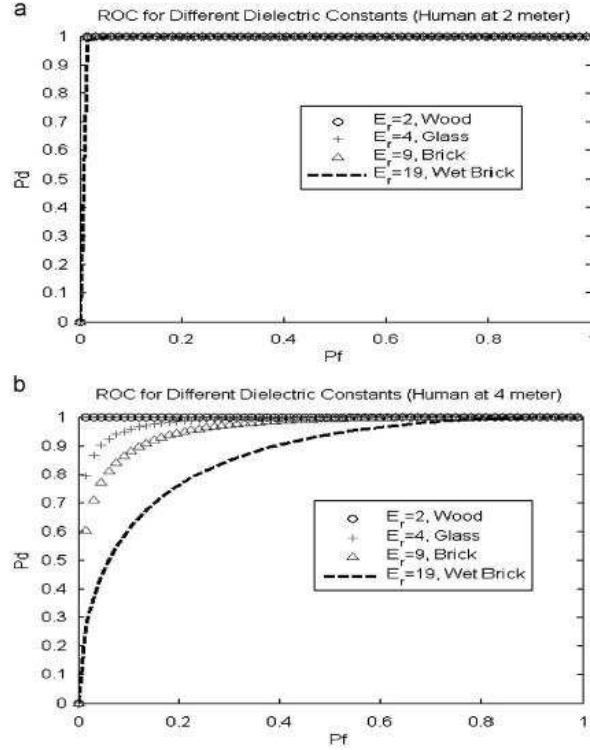
Figure 2.14: ROC curves for different wall dielectric constants for a human at distances of (a) 2 m and (b) 4 m ($P_d$ = probability of detection; $P_f$ = probability of false alarm). [25]

to occur when a noise signal breaks the threshold, but no human is present. A missed detection is when a low signal value from a human target fails to break the threshold. In order to find the probability of detection and the probability of false alarm, an appropriate hypothesis is created and a likelihood ratio test is performed. $H_0$ represents the hypothesis the absence of the human and was formed by subtracting the real-time background interference from an average of background interferences. $H_1$ represents the presence of a human. Using that information, Dr. Narayanan created receiver operating characteristic (ROC) curves. [25] Dr. Narayanan's resulting ROC curves are shown in Fig. 2.14.

Overall, the design and results of Dr. Narayanan's research with a noise radar system using the SDR concept fits well with the objectives of this research. The goal of this research is to develop and build a network of sensors that can monitor human

26

and non-human activity indoors and outdoor. This network of sensors can later be integrated into the QUEST processor. Dr. Narayanan's research and results prove that the SDR noise radar can locate human targets through walls. Also, the SDR concept greatly aids in integrating the sensor with the QUEST processor by digitizing the time delay and correlation.

With signals in digital form, the time delay is just a digital parameter that can be set as necessary by the QUEST processor, unlike cable delay lines that a computer processor could not affect. Digital signals also mean that correlation is accomplished in software. The QUEST processor can be integrated so that it is able to change the correlation length of the transmit and receive signals. Correlation length affects the signal-to-noise ratio (SNR). The longer the correlation length the greater the SNR. Correlation length and its relationship to the SNR will be discussed in more detail in the next chapter. If the correlation occurred in hardware, the QUEST processor could not change any parameters, but correlation length in a digital correlator is just another parameter to be set in the software. If the target shows a weak response, the QUEST processor would be able to increase the correlation length thus increasing the SNR and allowing for better visibility of the target. The drawback to increased correlation length is processing time. The longer the length, the more time it takes to correlate the signals. The QUEST processor could weigh the benefits and drawbacks of an increased ability to locate the target verses the time it take to process the data. Giving the QUEST processor the ability to make choices on the correlation length or the time delay, increase the interaction between the noise radar sensor and its processor. The goal of increased interaction is to decrease the need for human intervention, speed up results, and possibly detect items of interest that the human eye might miss. The SDR concept noise radar seems an ideal sensor for integration with the QUEST processor.

This thesis proposes to pattern its noise radar design after that of Dr. Narayanan's SDR noise radar. Also, this thesis seeks to expand upon the work Dr. Narayanan has accomplished and build a network of noise radar systems. The main goal is to

locate a target's (x, y) position using a network of simultaneously operating noise radar systems.

# III.  Theory

This chapter introduces the generalized theory that radars operate with and then specifically discusses UWB noise radars. First, in Section 3.1 the radar range equation and radar cross section are developed. Mathematical development of these two concepts helps to gain an overall picture into how radars operate and how specific performance parameters affect the operation of the radar system. Section 3.2 looks at noise radar theory and details the mathematical representation of cross-correlation. Correlation is the key element that allows noise radars to operate. Section 3.3 discusses digital noise radars and the specific elements of how these systems operate. It also discusses how digital radars were developed from the Software Defined Radio (SDR) concept. Also, this section explains how correlation is accomplished digitally. Section 3.4 looks at wall attenuation. It examines how electromagnetic waves can be transmitted through walls and the multiple reflection that can occur at the interfaces of different materials in the wall. Section 3.5 summarizes the chapter.

## 3.1   Radar Range Equation and Radar Cross Section

The radar range equation relates the range of the radar to its target to the characteristics of the antenna, receiver, transmitter, target, and environment [36]. This equation not only identifies the maximum range at which a target can be detected, but it also is an important tool in understanding radar systems. The noise radar is a radar that transmits a noise waveform. Though it uses noise as its signal it still operates within the realm of the radar range equation. The next part of this section will derive the radar range equation.

It is assumed that the transmitted power $P_t$ is radiated by an isotropic antenna, an antenna that radiates uniformly. If this is true, then the power density at distance of R from the radar is equal to the radiated power divided by the surface area of an imaginary sphere with a radius of R, or [36]:

$$Power\ density\ at\ a\ range\ of\ R\ from\ an\ isotropic\ antenna = \frac{P_t}{4\pi R^2} \qquad (3.1)$$

However, radars tend to use antennas that are directive and concentrate the radiated power $P_t$ in a specific direction. The gain $G_t$ of an antenna is a measure of the power density increase in one area from that of a isotropic antenna. Thus, the power density aimed at a target with a directive antenna with a gain of $G_t$ can be stated as [36]:

$$Power\ density\ at\ a\ range\ of\ R\ from\ a\ directive\ antenna = \frac{P_t G_t}{4\pi R^2} \qquad (3.2)$$

The transmitted wave will hit the target and be reradiated in many directions, but the reradiation of interest is the power density that is captured by the target and radiated back to the receive antenna. The radar cross section $\sigma$ determines the power density captured by the target. The radar cross section (RCS) is defined by the equation [36]:

$$Power\ density\ captured\ by\ target = \frac{P_t G_t \sigma}{4\pi R^2} \qquad (3.3)$$

The power captured by the target is then radiated back towards the radar, spreading out like an sphere until it reaches the radar. The power density reradiated back to the radar at a distance of R can then be stated as [36]:

$$Power\ density\ at\ recieve\ antenna = \frac{P_t G_t \sigma}{4\pi R^2} \cdot \frac{1}{4\pi R^2} \qquad (3.4)$$

The antenna only captures a portion of the energy from the target and is dependent on the incident angle. The total received signal power is given as the product of the effective aperture area $A_e$ of an antenna and the incident power density. The effective area is defined as [36]:

$$A_e = \frac{\lambda^2 G_r}{4\pi} \qquad (3.5)$$

where $G_r$ is the gain of the recieve antenna. The total power received power $P_r$ can then be calculated with the equation [36]:

$$P_r = \frac{P_t G_t \sigma}{4\pi R^2} \cdot \frac{1}{4\pi R^2} \cdot \frac{\lambda^2 G_r}{4\pi} = \frac{P_t G_t G_r \sigma \lambda^2}{(4\pi)^3 R^4} \tag{3.6}$$

The equation can then be rearranged to form the commonly known form of the radar range equation [36]:

$$R = [\frac{P_t G_t G_r \sigma \lambda^2}{(4\pi)^3 P_r}]^{\frac{1}{4}} \tag{3.7}$$

The radar range equation is an important equation in the world of radars, but another important factor to understand is the RCS variable contained in the equation. The IEEE definition of RCS can be derived from the radar range equation. If the range radar equation is rearranged to equal the RCS ($\sigma$) then the equation looks like [7]:

$$R = \frac{(4\pi)^3 P_r R^4}{P_t G_t G_r \sigma \lambda^2} \tag{3.8}$$

The power density incident on the target can be expressed by [7]:

$$power \; density \; incident \; on \; the \; target = \frac{|\overline{E^i}|^2}{2\eta_0} = \frac{P_t G_t}{4\pi R^2} \tag{3.9}$$

where $|\overline{E^i}|$ is the incident electric field component and $\eta_0$ is the intrinsic impedance in free space. When Eq. 3.9 is applied to Eq. 3.8 the RCS can be written as [7]:

$$\sigma = \frac{(4\pi)^2 P_r R^2 \eta_0 2}{G_r \lambda^2 |\overline{E^i}|^2} \tag{3.10}$$

The power density scattered back to the reciever can be expressed as [7]:

$$\frac{|\overline{E^s}|^2}{2\eta_0} = \frac{P_r}{A_e} \tag{3.11}$$

where $|\overline{E^s}|$ is the scattered electric field component. Eq. 3.5 gives the value for $A_e$ and can be substituted into Eq. 3.11. This changes the power density returned back to the reciever to [7]:

$$\frac{|\overline{E^s}|^2}{2\eta_0} = \frac{4\pi P_r}{\lambda^2 G_r} \tag{3.12}$$

31

Now if Eq. 3.12 is substituted back into the equation for the RCS (Eq. 3.10) the RCS can be written as [7]:

$$\sigma = 4\pi R^2 \frac{|\overline{E^s}|^2}{|\overline{E^i}|^2} \tag{3.13}$$

To assure that the receive antenna is in the far zone the limit $R \to \infty$ is applied to the equation and it can now be written as:

$$\sigma = \lim \quad R \to \infty \quad 4\pi R^2 \frac{|\overline{E^s}|^2}{|\overline{E^i}|^2} \tag{3.14}$$

Eq. 3.14 is the IEEE definition of RCS [17]. Though this definition is exact, calculation of the RCS value using this equation can be difficult and time consuming. Fortunately engineers and mathematicians have come up with equations to quickly calculate RCS values using a technique called physical optics. These equations are estimates and known as hip-pocket formulas. These formulas assume that the wavelength is much smaller than the target [17]. Two exemplar formulas are for a flat plate and a cylinder. The hip-pocket formula for a flat plate is [17]:

$$\sigma = \frac{4\pi A^2}{\lambda^2} \tag{3.15}$$

where $A$ is the area of the flat plate and $\lambda$ is the wavelength.

The hip-pocket formula for a cylinder with a radius of $r$ and a length of $l$ is [17]:

$$\sigma = \frac{2\pi r}{\lambda} l^2 \tag{3.16}$$

Although these formulas are not accurate when the wavelength is the same length or larger than the target, they can help identify the targets with the largest and smallest relative RCS values. This is the case with the frequency band of the noise radar system in this thesis. The frequency range is from 400 MHz to 800 MHz and the wavelength is relatively large in comparison to most targets, but a quick calculation can identify the relative strength of the RCS of each target.

Noise radars operate within the bounds set by the radar range equation and the RCS equation. Energy is sent out as pulses, continuous waves, or continuous noise. The energy strikes a target and returns back to the radar. The radar range equation and RCS mathematically describe this process and show how the range of the radar relates to the characteristics of the antenna, receiver, transmitter, target, and environment. The RCS is important to understand as well. The RCS identifies the factor of energy scattered from the target. Understanding how radars operate and their interaction with targets helps to understand the specific theory behind noise radars and how they operate.

## 3.2 UWB Noise Radar Theory

A UWB noise radar transmits a noise signal $x(t)$ at a target of distance R. The time taken for the signal to get to the target and return is $t_o = 2R/c$ where $c$ is the speed of light. The return signal can then be expressed as $y(t - t_o)$. The return signal, $y(t - t_o)$ is then correlated with the time delayed version of the transmitted signal $x(t - t_d)$ where $t_d$ is the time delay. Correlation is the key to making the noise radar work. If the time delayed noise is not captured or stored then the received signal has no value. To identify a target both the transmit and receive signal need to be correlated together. Correlation of two separate signals is also known as cross-correlation. The mathematical representation of cross-correlation is [3]:

$$C_{yx}(T) = \int_0^{T_{int}} y(t - t_o)x^*(t - t_d)dt \qquad (3.17)$$

where $T = t_o - t_d$. The maximum response of $C_{yx}$ would be when $T = 0$, when the round trip time to the target and back matches the internal delay (i.e. $t_0 = t_d$). The range resolution for the radar is expressed by $\Delta R = c/2\beta$ where $\beta$ is the signal bandwidth [3].

Correlation of the transmit and receive signals is the cornerstone function in making the noise radar work. Many implementations of radars rely on mixers and

filters for correlation. Instead, the noise radar design in this thesis relies on a digital correlator that correlates the transmit and receive signal in software. The correlation program used in this thesis is written in the Matlab® programming environment. The digitization of the signals and use of a digital correlator make this type of noise radar a digital noise radar. Section 3.3 further discusses digital noise radars, the concept that makes them possible, digital correlation, and some of the advantages of digital noise radars.

## 3.3   Digital Noise Radar

Analog UWB noise radars can be bulky with cable delay lines and other hardware components. A digital noise radar offers a more compact radar system and more signal processing options [25]. The the first step towards digitizing noise radar systems came in 1989 when researchers began working with a concept that later became known as software defined radio (SDR) [8]. Since then, SDR has been successfully applied in wireless technology, global positioning systems, and other personal communication applications [43] [48]. Recently, Dr. Narayanan took advantage of the SDR concept and applied it to noise radars [25]. His SDR implementation of the noise radar allowed correlation and image processing to be accomplished in software rather than in hardware. The next few subsections discuss the SDR concept, digital delay, and digital correlation.

*3.3.1   Software Defined Radio (SDR) Concept.*   The software defined radio concept replaces the hardware components of mixer, filters, amplifiers, modulators/demodulators, and detectors with software components on a computer or on embedded computing devices. With the signal processing handed over to software rather than specialized hardware components, the functionality and flexibility of the radar increases. A simple change in the software can completely change the previous set of operating instructions. To change the operating instructions in a hardware radio a new design and components are necessary. The SDR concept become a reality

through advancements in digital electronics, digital signal processing software, and faster analog-to-digital converters (ADC) [43] [48] [8].

An ideal SDR system would have a receiver with the ADC directly connected to the receiving antenna. For the transmitter, a digital signal processor would generate a stream of numbers that would be sent to a digital-to-analog converter (DAC), and then out of the transmitting antenna. This scheme cannot be completely achieved yet due to limits in technology. Current ADCs are not capable of picking up sub-microvolt radio signals, so a low noise amplifier (LNA) needs to be introduced. The addition of the LNA requires that a bandpass filter be placed between the antenna and the LNA to filter out unwanted signals before amplification [8]. Even with the addition of the LNA and bandpass filter the SDR concept has great benefits. The greatest advantages are reduced hardware costs, rapid upgrades, and an ability to change functions in software.

It is also prudent to note that the sample rate of the ADC and DAC are the major performance limiters in the SDR scheme. Performance in digital signal processing is directly related to the rate at which the signals are sampled.

*3.3.1.1   SDR Concept Applied to the Noise Radar.*    In an analog noise radar system, like the one shown in Fig. 2.8, there are hardware components like mixers, modulators/demodulators, oscillators, and cable delay lines. Applying the SDR concept to a noise radar means doing away with these hardware components and replacing them with an ADC and software. Fig. 3.1 shows a detailed block diagram of a digital noise radar system. The receiver closely follows the SDR design concept with antenna to bandpass filter to LNA to ADC. The transmitting end differs due to the function and purpose of a noise radar verses a radio. The noise source is in analog form and can be amplified and sent out of the antenna without a DAC. To achieve the ability to digitally correlate the transmitted and received signals, the transmitted noise signal is sent through the ADC and stored for processing in the
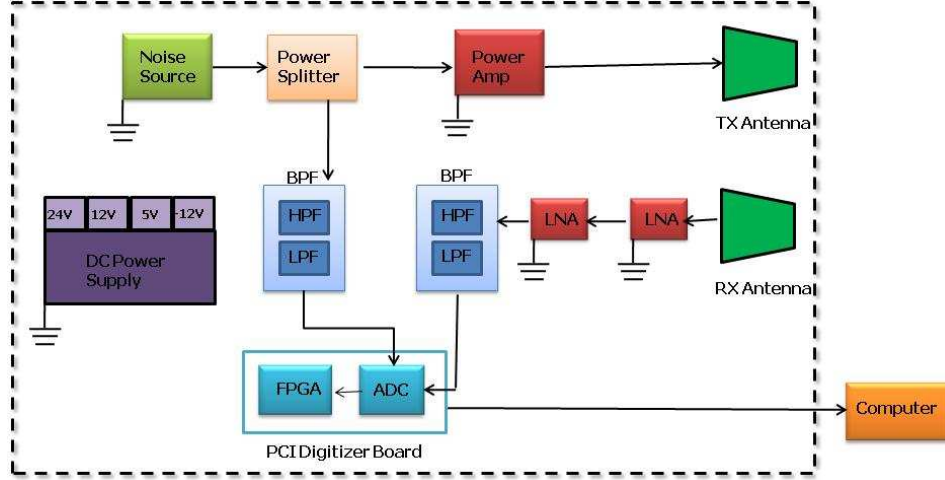
Figure 3.1:     Block Diagram of a UWB Noise Radar System

computer's software. Overall, this scheme reduces hardware and system bulk, and allows the use and flexibility that digital signal processing offers.

The SDR concept applied to the noise radar is particularly advantageous for the QUEST concept. The QUEST processor seeks to interact with the radar system in a way not previously considered. Giving the processor more freedom to interact effectively with a sensor system means that the system needs to function more in the digital realm. Digital signal processing offers the QUEST processor more flexibility in its interactions with the radar. Specific hardware components that perform signal processing limit the amount that the QUEST processor can interact or even change how the processing occurs. With processing done digitally or in software, the QUEST processor has the ability to insert or direct the radar's signal processing in a real-time or near real-time environment.

*3.3.2   Digital Delay.*     Traditional analog noise radar systems rely on physical cable delay lines to correlate the original noise signal and the received noise signal. These are bulky since a delay line system must have many cables with different lengths to be able to correlate targets at different ranges. Cable switches, amplifiers, and a controller are also necessary to run the delay line system [40]. With a digital noise radar, these items are unnecessary since the original signal and the received signal have

36

been digitally sampled and stored. This is accomplished with a high speed digitizer board directly sampling the radio frequency (RF) signal from both the transmitting and receiving antennas.

The sampling rate of the digitizer can be compared to the minimum delay step in a delay line. The higher the sampling rate, the smaller the delay step, and the greater a target's range resolution. This assumes that the limiting factor is the sampling rate. Bandwidth also plays a factor in range resolution. This relationship can be seen in the equation $\Delta R = c/2\beta$ where $\Delta R$ is the range resolution and $\beta$ is the signal bandwidth [3]. As the speed of digitizer's sampling rate increases this becomes less of a limiting factor and the bandwidth is the limiting factor in range resolution.

Digital sampling also allows for control over the data length that is sampled. The data length needs to be long enough to cover the search range of the radar and long enough to allow for cross correlation. The data length also has an effect on the SNR of the target detection. The longer the recorded data length, the longer the cross-correlation of the two signals can be, and this increases the SNR. The drawback to longer correlation is an increase in the amount of time needed to process the data. The next section looks at digital correlation and the mathematical derivation linking SNR and data length.

*3.3.3  Digital Correlation.*    A correlator is a hardware or software device that combines sampled voltage time series from one or more antennas to produce sets of complex vectors [6]. In doing this it compares how closely the signals resemble one another. A correlation of analog signals is accomplished with a mixer and low pass filter [13]. With digital signals, correlation is accomplished in software. In this thesis, the correlation is accomplished digitally using the `Matlab`® function xcorr. `Matlab`® defines its cross-correlation function xcorr by:

$$(3.18)$$

$$R_{xy}(m) = \begin{cases} \sum_{n=0}^{N-m-1} x_{n+m} y_n^* & m \geq 0 \\ R_{xy}^*(-m) & m < 0 \end{cases}$$

where $x$ and $y$ are length N vectors (and $N>1$) and where m is time lags or leads. If the vectors are not the same length Matlab® pads the shorter vector with zeros to make the length equal. The length of the output vector is equal to $2N - 1$.

If the strongest correlation peak within the output vector occurs at $m = 0$ then the two vectors are highly correlated. The $m = 0$ is the center point of the output correlation vector. Since the output vector has a length of $2N - 1$ the center point is at $N + 1$. The noise radar software pulls out the $N + 1$ point of the correlation vector, because a high correlation peak indicates that the receive signal matches the transmit signal. The receive signal could only match the random noise transmit signal if it was backscatter from a target. The noise radar shifts the received signal in time and correlates it at each time shift to the transmit signal. At each correlation the $N + 1$ of the output vector is pulled out and stored. When these points are plotted the highest correlation peaks indicate the time it took for the transmit signal to hit a target and return. With the points in time known, distance is easily calculated with the equation $R = ct/2$ where $R$ is the range, $c$ is the speed of light, and $t$ is the round trip time from the radar and back [36].

*3.3.3.1 Digital Correlation Statistics.* In a digital correlator, when the delay of the replica transmit signal is the same as the receive target echo, the two cross correlated signals can be seen as an autocorrelation that has a strong correlation coefficient. One is the highest value for the correlation coefficient and this means that the two signals are exactly the same. In a noise radar application the return signal has been changed by the target and environment. It is expected that a relatively strong correlation will exist compared to the random noise in the area, but that this value will still be much less than one. To detect a target that exists at an unknown distance, the correlation of the received signal and transmit replica needs shifting

38

delays applied to the received signal until a match of the transmitted and received signals is found. This process of shifting delays becomes the cross correlation process.

Cross correlation can be derived from the statistical estimate of the autocorrelation process. Hawkins, in his text on correlator theory, begins with autocorrelation, derives the cross correlation, and defines the signal to noise ratio (SNR) of the measured correlation coefficient [13]. First, he begins with a statistical definition of autocorrelation. The autocorrelation coefficient is then found by dividing by the variance. Then, the cross correlation can statistically be described with two joint Gaussian random variables with a mean of zero and stated as the Bivariate Gaussian probability distribution function. The cross correlation coefficient can then be found by dividing the cross correlation by the variance. This cross correlation coefficient is the expected value of the maximum value of the correlation function. The cross correlation coefficient is developed further and simplified using the correlation mean and variance. Last, Hawkins defines the SNR of the measured correlation coefficient.

Hawkins states in this text that the autocorrelation estimate, calculated as an ensemble average of $K$ temporal samples of the waveform $x(t)$ produced by the zero-mean Gaussian random process $X(t)$ with standard deviation $\sigma$ as [13]:

$$(3.19)$$

$$r_{XX}[n] = \mu_{r_{XX}}[n] \pm \sigma_{r_{XX}}[n] = \begin{cases} \sigma^2 \pm \sigma^2 \sqrt{\frac{2}{K}} & n = 0 \\ 0 \pm \sigma^2 \frac{1}{\sqrt{K}} & n \neq 0 \end{cases}$$

where n is the number of time lags or leads, $\mu_{r_{XX}}$ is the mean of the autocorrelation, and $\sigma_{r_{XX}}$ is the standard deviation of the autocorrelation.

The correlation coefficient of autocorrelation can then be described by:

$$\rho_{XX}[n] = \frac{r_{XX}[n]}{\sigma^2} \qquad (3.20)$$

The expected values of the correlation coefficients are then:

$$(3.21)$$

$$\rho_{XX}[n] = \mu_{\rho_{XX}}[n] \pm \sigma_{\rho_{XX}}[n] = \begin{cases} 1 \pm \sqrt{\frac{2}{K}} & n = 0 \\ 0 \pm \frac{1}{\sqrt{K}} & n \neq 0 \end{cases}$$

With this information we can consider the cross correlator. If $X$ and $Y$ are joint Gaussian random variables with zero mean and variance $\sigma^2$, then their probabilities of occurrence is governed by the Bivariate Gaussian probability distribution function that is given by [20]:

$$f_{XY}(x,y) = \frac{1}{2\pi\sigma^2\sqrt{1-\rho^2}} exp(-\frac{(x^2+y^2-2\rho xy)}{2\sigma^2(1-\rho^2)}) \qquad (3.22)$$

where the cross correlation coefficient ($\rho$) is [20]:

$$\rho = \frac{E[XY]}{\sqrt{E[X^2]E[Y^2]}} = \frac{\langle xy \rangle}{\sqrt{\langle x^2 \rangle \langle y^2 \rangle}} = \frac{\langle xy \rangle}{\sigma^2} \qquad (3.23)$$

and $-1 < \rho < 1$. $\langle \rangle$ denote the expectations of many examples. Now for $\rho \ll 1$, the exponent can be expanded and Eq. 3.22 can be written as [20]:

$$f_{XY}(x,y) \approx [\frac{1}{\sigma\sqrt{2\pi}}exp(\frac{-x^2}{2\sigma^2})][\frac{1}{\sigma\sqrt{2\pi}}exp(\frac{-y^2}{2\sigma^2})](1 + \frac{\rho xy}{\sigma^2}) \qquad (3.24)$$

The cross correlation coefficient from Eq. 3.23 is the expected value of the maximum of the correlation function. With the appropriate delay this maximum occurs at the center, or zeroth lag, of the correlator. If the sampling frequency is at least two times the bandwidth (full precision sampling), then the K-ensemble averaged correlator is directly proportional to $\rho$, shown by:

$$\begin{aligned} r_{XY} &= \mu_{r_{XY}} \pm \sigma_{r_{XY}} \\ &= \rho\sigma^2 \pm \sigma^2\sqrt{\frac{\rho^2+1}{K}} \end{aligned} \qquad (3.25)$$

$\mu_{r_{XY}}$, from Eq. 3.25, can be found by solving Eq. 3.23 for $E[XY]$.

$$\mu_{r_{XY}} = E[XY] = \langle xy \rangle = \rho\sigma^2 \tag{3.26}$$

$\sigma_{r_{XY}}$, from Eq. 3.25 can be derived through the following equation:

$$\sigma_{r_{XY}}^2 = \frac{1}{K}(E[(XY)^2] - (E[XY])^2) = \frac{1}{K}(\sigma^4 + \sigma^4\rho^2) \tag{3.27}$$

where $E[(XY)^2]$ is derived from:

$$E[(XY)^2] = \int_{\infty}^{\infty} \int_{\infty}^{\infty} x^2 y^2 f_{XY}(x,y) dx dy = \sigma^4(1 + 2\rho^2) \tag{3.28}$$

The cross correlation coefficient is:

$$\rho_{XY}[n] = \frac{r_{XY}[n]}{\sigma_{r_{XY}}^2} = \rho \pm \sqrt{\frac{\rho^2 + 1}{K}} \tag{3.29}$$

The SNR of the measured correlation coefficient is defined as:

$$SNR \doteq \frac{\mu_{r_{XY}}}{\sigma_{r_{XY}}} \tag{3.30}$$

When full precision sampling is used, then the SNR can written as:

$$\begin{aligned} SNR &= \rho\sqrt{\frac{K}{\rho^2 + 1}} \\ &\approx \rho\sqrt{K} \quad for \ \rho \ll 1 \end{aligned} \tag{3.31}$$

Eq. 3.31 yields the SNR for the digital cross correlator for $\rho \ll 1$. This means that the SNR is proportional to the square root of the number of samples. $\rho \ll 1$ is an allowable assumption because the received signal has traveled through the environment, struck a target, and returned to the radar. During the entire time of its travel, the environment and target distorted the signal in the form of phase delays,

41

amplitude changes, and additive environmental noise. When $\rho = 1$ it means that the correlation of the transmitted and received is exact. Knowing that the received signal has been changed, the likelihood of exact correlation is small. So, it would be a fair assumption that even a strong correlation would be $\rho \ll 1$.

The equation for SNR has realizable implications for a digital noise radar. An increase in the number of samples or correlated data length will increase the SNR. For example, an increase from a data length of 200 to 400 will increase the SNR by 2.5 dB. For each increase in correlated data length there is a corresponding increase in processing time. The optimal data length needs to be determined by an acceptable SNR for target identification and the limits set on processing time.

## 3.4 Wall Attenuation Theory

One of the goals of this thesis is to locate targets through walls. For a signal to pass through a wall the frequency needs to be under 1 GHz. Frequencies in this range have longer wavelengths that can penetrate through the width of the walls [12]. The frequency range that the noise radars in this thesis will operate within is 400 MHz to 800 MHz. This frequency range was based on experiments accomplished by one of Dr. Narayanan's PhD students. He found that the lowest signal loss due to the wall was in the 450 MHz to 750 MHz frequnecy band [18]. The frequency band used in this thesis is slightly outside 450 MHz to 750 MHz because a larger bandwidth was desired for increased range resolution. The range resolution of the radar system will be discussed further in the next chapter. The frequency range from 400 MHz to 800 MHz is known to be able to penetrate through walls to reach the target, but losses of the signal are expected. The thickness of the wall, its dielectric constant, and angle of incidence affect the propagating signal. As the signal travels through the wall it slows down and this propagation delay causes phase changes [4]. This phase change contributes to information loss in both target range and Doppler detection.

Materials that generally make up walls (like brick, wood, and concrete) are nearly lossless to a low frequency wave and this means that the attenuation constant
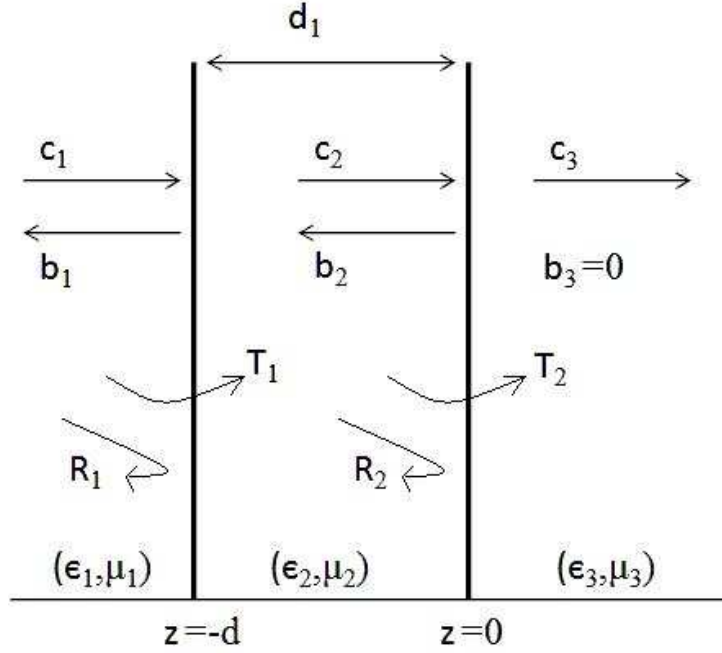
Figure 3.2:    Reflection and Transmission Coefficients for a Wave Propagating through a Wall.

is low. The attenuation constant can be calculated with the equation [4]:

$$\alpha = \omega\sqrt{\mu\varepsilon_r}(.5[\sqrt{1 + (\frac{\sigma}{\omega\varepsilon_r})^2} - 1])^{.5} \qquad (3.32)$$

where $\varepsilon_r$ the dielectric constant, $\sigma$ is the conductivity, $\mu$ is the permeability, and $\omega = 2\pi\ frequency$. For example, the dielectric constant of concrete is 7, the conductivity is 1 mS/m, and the permeability is 1 $N/A^2$ [10] [4]. Using the center frequency of the noise, 600 MHz, and the concrete's constitutive parameters the attenuation constant is near zero. This means that a concrete wall is mostly lossless at the frequency in which the noise radar will operate.

If the material of the wall is mostly lossless then we can reasonably assume that most of the energy lost in propagating through the wall is due to multiple reflections at the interfaces of different materials in the wall. Fig. 3.2 shows the reflection and transmission coefficients of a wave propagating through the wall. The variables $c_1$ and $b_1$ represent forward and reverse complex wave amplitudes. Their relationship is

defined by the matrix formulation [12]:

$$\begin{bmatrix} c_1 \\ b_1 \end{bmatrix} = \prod_{n=1}^{2} [A^{(n)}] \begin{bmatrix} c_3 \\ b_3 \end{bmatrix} \tag{3.33}$$

$$[A^{(n)}] = \frac{1}{T_n} \begin{bmatrix} e^{jk_{nz}d_n} & R_n e^{-jk_{nz}d_n} \\ R_n e^{jk_{nz}d_n} & e^{-jk_{nz}d_n} \end{bmatrix} \tag{3.34}$$

where

$$R_n = \frac{Z_n - Z_{n-1}}{Z_n + Z_{n-1}} \quad , \quad T_n = 1 + R_n \tag{3.35}$$

$$Z_n = \frac{\eta_n k_n}{k_{nz}} \quad , \quad k_{nz} = \sqrt{k_n^2 - k_z^2} \quad , \quad k_z = k_0 \sin(\theta_i) \tag{3.36}$$

and $\theta_i$ is the angle of incidence. It is assumed that the polarization of the reflected and transmitted waves are in the same direction as the incident wave. Also, multipath effects behind-the-wall are not taken into account because UWB radars tend to have good immunity from multipath effects because of their high resolution.

The incident electric field component $\overline{E^i}$, the reflected electric field component $\overline{E^r}$, and the transmitted electric field component $\overline{E^t}$ are given by [12]:

$$\overline{E^i} = \widehat{x} E_0 e^{-jk_z z} \tag{3.37}$$

$$\overline{E^r} = \widehat{x} \Gamma E_0 e^{jk_z z} \tag{3.38}$$

$$\overline{E^t} = \widehat{x} T E_0 e^{-jk_z z} \tag{3.39}$$

where

$$\Gamma = \frac{b_1}{c_1} \quad , \quad T = 1 + \Gamma \tag{3.40}$$

and where $E_0$ is the amplitude of the incident electric field.

The formulation of the incident, reflected, and transmitted electromagnetic fields give the ability to calculate these electromagnetic fields as long as $E_0$ is known. Also, this allows physical insight into how a wall or other obscuring object can allow most of the signal to pass through, yet still some part of the signal reflects back.

### 3.5  Chapter Summary

This chapter introduced the generalized theory that radars operate with and then specifically discussed UWB noise radars. The development of radar range equation showed how items like range, and the characteristics of the antenna, receiver, transmitter, target, and environment relate to each other. It was understood that a noise radar has the same relationships described in the radar range equation though it uses a noise waveform for its transmit signal. The mathematical representation of correlation and why correlation was a key element in noise radars was discussed. Also, the specifics of digital noise radars were discussed and how these systems operate. Last, wall attenuation was examined. Electromagnetic waves at the frequency range of 400 MHz to 800 MHz traveling through concrete (a substance many building walls are made of) have an attenuation constant near zero. This means that the wall itself does not damp the signal noticeably. Instead, loss of signal strength can occur at the interfaces of different materials in the wall. Though reflections occur most of the signal is capable of propagating through a wall at the desired frequency range.

# IV. Noise Radar Hardware Design and Software Signal Processing

T his chapter describes the overall hardware and software design for the network of radar systems. Section 4.1 looks at the overarching hardware design of the network and the design of each noise radar system. Sections 4.2-4.9 discuss each hardware component in detail. Table 4.1 lists all the hardware components, manufacturers, and basic specifications. Section 4.10 looks at the the network of desktop computers and the arbitrary waveform generator. Section 4.11 details the software algorithm used for correlation and imaging. Section 4.12 summarizes the chapter and the network of noise radar systems.

## 4.1 Hardware Design Overview

Fig. 4.1 shows an overview block diagram of the noise radar system and a possible target scenario to depict how the hardware is utilized in this thesis. The concept uses three separate noise radar systems positioned around a room to achieve an accurate position location of the target. These individual systems are linked together through a computer network where the data from each radar is processed into a consolidated output. The three desktop computers, each containing a digitizer, are located together on a cart with wheels. Also, located on the bottom of the cart are the radar boxes containing the noise sources, amplifier, and filters. The ethernet hub, power cords, and other cabling are located on the cart as well. The antenna pairs for each system, positioned on an antenna stands, are connected to the appropriate radar boxes with 25 ft cables. The extended cables and cart make moving the radar systems easier and allow the antennas, read location of radar systems, to be easily placed apart from one another. A keyboard, mouse, and monitor are connected to the desktop computer of Radar System 1 to control all three systems. An arbitrary waveform generator (AWG) set to generate rectangular pulses is connected to each of the digitizer's external trigger ports. Fig. 4.2 shows several pictures of the radar systems.
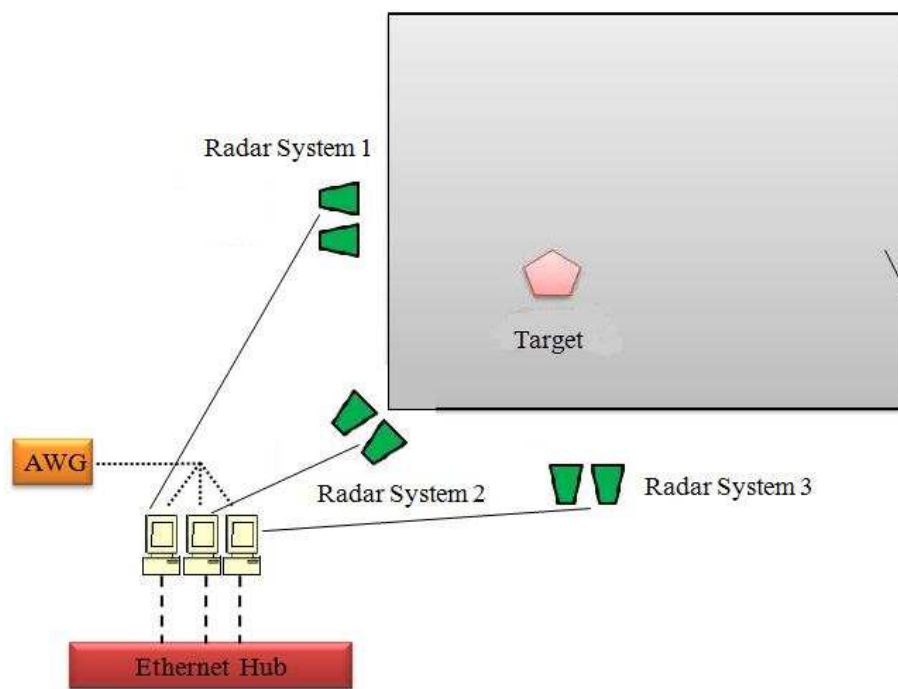
Figure 4.1:    Overview of a Network of UWB Noise Radar Systems and Possible Target Scenario

(a) Radar Systems 1, 2, and 3's Computers and Radar Boxes
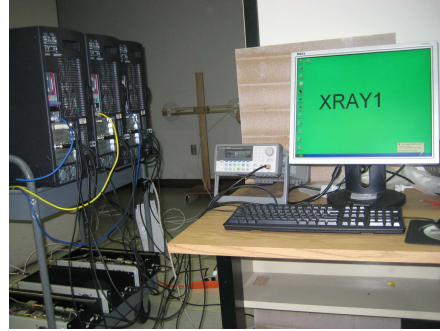


(b) Radar Systems 1, 2, and 3's Computers, Monitor Display, the AWG, and a Antenna Stand in Back
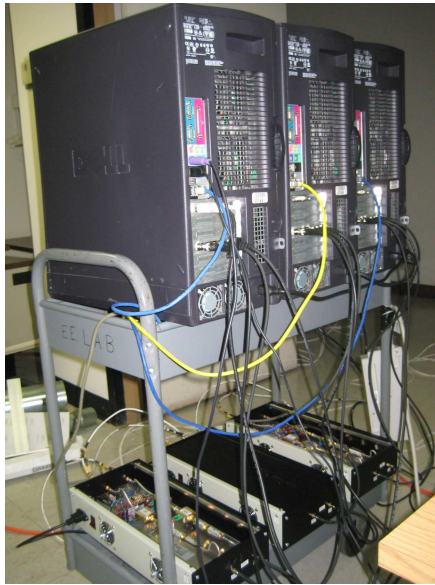


(c) Radar Systems 1, 2, and 3's Computers with Connections to Radar Boxes



(d) Opened Radar Box of Radar System 1

Figure 4.2:    Pictures of the 3 Radar Systems Mounted on Cart
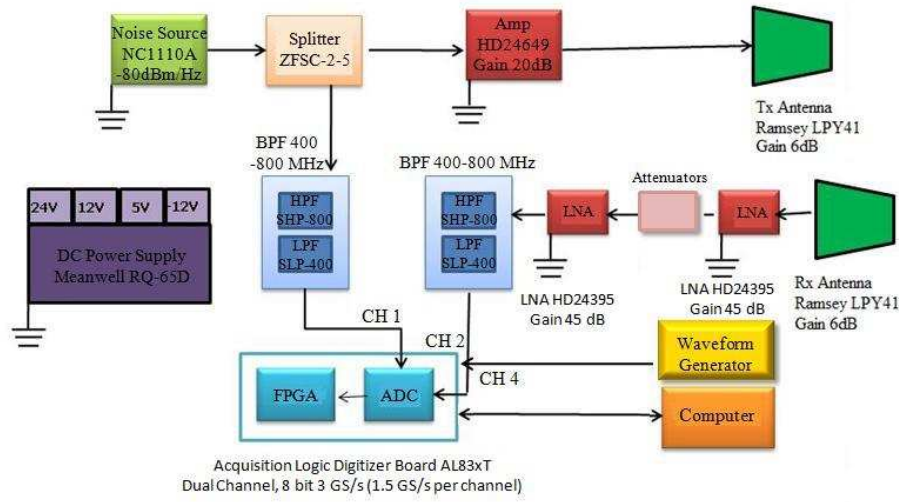
Figure 4.3:    Block Diagram of UWB Noise Radar System

Fig. 4.3 shows a detailed block diagram of an individual UWB noise radar system.    Table 4.1 shows a summary of each component, the manufacturer, part number, and basic specifications.

## 4.2    Power Supply

The power supply is a commercially available component manufactured by Meanwell. The power supply requires an input of 115 V AC. It has outputs of GND, 24 V, 12 V, -12 V, and 5 V. It supplies power to the noise source and all of the amplifiers.

## 4.3    Noise Source

The noise source is commercially available from Noise Com Inc.  The noise source can provide a random noise signal from 10 Hz to 6 GHz. It produces white Gaussian noise as high as +13 dBm. When used within the noise radar system it is expected to produce noise at +10 dBm, with an output power of -80 dBm/Hz, and with a flatness of ±2.0 dB. Ideally, the noise source should provide a flat region so that a uniform power density is provided in the frequency range of interest, approximately 400 MHz

Table 4.1:    List of Noise Radar Components and Specifications

| Component | Supplier | Part Number | Specifications |
|---|---|---|---|
| Power Supply [21] | Meanwell | RQ-65D | Outputs GND, 24 V, $\pm$12 V, 5 V |
| Noise Source [29] | Noise Comm Inc | NC1110A | Pwr 10 dBm, Output -80 dBm/Hz |
| Splitter [24] | Mini-Circuit | ZFSC-2-5 | Bandwidth 10-1500 MHz |
| Amp [15] | HD Comm Corp. | HD24649 | Gain 20 dB |
| LNA [14] | HD Comm Corp. | HD24395 | Gain 45 dB, noise figure of 0.8 dB |
| HPF [23] | Mini-Circuit | SHP-400 | Passband $400 - 3200$ MHz |
| LPF [22] | Mini-Circuit | SLP-800 | Passband DC$-$800 MHz |
| Antennas [32] | Ramsey | LPY41 | Gain 6 dB |
| Antenna Stands | Custom Build | None | Antenna Height: Max 4 ft Min 1 ft |
| Digitizer Board [1] | Acquisition Logic | AL83xGT | 2 Channel, 8 bit 1.5 GS/s per channel |
| AWG | Agilent | 33250A | 80 MHz sine and square waveforms |

to 800 MHz. Fig. 4.4 shows the power spectrum of the noise source in the frequency range of interest. It verifies that from 400 MHz to 800 MHz a flat region in the power spectrum exists. The noise source signal is then fed into a power splitter with one output leading towards the transmitting antenna and the other output leading to the PCI Digitizer Board.

## 4.4   Power Splitter

The power splitter is an inexpensive commercially available part from Mini-Circuit. It has a wide bandwidth from 10 Hz to 1500 MHz and a typical insertion loss of 0.5 dB. It splits the noise signal between the power amplifier and the PCI Digitizer Board.

## 4.5   Power Amplifier

One output, after the power splitter, leads to the power amplifier. This amplifier boosts the signal output to ready it for transmission through the antenna and into the environment. The amplifier is a commercially available part manufactured by HD Communication Corp. It has a frequency range of 100 Hz to 1000 MHz, a gain of 45 dB, and a noise figure of 3.5 dB.
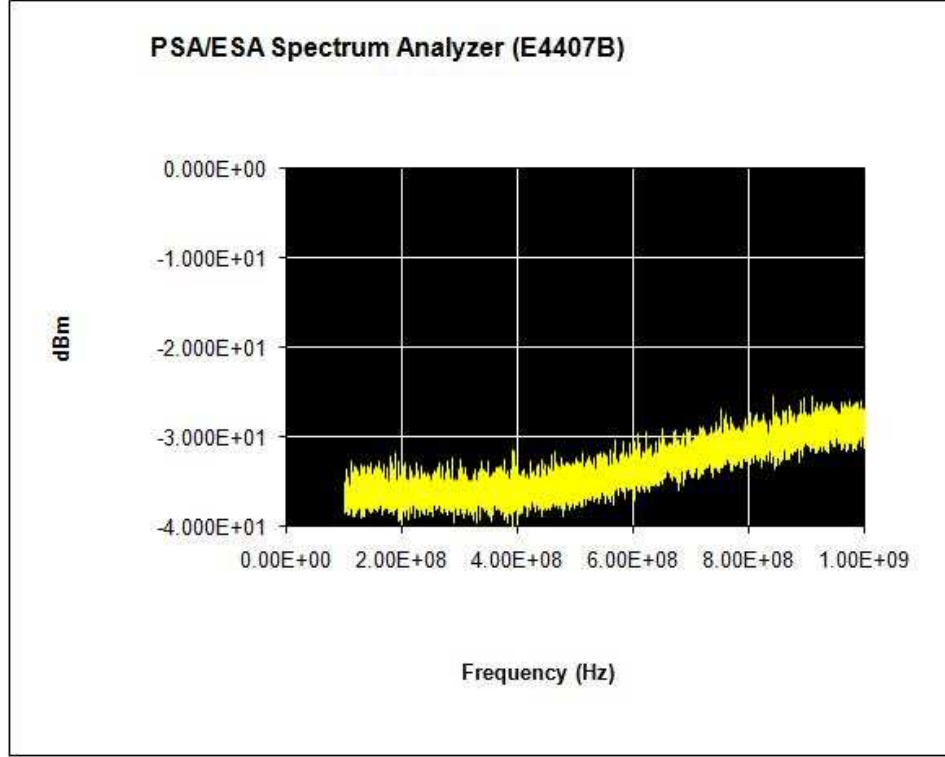
Figure 4.4:    Power Spectrum of the Noise Source

## 4.6   Antennas

The receive and transmit antennas are identical. Both are inexpensive commercially available parts from Ramsey Electronics. The antenna is a log periodic yagi antenna with a frequency range of 400 MHz to 1000 MHz and a gain of 6 dB. These antennas are small, light weight, thin and directional. They are simple, require no tuning, are fairly rugged, and feature a SMA connector. The antennas have a balloon shaped antenna pattern shown in Fig. 4.5 [11].

*4.6.1  Antenna Stand.*    The antenna stand was designed and built with consideration for basic functionality, simplicity, low cost, and ease of construction. The stand itself is made of wood so as not to cause strong reflections. The antenna holder is also made of a good electric insulator material that will not affect the antenna pattern or polarization. The stand allows for adjustment of the height of the antennas from the ground, the spacing between the antennas, and the polarization. The height

51
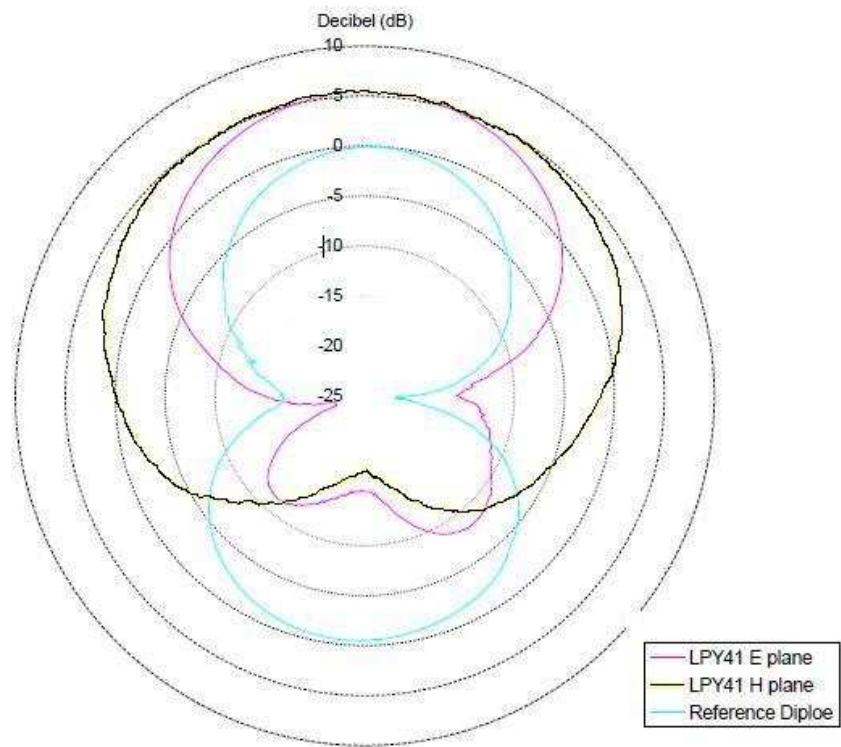
Figure 4.5:    Measured Antenna Pattern of the Log Periodic Yagi Antenna [11]

Figure 4.6:     Picture of Antenna Stand

can be adjusted from 6 inches off the ground to a maximum of just under 4 ft. The spacing can range from the edges of the antennas touching to 2.5 ft between the centers of each antenna. Fig. 4.6 shows a picture of the antenna stand. The antennas can also be adjusted to be either in horizontal or vertical polarization. Throughout all the experiments conducted during this thesis, each antenna operated in the horizontal polarization. The choice of polarization was based on experiments accomplished by one of Dr. Narayanan's students. He found that the antennas had less coupling in the horizontal polarization [18].

## 4.7   Low Noise Amplifier (LNA)

The received antenna signal is sent into two LNAs in series. The return signal is very small and needs to be above that of the quantization level of the PCI Digitizer Board's ADC to be accurately sampled. In simulations, the gain factor provided by the LNA was one of the most influential pieces in target detection. For more details

on the simulation project see Appendix D. An increase in gain increases the detection range. So it was with great care that the LNA component was chosen. A low noise figure was very desirable as well as an acceptable gain figure and a reasonable cost. The LNA from HD Communication Corp. was chosen because of its low noise figure, acceptable cost, and its ability to be cascaded for an adequate gain.

Each LNA has a gain of 20 dB, a frequency range of 100 MHz to 1400 Mhz, and a noise figure of 0.8 dB. So as not to saturate the signal, attenuators sit between the two amplifiers. Each radar system's attenuation is different, because of the small variations in each LNA. Radar system 1 has 6 dB of attenuation. Radar system 2 has 9 dB of attenuation. Radar system 3 has 6 dB of attenuation. These values were decided upon through experimentation. A flat metal board was 1 m from each system. This was assumed to be the worst case scenario or the highest return that could be seen. The attenuator values were adjusted keep the overall gain at an appropriate level.

Fig. 7(a) shows the reference noise source that was passed through one LNA and then both LNAs with the attenuator in between. This reference noise signal represents a very weak signal return. Fig. 7(b) shows the power spectrum of the reference signal after passing through one LNA. Fig 7(c) shows the power spectrum of the reference signal after passing through the first LNA, a 3 dB attenuator, and the second LNA. The reference signal was at about -63 dBm at 600 MHz. After it passed through the first LNA it was at about -42 dBm at 600 MHz, a gain of 21 dBm which was about what was expected. After it passed through the first LNA, the 3 dB attenuator, and the second LNA the signal was at about -27 dBm. The gain was about 18 dBm and this is as expected since a 3 dB attenuator sat between the two LNAs.

### 4.8   Bandpass Filter (BPF)

The BPF is actually composed of a high pass and a low pass filter. Together the two filters achieve an approximate frequency range of 400 MHz to 800 MHz. Both the high pass and low pass filters are inexpensive commercially available parts manufac-
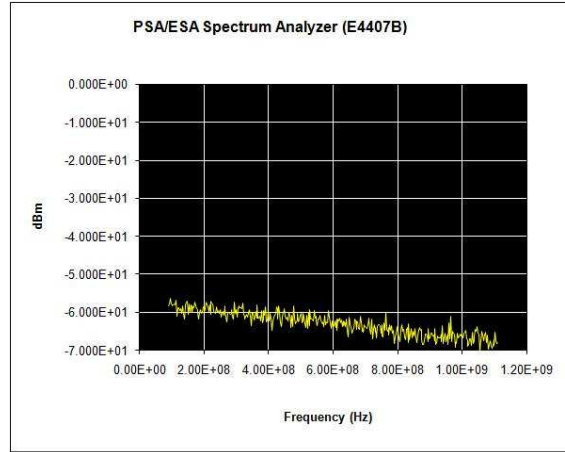
(a) Power Spectrum of the Reference Noise Signal
Representing a Weak Signal Return from a Target
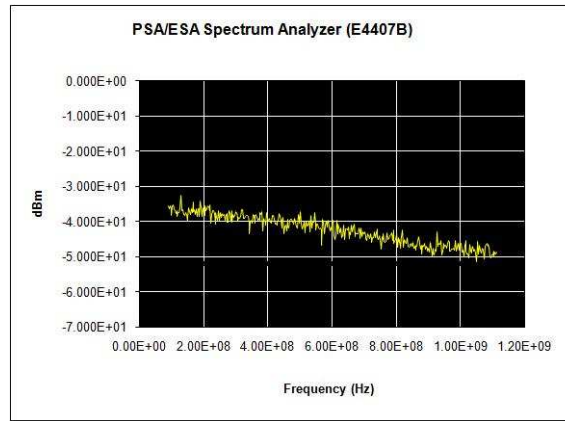


(b) Power Spectrum of the Reference Signal After
Passing Through One LNA
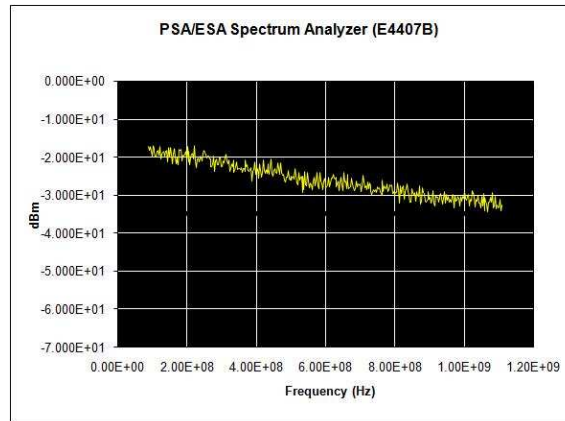


(c) Power Spectrum of the Reference Signal After
Passing Through Both LNAs and a 3 dB Attenua-
tor

Figure 4.7:    Power Spectrum of a Representative Returned Signal After Passing
Through One LNA and Both LNAs

55
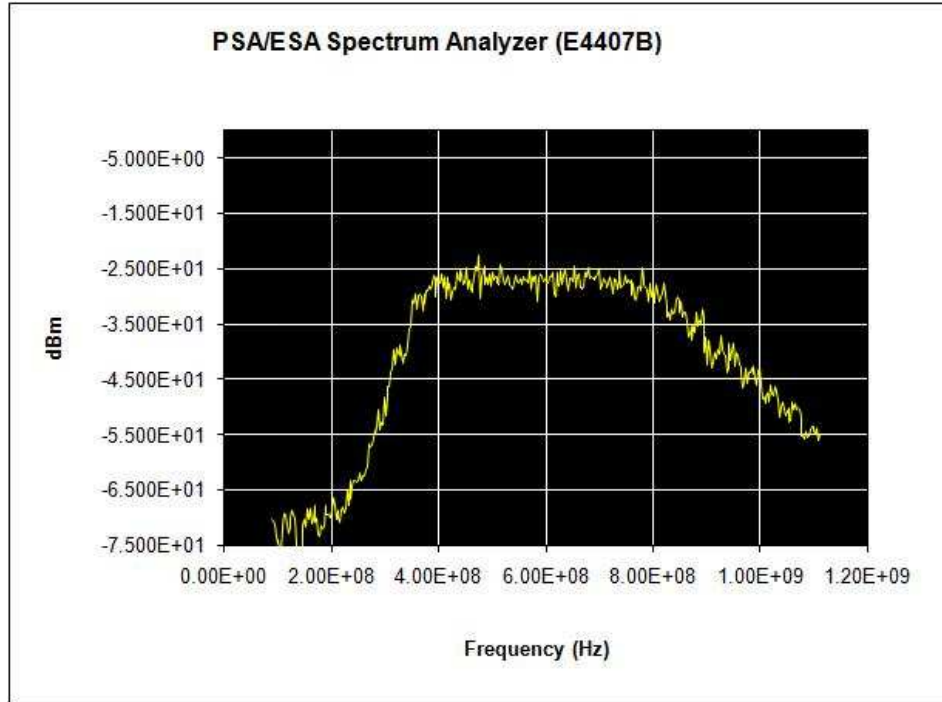
Figure 4.8:     Passband of BPF

tured by Mini-circuit. The low pass filter has a passband (loss < 1.3 dB) frequency range of DC to 800 MHz. 3 dB attenuation occurs at approximately 990 MHz. The high pass filter has a passband (loss < 1.3 dB) frequency range from 395 MHz to 3200 MHz. 3 dB occurs on the low frequency end at 360 MHz. Fig. 4.8 shows the results of the noise source signal when passed through the BPF. This shows that the passband is approximately 400 MHz to 800 MHz as expected.

Two BPF are utilized in the radar system. One is placed directly after the power splitter and the other is positioned after the low noise amplifier. The purpose of the BPF is to reject the frequencies that lie outside the desired frequency range. It assures the outgoing signal has the frequency best suited for wall penetration. For the incoming signal, it filters out the lower and higher frequency noise from the environment. Then, all that is left is the frequencies of interest, those that were originally transmitted out into the environment.

The bandpass filter makes the bandwidth approximately 400 MHz. 400 MHz bandwidth means that the range resolution is 0.375 m calculated from the equation $\Delta R = c/2\beta$ where $\Delta R$ is the range resolution and $\beta$ is the signal bandwidth [3]. This means that the target's location will be accurate to within 0.375 m.

## 4.9  PCI Digitizer Board

The SDR concept calls for a high speed ADC and a memory storage mechanism to store the transmit and receive digital signals. The PCI Digitizer Board from Acquisition Logic accomplishes this task. It samples and converts the analog signal of the transmit signal and the receive signal into a digital format and puts the information into data files. Acquisition Logic's AL83xGT PCI Digitizer Board has dual-channel analog-to-digital converter (ADC) that samples the analog signal with 8 bits of resolution at a rate of 1.5 GHz for each channel. Fig. 4.9 shows a picture of the board. The sampled data streams lead into a Field Programable Gate Array (FPGA) and are stored in onboard memory. The data is then transferred over to a computer or laptop over a 64-bit/66 MHz PCI bus. The data is stored in a file with each data point as raw signed binary data. Fig. 4.11 show the results of a 750 MHz signal sent through Channel 1 of the PCI Digitizer Board. Fig. 4.10 shows the results of a noise signal sent through Channel 2 of the PCI Digitizer Board. The 750 MHz sine wave from Channel 1 has a triangular wave pattern as predicted by Nyquist's theory since its frequency is half that of the 1.5 GHz sampling rate [36]. It also has a frequency peak at 750 MHz. The noise signal from Channel 2 has sampling that appears correct in the time and frequency domain.

The sampling frequency of the digitizer adds a limitation to the range accuracy. The time between samples is a finite time and divisions between are not possible by the very nature of the digital sampling. With a sampling frequency of 1.5 GHz the time between samples is 1/1.5 GHz or $0.66667 \text{x} 10^{-9}$ seconds. In this amount of time, the target range that is possible can be calculated with the equation $R = \frac{ct}{2}$ where R is range, c is the speed of light, and t is the round trip time [36]. The resulting

Figure 4.9:　　Acquisition Logic's AL83xGT PCI Digitizer Board

value is 0.1 m. This 0.1 m is less than that of the range resolution determined by the bandwidth. In this case, it is not the limiting factor.

## 4.10　Desktop Computer Network and AWG

This section discuses the desktop computer network and its components. The computer network consists of three commercially available desktop computers and a D-Link 10-T Ethernet Hub. The Windows Remote Desktop program is used to link all three computers so that each could be viewed on one computer. Radar System 1 has a monitor, mouse, and keyboard connected to it to control all three computers. If the test calls for a moving target an AWG is necessary. The AWG is an Agilent 33250A. If needed, the AWG is connected by a cable that extends from its output and then its signal is split along three same-length cables to each digitizer's external trigger port. The AWG synchronizes the timing of the data capture for each radar system. The synchronization necessity is discussed more in Section 4.11.

## 4.11　Signal Processing Software Algorithm Description

This section describes the signal processing software algorithm and how it works. The purpose of the software algorithm is to take the raw noise signal data files captured
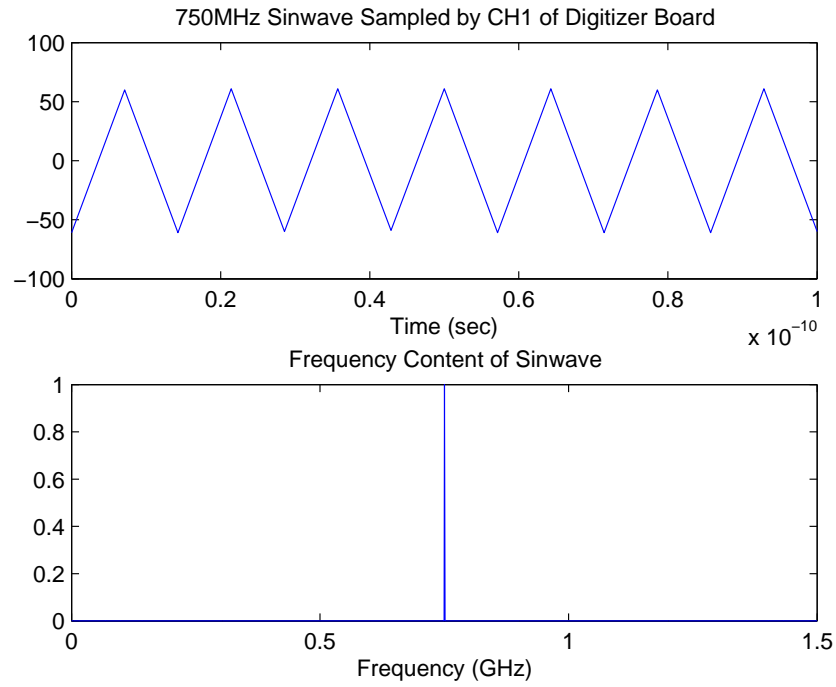
Figure 4.10:    750 MHz Sine Wave Sampled by CH1 of Digitizer Board and its Frequency Content
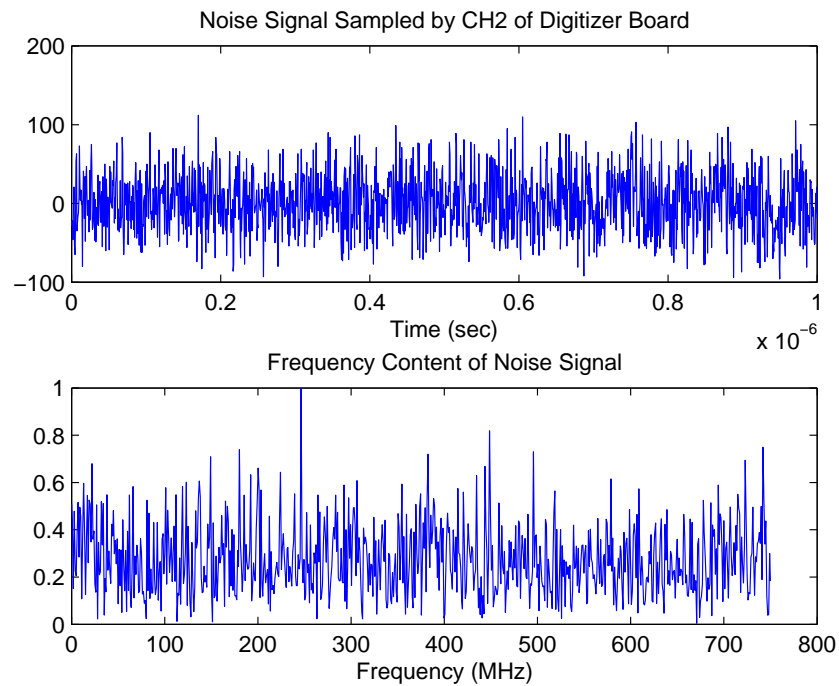


Figure 4.11:    Noise Signal Sampled by CH2 of Digitizer Board and its Frequency Content

by the digitizer and process them into two-dimensional image matrices that then can be interpreted by a human or computer. It accomplishes this in the Matlab® programming environment with three main steps (See Appendix A for an example of the code). The first step pulls in raw data files, organizes them into a usable format, and filters them. The second step correlates the replica transmit noise signal to the received noise signal and creates the one-dimensional time vectors from each system. The third step combines the individual results of each system into a consolidated data matrix and plots a two-dimensional image. These three steps give an overarching view of how the software algorithm works.

Before each step is covered in detail, several terms and concepts need to be discussed to aid in understanding the details of the algorithm. First, capture of the raw data, and recording it to files is accomplished with the digitizer's recorder application. The recorder application names the data file, sets the trigger source, sets the number of samples per acquisition, and sets the number of acquisitions. A standardized naming convention is used to help automate pulling the data files into Matlab® . The convention is as follows; system number, test number, and channel number. For example, system 2, test 1, received signal would be written $Sys2\_1\_CH2$.

The trigger source can be software defined or externally defined. A software defined trigger source is used for stationary target since there is no need for synchronizing the timing of data capture for radar systems 1, 2, or 3. (Note: Each system has a digitizer recorder program that needs to be separately set.) This is not true with a moving target and each radar system needs to capture data at the same time to accurately find the location of the target at a given point in time. An external trigger source, a pulse generator, is used for motion capture. The AWG assures that each radar system's digitizer is capturing data at the same moment.

The number of samples per acquisition is the number of data points in a single transmit and receive signal that will be correlated against one another. The number of acquisitions is the number of times the digitizer will trigger and capture the specified

number of samples. Twenty acquisitions of 5000 samples would be one data file with 20 sets of 5000 samples. The data file is written in raw signed binary and put into one column. So, 20 acquisitions of 5000 samples would be written as one single column containing 100,000 rows of data. The digitizer recorder application also allows for adjusting the sample rate and the number of channels sampled. These settings remain at the 2 channel sampling, to get both the transmitted and received data, and at a sample rate of 3.0 GHz for the card or 1.5 GHz for each channel. The digitizer samples each channel simultaneously. A good understanding of the digitizer's recorder application and how the data file are written is important to understand the software algorithm.

The first step pulls the data files into the Matlab® workspace. It then reshapes the data from one column to a matrix with the number of acquisitions by the number of samples. Then a filter is applied to each acquisition. The algorithm makes use of Matlab® functions to read in the binary data, reshape it, and apply a digital filter. The digital filter is to make up for a short coming in the hardware. The hardware filter cuts off at 800 MHz. The digitizer has a sample rate of 1.5 GHz. At the Nyquist rate the best it can sample without aliasing is at 750 MHz. The digital filter filters out frequencies higher than 750 MHz to minimize errors.

The second step correlates the transmitted and received signal to get a one-dimensional time vector for each radar system. Other processes, like averaging and background subtraction, are performed on the one-dimensional time vector to increase the likelihood of target detection. The correlation process uses the Matlab® function xcorr and a loop. The loop allows for a portion of the transmitted signal to be compared along a portion of the received signal at incrementally increasing time period. For example, the first loop compares the transmit signal, tx(t), to the receive signal, rx(t). The next increment of the loop compares the same transmit signal, tx(t), to a time shifted receive signal, rx(t+1). One increment shift is equal to the time step between samples which is the inverse of the sampling frequency. In this case the time step is equal to $1/(1.5 \times 10^9)$ or 0.66 ns. Each comparison of the transmitted

and received signal results in a correlation vector and the midpoint of each vector (the autocorrelation value) is saved. Each increment of the loop compares the next point in time of the received signal to the transmit signal and a vector is created from the saved autocorrelation values. A peak in the autocorrelation value means that there is a high correlation or match of the transmitted and received signal. A peak at x point in time in the vector made from the autocorrelation values (the correlation vector) means that the received signal has hit a target and took x time round trip to return to the radar. A correlation vector is created for each simultaneously captured transmitted and received signal.

An averaging of several correlation vectors is then applied. All the experiments done during the course of this thesis took 20 correlation vectors added them together and divided by 20. This averaging process increased the likelihood of target detection because it increased the signal-to-noise ratio. This works because the target's correlation peak remains in the same location in the correlation vector. The correlation strength of the noise in the correlation vector has random peaks and valleys. Although its peaks and valleys are lower in correlation strength than the target, the averaging process allows some of noise to cancel each other out and then be averaged. This makes the noise surrounding the target lower and in effect increases the signal-to-noise ratio.

Another task accomplished during step two is background subtraction. After all the tests in a specific test scene were accomplished, a background shot of the area or room was taken. This background shot was the test scene without any targets. During testing is was found that subtracting out the background greatly increased target detection. In some of the test scenes, the back and side areas were very cluttered and, if a wall was present, it offered reflections and multipath problems. The clutter of the background often obscured the target making it difficult to detect. By taking a background shot and subtracting it from the collection the clutter caused by the background is reduced. In the software, the algorithm simply subtracts the background's averaged correlation vector from that target's averaged correlation vector. Overall,

step two correlated the transmitted and received signal to get a one-dimensional time vector for each radar system that was processed to increase the likelihood of target detection.

The third and final step combines the data of each system into a consolidated matrix and graphs the results. Each radar system has a correlation vector that relates to a specific point in time. The correlation vector from each system contains the one-dimensional information of the time from the radar to the target and back. The round trip time is easily converted to range by the equation $R = ct/2$ [36]. $R$ is understood to be the range, $c$ is the speed of light, and $t$ is the round trip time. All that is known is that the target is somewhere in a semi-circle x meters from the radar. With three radar systems it is possible to triangulate the exact location of the target, getting an (x, y) position. First each systems location (x, y) location is entered into the program. Then, a matrix is created taking the one dimensional correlation vector and spreading it out radially from the radar's location. This is accomplished for each system. Then, the three matrices are summed and graphed. The targets are located where the rings of each system overlap. This overlap should be the highest amplitude in the scene. To minimize the errors due to each system's individual gain, each correlation vector is normalized before consolidation. In summary, the third step accomplishes the tasks necessary to graph the results.

This section described the signal processing software algorithm and how it works. The software algorithm takes the raw noise signal data files captured by the digitizer and process them into two-dimensional image matrices. This is accomplished in the `Matlab`® programming environment in three main steps. The first step pulls in raw data files, organizes them into a usable format, and filters them. The second step correlates the replica transmit noise signal to the received noise signal and creates one-dimensional time vectors from each system. The third step combines the individual results of each system into a consolidated data matrix and plots a two-dimensional image.

## 4.12  Summary of the Chapter and the Network of Noise Radar Systems

This chapter described the overall hardware design for the radar system, the individual components, the network of desktop computers, and the software that performed the correlation and plotted the two-dimensional images. Table 4.2 summarizes the network of noise radar systems.

Table 4.2:  Summary of the Network of Noise Radar Systems

| Parameter | Value |
|---|---|
| Number of Systems | 3 |
| Networked Together | Yes |
| Frequency | 400 MHz-800 MHz |
| Polarization | HH |
| Antenna Gain | 6 dB |
| Analog-to-Digital Conversion | 8 Bits |
| Sampling Rate | 1.5 GHz/per channel |
| Range Resolution | 37.5 cm |
| Correlator | Digital |

# V. Research Methodology

This chapter highlights the research methodology and procedures used during the experiments. Section 5.1 states the purpose and objective of the experiments conducted for this thesis. Section 5.2 describes the methods and procedures followed while conducting experiments. Section 5.3 identifies the targets used in testing and analyzes characteristics of each target. Section 5.4 describes each test scenario. Table 5.1 lists all the test scenarios that will be analyzed in the main body of this document. Appendix B lists all the tests conducted during the course of this research. Section 5.5 summarizes the chapter.

## 5.1 Purpose and Objective

The overall purpose of this research is to build a network of noise radar systems that can operate simultaneously without interference, locate multiple human or non-human targets, and track human movement through a room. Another goal is to design this network of sensors in a manner that will allow for integration with the QUEST processing kernel. The main objective is to characterize the noise radar systems and create two-dimensional images of areas that will later be analyzed by the QUEST processing kernel. In future studies, the QUEST kernel will be integrated with the noise radar systems and interact with it, affecting and changing the data collection and processing parameters.

## 5.2 Methods and Procedures

This section looks at the method used for choosing specific test scenarios and the procedures to set up a test scenario. The method for choosing test scenarios was based on the idea of working from the simplest task to the most complex task. Since this hardware was built during the course of this thesis, the first objective was to have each of the three radar systems individually find a stationary target. Second, the three systems must be networked together, find a stationary target, and create a two-dimensional image of the area of interest. Third, the radar systems must locate

several targets and create a two-dimensional image. Fourth, the radar systems must locate targets with clutter, like chairs, in the area of interest, and create a two-dimensional image. Last, the radar systems must follow a moving target through an empty and cluttered room, and create a two-dimensional image.

The generalized procedures for setting up and running a test scenario are as follows:

1. Define test area and decide upon test matrix.

2. Place antenna stands in appropriate positions and mark location in terms of (x,y) coordinates

3. Assure all cable connections are solid.

4. Turn on computers, if necessary, and connect to each computer through Windows Desktop Remote

5. Turn on each noise radar system with red switch on radar box and allow about five minutes time for noise source to stabilize before taking data.

6. Check that each system's received signal (CH2) is within -2 to 2 volts and not below that of the transmitted signal. The digitizer's maximum voltage range is -2 to 2 volts. Use digitizer's oscilloscope program to check the received signal's strength. Add or subtract attenuators at the radar box's receive signal input based on the received signal's input to correct signal strength.

7. Open each system's digitizer record program and enter the appropriate data based on test matrix.

8. Set up a calibration object with a uniform RCS pattern equidistance from each radar system. (The calibration object's correlation strength for each system is used to normalize the different gains of each system. Also, each radar system has slight variations in the antenna cable length and path length between hardware components. With an object at a known distance from each radar system the variations in path length can be compensated for. Both normalization and path

length variations are accounted for in all of the experiments accomplished in this thesis.)

9. Set up the test scene.

10. Collect data using each system's digitizer record program.

11. Repeat test setup and data collection steps until all tests in the test matrix are complete.

12. Take a background shot of the area. (Background shots were taken for each test scenario shown in this thesis. The background shot was used for background subtraction.)

13. Consolidate all the data files from each radar system into one folder.

14. Enter appropriate data into the correlation software program, run the program, and graph the results.

Also of note is that the position of the radar is stated as the center point between the two radars and at the furthest edge of the antennas from the stand.

The methodology and procedures discussed in this chapter are fairly straight forward. The methodology of experiments starts with the most basic and moves up to the most complex. The procedures were designed with simplicity in mind and could be simplified further. For example, an overarching software program could control each digitizer's record program instead of controlling each independently.

## 5.3    Analysis of Targets

The target of most interest is a human target. However, this is not the only target used in test scenarios. Three types of targets were utilized, a 6 ft tall by 6 in diameter metal tube, a 5 ft tall by 8 in diameter metal tube, and two human targets. Fig. 5.1 shows pictures of the various targets.

The three types of targets have interesting characteristics. The tubes are known good reflectors because of their metal construction. The human is assumed to be an

(a) 6 ft Tall by 6 in Diameter Metal Tube (b) 5 ft Tall by 8 in Diameter Metal Tube



(c) Two Human Targets

Figure 5.1:     Pictures of Three Types of Targets Used During Experiments

adequate reflector because Dr. Narayanan from Pennsylvania State was able to detect a human through a wall [25]. The analysis of the targets should help to see how the human target's reflectivity compares to the metal tubes' reflectivity. Another interesting characteristic is each target's shape. The 8 in diameter metal tube is uniformly round. This means that the radar cross section (RCS) will be uniform at various angles. The 6 in diameter tube has two pieces of tubing connected together in an uneven fashion. With this shape the RCS is expected to change as the object is rotated. The human will also have a different RCS as he is rotated due to his non-uniform shape.

The hip-pocket formula for a cylinder can be used to get an idea of what the RCS would be for the two cylinders. The hip-pocket formula for a cylinder with a radius of $r$ and a length of $l$ is [17]:

$$\sigma = \frac{2\pi r}{\lambda} l^2 \tag{5.1}$$

where $\lambda$ is the wavelength. Using this equation, the RCS for the 8 in diameter is 34.72 dBsm, using the center frequency 600 MHz for $\lambda$. The RCS for the 6 in diameter tube is 35.06 dBsm, using the center frequency 600 MHz for $\lambda$. This quick calculation means that the 8 in diameter tube and the 6 in diameter tube have RCS values that are very similar. This calculation is only an estimate since the hip-pocket formula assumes that the wavelength of the signal is small compared to the target. This is not true for a center frequency of 600 MHz. The wavelength is calculated with $\lambda = \frac{c}{f}$ where $c$ is the speed of light and $f$ is the frequency [17]. For a center frequency of 600 MHz the wavelength is 0.5 m. The wavelength is not small in comparison to the target, but the calculation suggests that the RCS of both targets might be similar.

Test measurements accomplished by a PhD student working with Dr. Narayanan at Pennsylvania State University determined that the RCS of a human target facing forward, depending on the size of the human, could range from -1 dBsm to 1 dBsm [18]. Although the calculations for the 8 in and 6 in diameter tube may have error in them,

it is clear that the human will have a much lower RCS value. RCS values are important because RCS will relate directly to the correlation strength. The higher the RCS value, the stronger the return signal, and the stronger the correlation between the transmit and receive signals. So, the metal tubes will most likely have higher correlation strength values than the human.

Also, the RCS at various angles is of concern with the radar system used in this thesis. With each radar system placed at various places around the room, each radar will have a different angle looking at the target. The 8 in diameter tube will look the same no matter what angle the radars are facing it, but the 6 in diameter tube and the human might appear different. These differences may skew overall results or may offer insight into why certain effects occur in the results.

Rotation of each object at eight different angles was accomplished and documented. All measured values were obtained in the AFIT bldg 194 using only one radar system. Each target was placed 3ft or approximately 0.9 m in front of the radar system's antennas. Each system's antenna height was not changed at any time throughout any of the test scenarios presented in this thesis. Each object was set to begin rotation at the 0° position and rotated to 315°, 45° at a time, in a clockwise motion. The clockwise direction is taken from the perspective of looking down on the object. Fig. 5.2 shows the 0° position for each object. In this experiment, only the taller human was rotated.

Fig. 5.3 shows the results of rotating the 8 in diameter tube. The results for the 8 in diameter uniformly shaped tube differed slightly, but each had a similar pattern, as expected. The difference could be attributed to the tube not being perfectly round, effects introduced by the environment, and the limitations of the accuracy the radar system.

Fig. 5.4 shows the results of rotating the 6 in diameter tube. The results for the 6 in diameter tube differed only slightly, but each had a similar pattern. This means
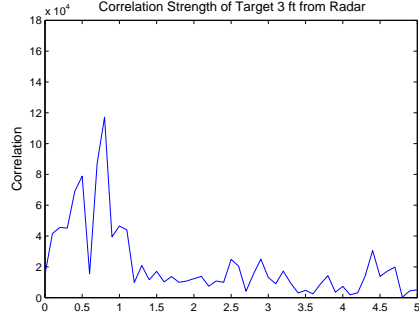
(a) 6 ft Tall by 6 in Diameter Metal Tube at 0° Rotation



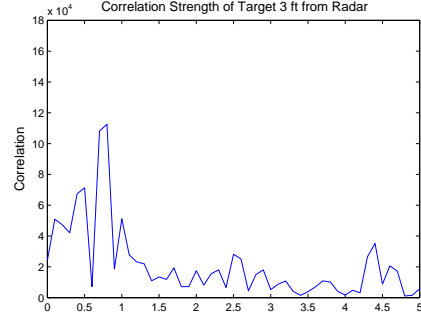(b) 5 ft Tall by 8 in Diameter Metal Tube at 0° Rotation



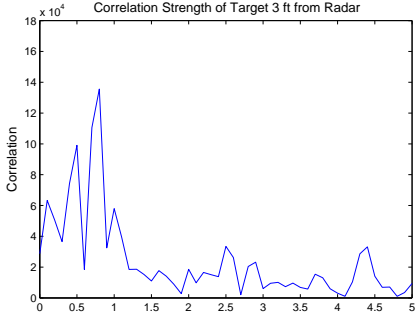(c) Human Target at 0° Rotation

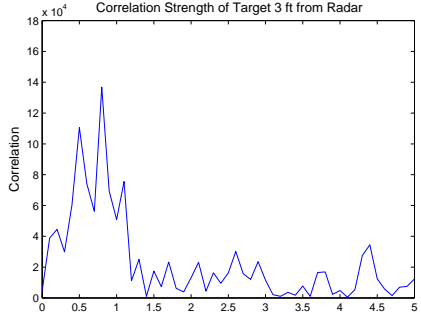Figure 5.2:    6 in and 8 in Diameter Metal Tubes and Human at 0° Rotation

(a) 8in Diameter Metal Tube at 0°

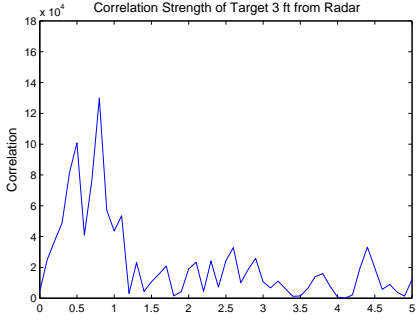(b) 8 in Diameter Metal Tube at 45°

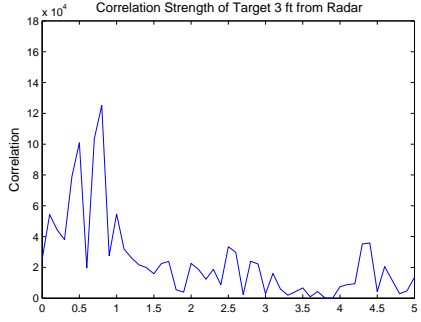(c) 8 in Diameter Metal Tube at 90°
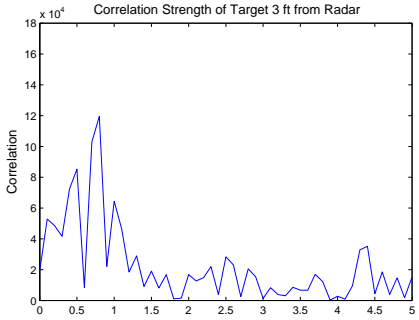
(d) 8 in Diameter Metal Tube at 135°
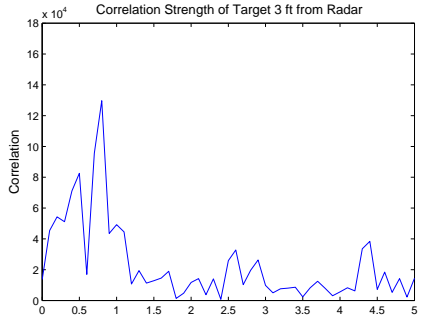
(e) 8 in Diameter Metal Tube at 180°

(f) 8 in Diameter Metal Tube at 225°

(g) 8 in Diameter Metal Tube at 270°

(h) 8 in Diameter Metal Tube at 315°

Figure 5.3:    Plots of Correlation Strength of 8 in Diameter Metal Tube Rotated from 0° to 315°

that no matter what angle each radar looks at this tube its non-uniformity will not create a large impact in results.

Fig. 5.5 shows the results of rotating the human. The results for the human target differ from that of the tube. These results have much more variation. The human target at 0°, 180°, 90°, and 270° (the front, back, and side views) have one peak that is much higher than the others. The views at other angles generally have two tall peaks. This adds some ambiguity to the exact location of the target. The symmetry of the human and the results due to that symmetry are worthy of note. For example, the front and back shots of the human appear very similar. In general, shots that are 180° apart have results with similar correlation patterns. Overall, the results of rotating the human mean that if the radars are at different viewing angles possible error is introduced because different correlation patterns are produced. Especially, in the viewing angles that show two similar strength peaks. These might appear as two targets or make the range of the target less accurate.

The human target results also show that the correlation strength is generally lower than that of the metal tubes. Only in the case of the human target rotation at 180° is the human's correlation strength higher. This correlation strength seems out of place since it is so much higher than any of the other correlation strengths. It might be due to environmental factors or a material in the human's clothing. More human rotational tests would need to be performed to see if this was a constant trend. But for the purposes of this thesis the assumption is that the human's correlation strength will not be as high as that of the metal tubes.

## 5.4   Test Scenarios

This section looks at the various test scenarios. These test scenarios follow the methodology of working from the most basic of target acquisitions to the most complex. In the first scenario, the three radar systems look through a wall at a stationary human target, facing the radar system's antennas. Fig. 5.6 shows a diagram of this test scenario. The wall is approximately 5 in or 13 cm thick and the radar's
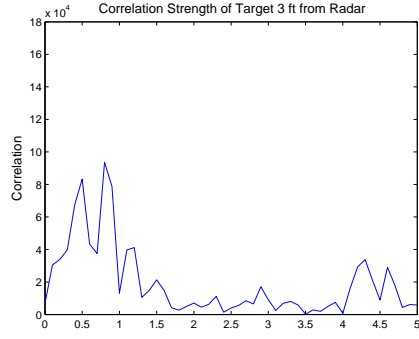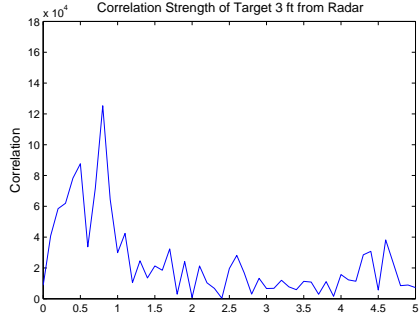
(a) 6 in Diameter Metal Tube at 0°
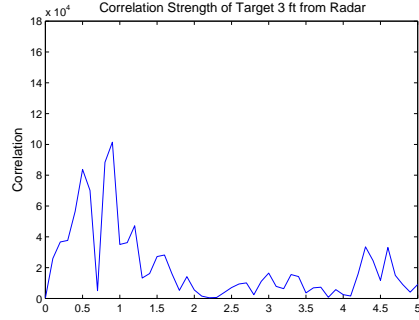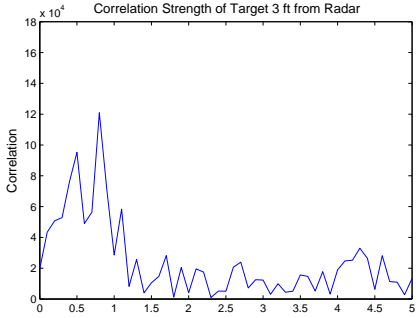
(b) 6 in Diameter Metal Tube at 45°
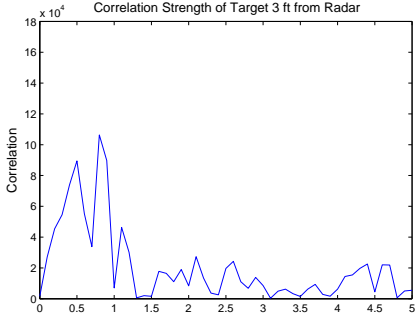
(c) 6 in Diameter Metal Tube at 90°

(d) 6 in Diameter Metal Tube at 135°

(e) 6 in Diameter Metal Tube at 180°
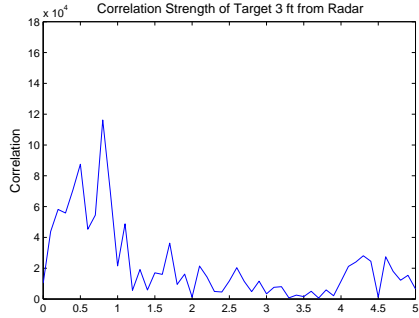
(f) 6 in Diameter Metal Tube at 225°
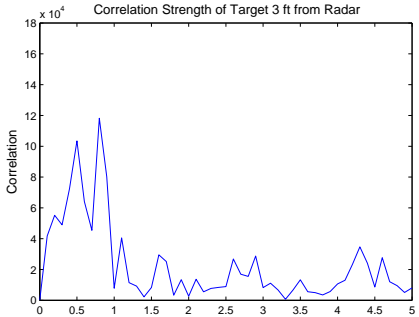
(g) 6 in Diameter Metal Tube at 270°
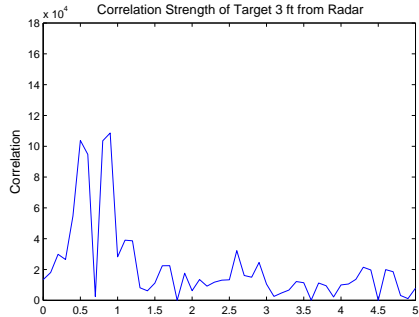
(h) 6 in Diameter Metal Tube at 315°

Figure 5.4: Plots of Correlation Strength of 6 in Diameter Metal Tube Rotated from 0° to 315°
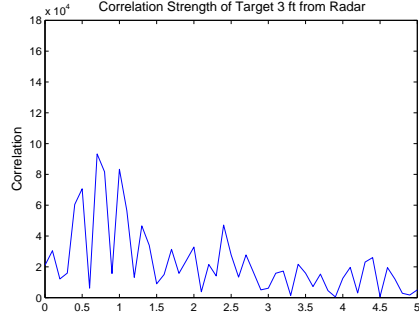
(a) Human at 0°
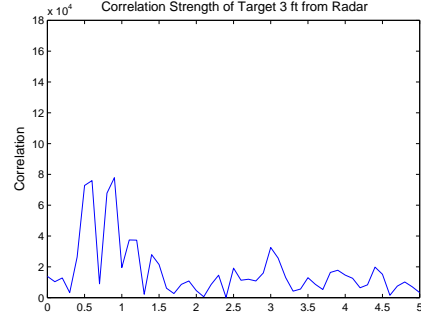
(b) Human at 45°
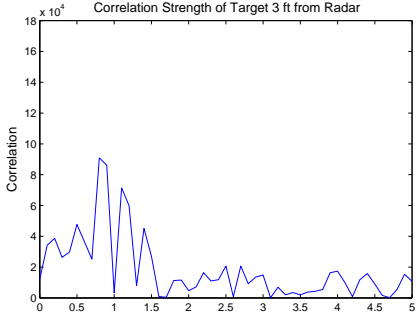
(c) Human at 90°
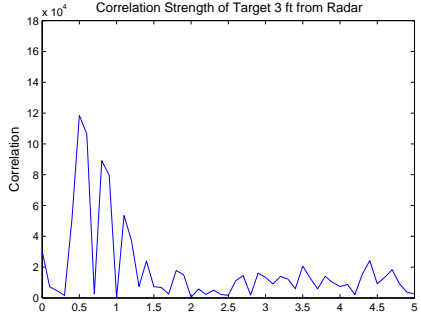
(d) Human at 135°
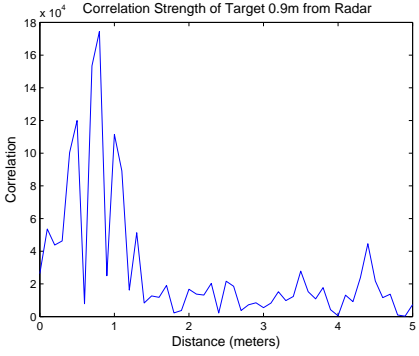
(e) Human at 180°
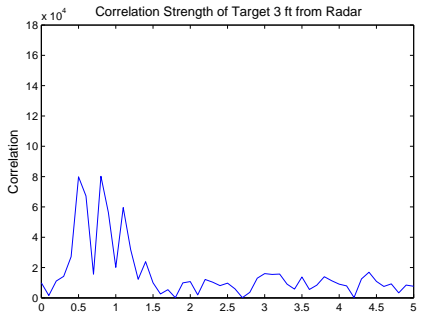
(f) Human at 225°
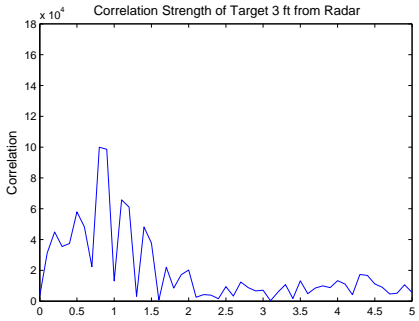
(g) Human at 270°
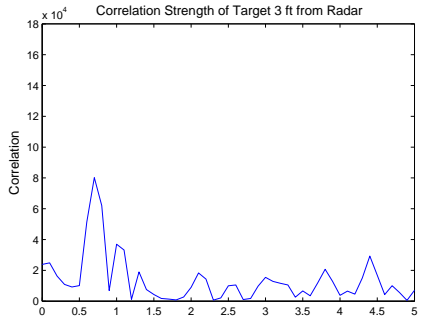
(h) Human at 315°

Figure 5.5:    Plots of Correlation Strength of Human Rotated from 0° to 315°
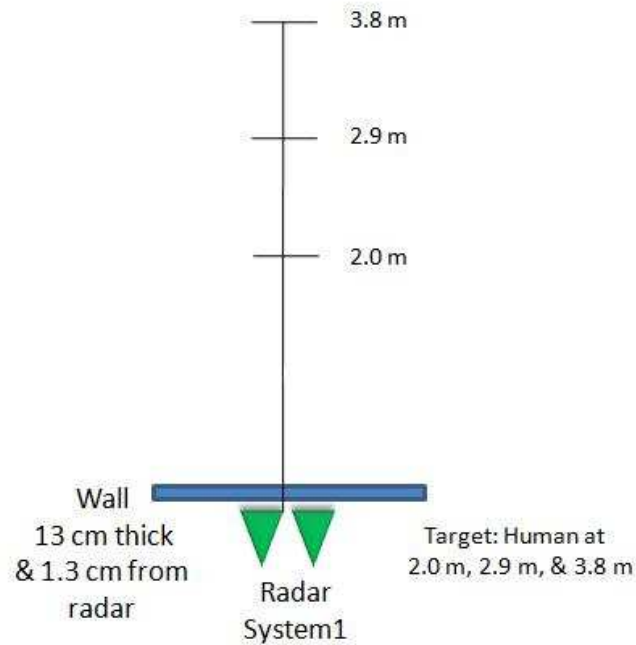
Figure 5.6:    Example Test Scenarios of Individual Radar System with One Stationary Human Target in Three Different Locations

antennas are 0.5 in or 1.3 cm from the wall. On separate tests the human is moved from 2 m to 3.8 m from the radar systems.

In the second scenario, the three systems are networked together to find a stationary target. Fig. 5.7 shows a example diagram of this type of test scenario. The radars are placed in a row, 1.3 cm from a wall 13 cm thick. The end radar is at a diagonal to the corner of the wall. Individually, the three types of targets are placed in the room.

In the third scenario, the three radar systems must locate several targets and create a two-dimensional image. This scenario has several variations, combinations include two metal tube targets, two human targets, and one human and one metal tube. Fig. 5.8 shows a example diagram of this type of test scenario. The radars are placed in a row, 1.3 cm from a wall 13 cm thick. The end radar is at a diagonal to the corner of the wall. Two metal tubes are placed in the room.
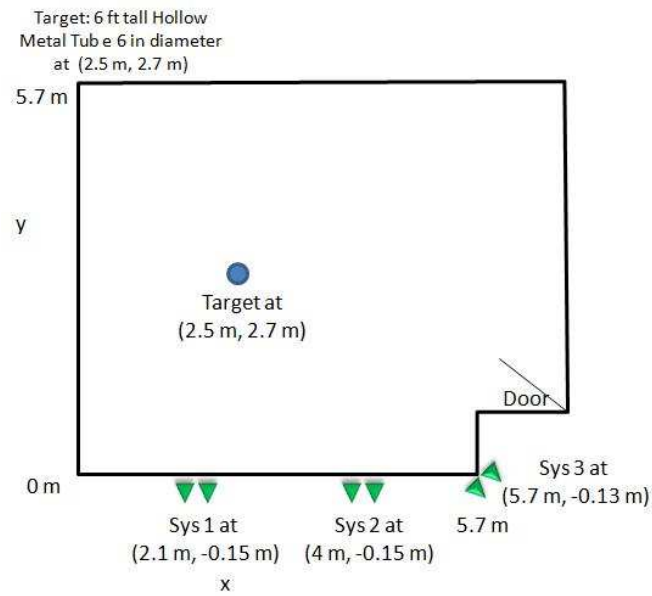
Figure 5.7:    Example Test Scenario of Networked Radar Systems Where Only One Stationary Target Exists at a Time
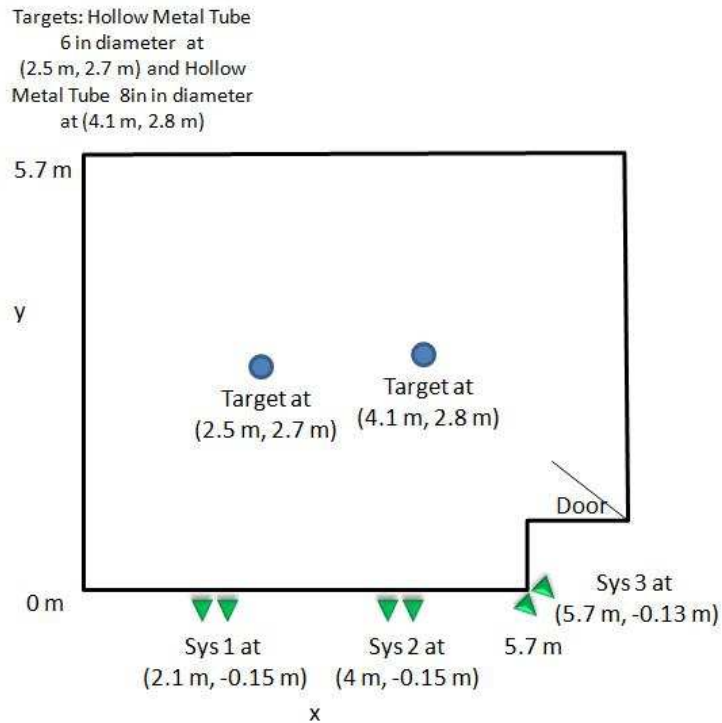


Figure 5.8:    Example Test Scenario of Networked Radar Systems with Two Stationary Target
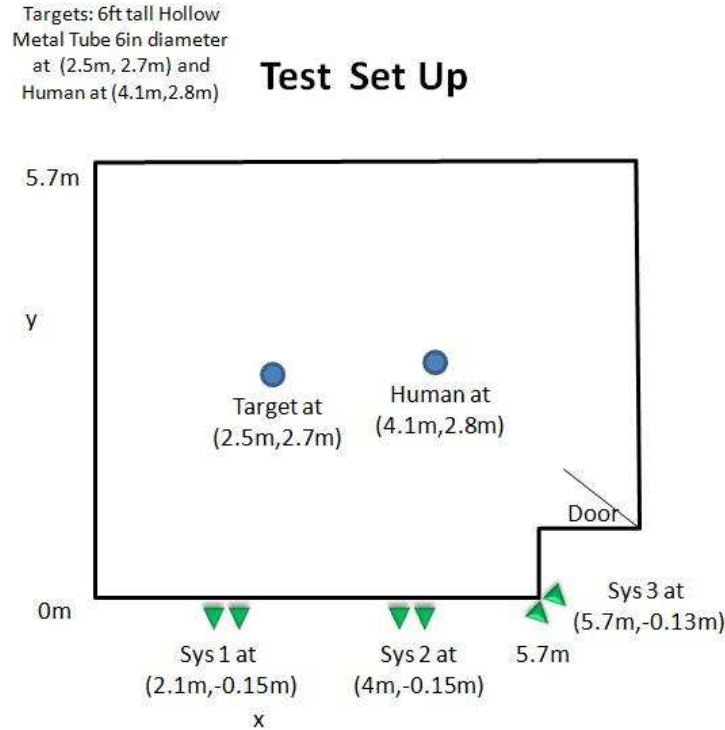
Figure 5.9: Example Test Scenario of Networked Radar Systems with Two Stationary Targets and Clutter in the Area of Interest

Fourth, the radar systems must locate targets with clutter, like chairs or other objects, in the area of interest, and create a two-dimensional image. Fig. 5.9 shows a example diagram of this type of test scenario. In this example, the radars are looking through open air and not through a wall. Experiments were accomplished through walls and through air. No significant difference in the results were found. There was only one difference. Without the wall higher attenuators were needed on the received signal's input to the radar box to keep the voltage between -2 and 2 volts. In this test scenario, the radars are placed in a row looking into a room with an open area that contains two humans and a chair. The chair is located between the two humans.

Last, the radar systems must follow a moving target through an empty and cluttered room, and create a two-dimensional image. Fig. 5.10 shows a example diagrams of this type of test scenarios. The radars are placed in a row, 1.3 cm from a wall 13 cm thick. The end radar is at a diagonal to the corner of the wall. A human

walks through the room diagonally, starting in the bottom right of the room moving to the top left of the room.

The test scenarios given represent the some of the test scenarios used in this thesis. Table 5.1 gives a full account of all tests that are discussed in the results section.

## 5.5 Chapter Summary

This chapter highlighted the research methodology and procedures used during experiments. The overall purpose of this research was to build a network of noise radar systems that could operate simultaneously without interference, locate multiple human or non-human targets, and track human movement through a room. The method for choosing test scenarios was based on the idea of working from the simplest task to the most complex task. This concept meant that the first task was to get each system working individually and the last task was to track a human's movements through a wall. The test scenarios were all developed with this method in mind. The test scenarios used three types of targets, a 6 ft tall by 6 in diameter metal tube, a 5 ft tall by 8 in diameter metal tube, and two human targets. Each target was rotated from 0° to 315° to see how viewing angle changed the correlation strength. The two metal tubes had mostly consistent correlation strengths at each angle, but the human's correlation strength showed much more variation at each angle. This indicated that each of the three radar systems could have varying correlation strengths depending on its viewing angle.
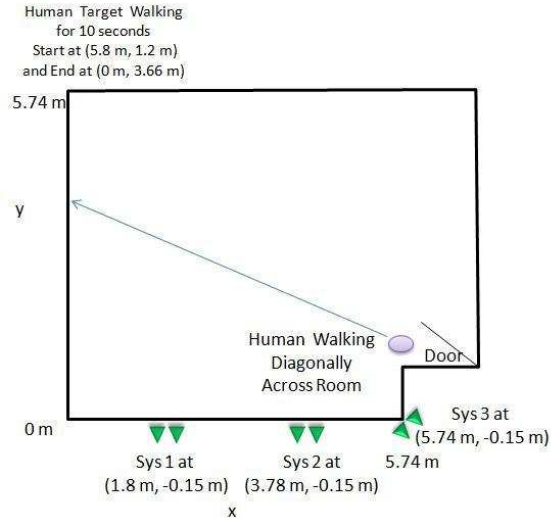
(a) Test Scenario of a Human Moving through an Empty Room
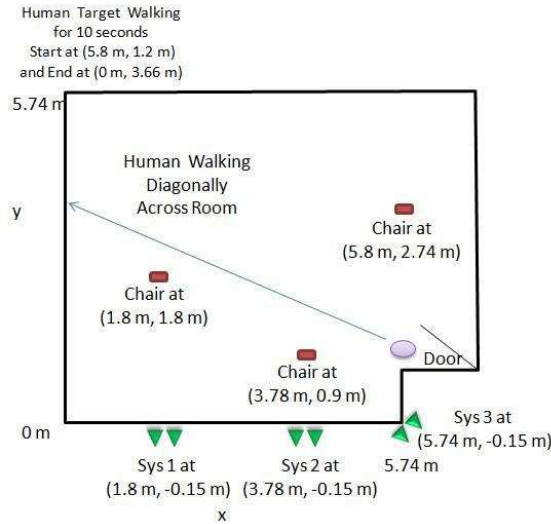


(b) Test Scenario of a Human Moving through a Room with Three Chairs

Figure 5.10: Example Test Scenarios of Networked Radar Systems with a Human Moving through a Room

80

| Test | Thru wall /Thru air | Target(s) Location (in meters) | Antenna Placement (in meters) | 1D /2D Image(s) |
|---|---|---|---|---|
| 1 | Thru wall | 1 Human at (0, 2), (0, 2.9), (0, 3.8) | (0, 0) | 1D |
| 2 | Thru wall | 6 in Tube at (2.5, 2.7) | Sys1 (2.1, -0.15) Sys2 (4, -0.15) Sys3 (5.7, -0.13) | 2D |
| 3 | Thru wall | 8 in Tube at (4.1, 2.8) | Sys1 (2.1, -0.15) Sys2 (4, -0.15) Sys3 (5.7, -0.13) | 2D |
| 4 | Thru wall | Human at (4.1, 2.8) | Sys1 (2.1, -0.15) Sys2 (4, -0.15) Sys3 (5.7, -0.13) | 2D |
| 5 | Thru wall | 6 in Tube at (2.5, 2.7) 8 in Tube at (4.1, 2.8) | Sys1 (2.1, -0.15) Sys2 (4, -0.15) Sys3 (5.7, -0.13) | 2D |
| 6 | Thru wall | 6 in Tube at (2.5, 2.7) Human at (4.1, 2.8) | Sys1 (2.1, -0.15) Sys2 (4, -0.15) Sys3 (5.7, -0.13) | 2D |
| 7 | Thru air | Human 1 (2, 1.3) Human 2 (3.9, 3.1) | Sys1 (1, 0) Sys2 (2.9, 0) Sys3 (4.8, 0) | 2D |
| 8 | Thru air | Human 1 (2, 1.3) Human 2 (3.9, 3.1) Chair (3.3, 1.3) | Sys1 (1, 0) Sys2 (2.9, 0) Sys3 (4.8, 0) | 2D |
| 9 | Thru wall | Human Motion Start (5.8, 1.2) End (0, 3.66) | Sys1 (2.1, -0.15) Sys2 (4, -0.15) Sys3 (5.7, -0.13) | 2D |
| 10 | Thru wall | Human Motion Start (5.8, 1.2) End (0, 3.66) Chairs (1.8, 1.8), (3.78, 0.9), (5.8, 2.74) | Sys1 (2.1, -0.15) Sys2 (4, -0.15) Sys3 (5.7, -0.13) | 2D |

Table 5.1: Test Matrix

# VI.  Results and Analysis

This chapter analyzes the results of tests accomplished with the noise radar system. It also details the effect that data length had on the results. Section 6.1 presents and analyzes the results of a single radar with a single target. In Section 6.2 the results of single target with the networked system are presented and analyzed. Section 6.3 looks at the results of the networked radar systems with multiple targets. In Section 6.4 the results of the networked radar systems with targets and clutter in the area are presented and analyzed. Section 6.5 presents and analyzes the results of a human target moving through a room with and without clutter. Section 6.6 shows the effects data length has on the image results. Section 6.7 summarizes the results. Appendix B lists all the tests conducted during the course of this research and Appendix C displays more test scenarios with results.

## 6.1  Results of Single Radar System and Single Target

This section covers the setup, results, and analysis of a single radar system looking at a single stationary target. A radar system looked through the wall at a stationary human target, facing the radar system's antennas. Fig. 6.1 shows a diagram of this test scenario. The wall is approximately 5 in or 13 cm thick and the radar's antennas are 0.5 in or 1.3 cm from the wall. The wall used during all of the through-the-wall experiments is a plaster board wall with many metal and wood studs between the plaster board sheets. In placing the radar antenna some care was taken to avoid metal studs. If one of the antennas was placed in directly in front of a metal stud then the target was not able to be located. The radar's signals do not travel through metal. Instead they are reflected. If the transmit antenna is in front of a metal stud then the transmit signal never reaches the target making a correlation with the received signal impossible. If the receive antenna is in front of a metal stud the backscatter of the target is reflected back into the room and does not make it to the receive antenna. On separate tests the human is moved from 2 m to 3.8 m from the radar systems. Fig. 6.1 shows a diagram of the radar location relative to three
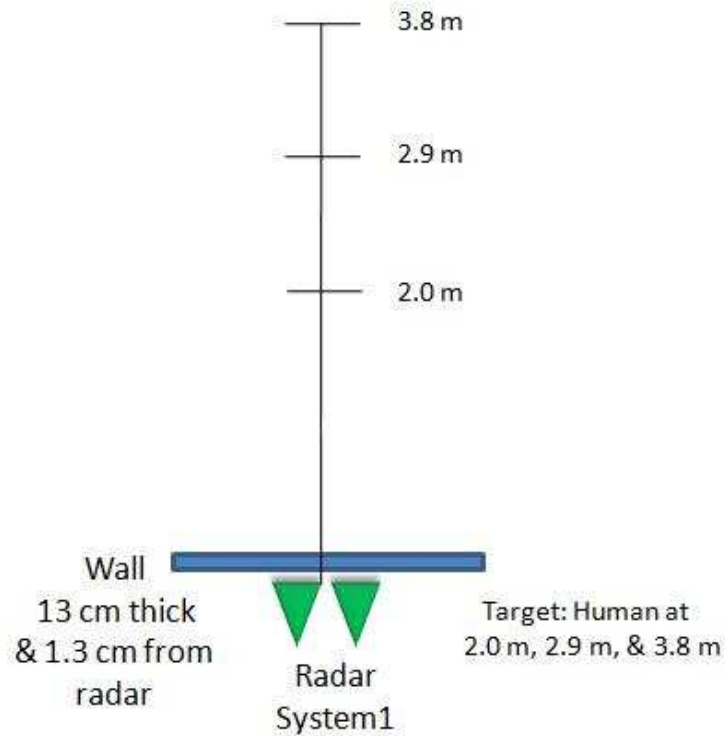
Figure 6.1: Diagram of Individual Radar System with One Stationary Human Target in Three Different Locations

positions of the human target. Fig. 6.2 shows pictures of the equipment setup and the human target at the three test positions.

Fig. 6.3 shows the resulting one-dimensional plots of the target's location in meters. Only radar system 1's results are shown, because the results for each radar system are very similar. The target was located at 2 m, 2.9 m, and 3.8 m and it is expected that peaks denoting a target would be at 2 m, 2.9 m, and 3.8 m. The resulting plots show peaks at approximately these locations correctly locating the human target at each position. Also of note, is the strength of the correlation peak at the three distances. As the target moves further away the correlation peak's strength lessens. This makes sense since distance attenuates signal strength. Attenuation in the received signal lessens the correlation value. A human target at 2.9 m is starting

(a) Radar System Setup



(b) Target: Human at 2 m



(c) Target: Human at 2.9 m



(d) Target: Human at 3.8 m

Figure 6.2:    Pictures of Radar System Setup and Test Scenes with Human Target
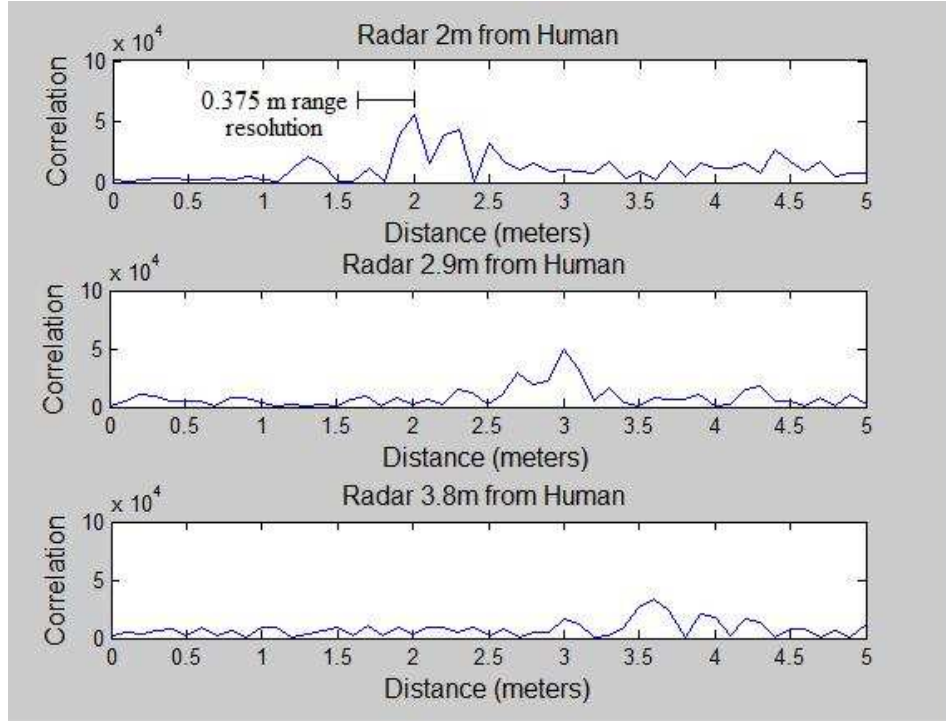
Figure 6.3: Location Results for Radar System 1 Looking Through a Wall at a Human Target that Moves from 2 m, 2.9 m, and 3.8 m

to become much less distinguishable from the noise floor. Human targets at much further distances become less likely to detect.

## 6.2 Results of Networked Radar Systems and Single Target

This section covers the setup, results, and analysis of the networked radar systems and a single target. The three radar systems are networked together to find a stationary target. The radars are placed in a row, 1.3 cm from a plaster board wall 13 cm thick. The end radar is at a diagonal to the corner of the wall. In the first test, the 6 in tube is placed at (2.5 m, 2.7 m). In the second test, the 8 in diameter metal tube is placed at (4.1 m, 2.8 m). In the third test, the human is placed at (4.1 m, 2.8 m). Fig. 6.4 shows diagrams of each test scene. Fig. 6.5 shows pictures of the equipment setup and positions of the targets.

Fig. 6.6 shows the resulting two-dimensional plots locating each target's position. In the first scene, the 6 in diameter tube is at (2.5 m, 2.7 m) and a high intensity
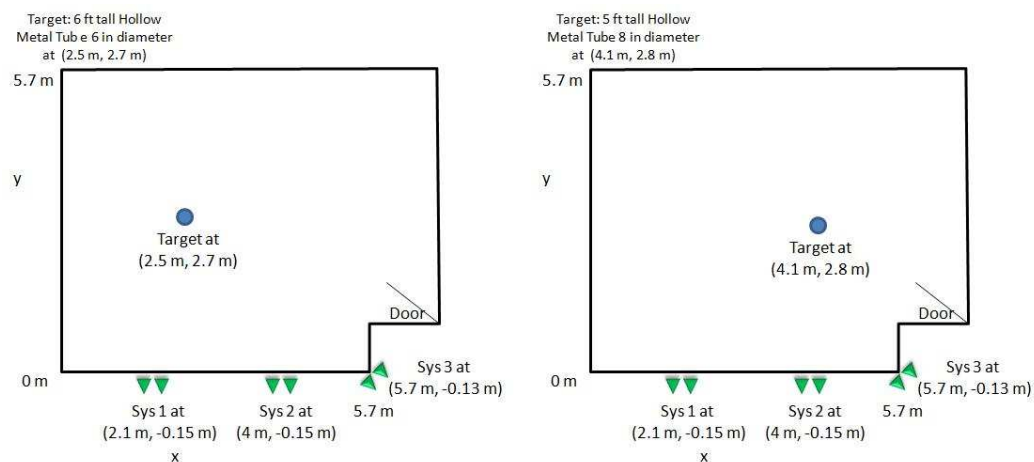
85

(a) Target: 6 in Diameter Metal Tube at (2.5 m, 2.7 m)

(b) Target: 8 in Diameter Metal Tube at (4.1 m, 2.8 m)
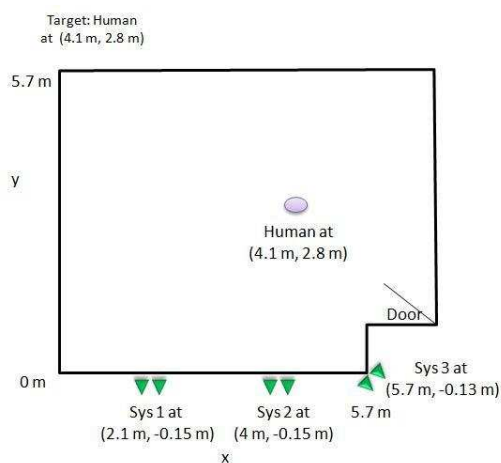


(c) Target: Human at (4.1 m, 2.8 m)

Figure 6.4:    Diagrams of Networked Radar Systems Test Scenes with Single Targets

86

(a) Radar Systems Setup


(b) Target: 6 in Diameter Metal Tube at (2.5 m, 2.7 m)


(c) Target: 8 in Diameter Metal Tube at (4.1 m, 2.8 m)


(d) Target: Human at (4.1 m, 2.8 m)

Figure 6.5:     Pictures of Networked Radar Systems Setup and Test Scenes with Single Targets

correlation depicted as a red to orange spot at this point is expected. The results show a red spot at approximately (2.3 m, 2.8 m) this location is not the exact location of the target, but it is within the 0.375 m range resolution.

The second scene placed the 8 in diameter tube at (4.1 m, 2.8 m) and a red spot is expected at this location. The results show a red spot at approximately (4.2 m, 2.8 m), which is very close to what was expected. There is also another yellow-orange spot at (4 m, 3 m) which is probably also due to the target. The one-dimensional rotation plots of the 6 in tube target show that a peak exists and then usually there are other lower strength peaks on one or both sides of the main peak. These other peaks can create false targets or clutter near the actual target. In some instances the actual location of the target is between these hot spots. More examples of this will be shown in later results. With training and repetition of examples it becomes easier to identify the location of real targets and see false targets and clutter.

The third scene placed the human target at (4.1 m, 2.8 m) and a red spot is expected at this location. The results show a red spot at approximately (3.6 m, 2.9 m) the y value is within error limits but the x value is slightly outside the 0.375 m range resolution. There are several explanations for the error. The first is that all the radars are at least 3 m in distance from the radar. Three meters comes close to the maximum distance that the noise radar can detect a human target. Notice that there also exists a dotted ring coming from radar system 2's location. This radar is the closest radar system getting the strongest return and accurately locating the target from its distance. This ring passes through the target's expected location and a orange-yellow spot is located at approximately (4.1 m, 3 m). The other two radars are not contributing high correlation peak strengths due to their distance from the target. So, a higher degree of error is possible when operating at the system's range limits for a human target.

(a) Target: 6 in Diameter Metal Tube at (2.5 m, 2.7 m)

(b) Target: 8 in Diameter Metal Tube at (4.1 m, 2.8 m)
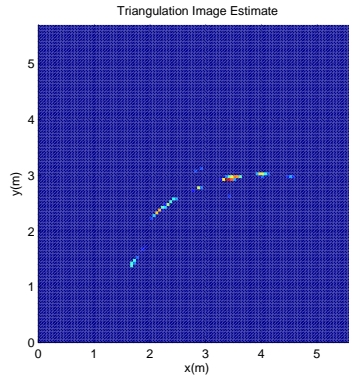


(c) Target: Human at (4.1 m, 2.8 m)

Figure 6.6:    Location Results of Networked Radar Systems Looking Through a Wall at a Single Target

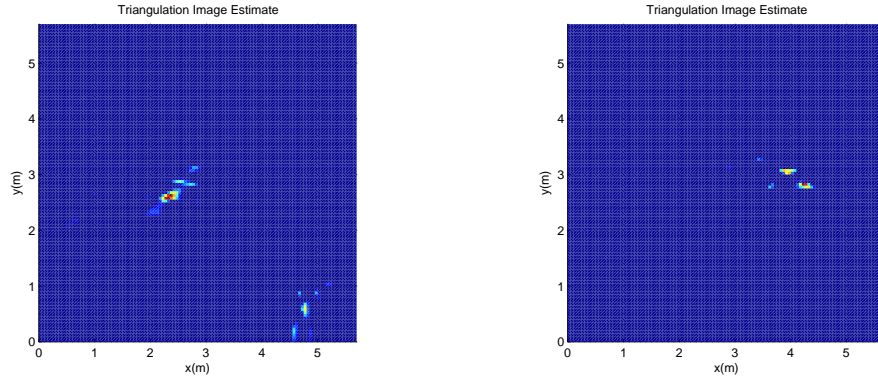## 6.3   Results of Networked Radar Systems and Multiple Targets

This section covers the setup, results, and analysis of the networked radar systems and multiple targets. The three radar systems are networked together to find the stationary targets. The radars are placed in a row, 1.3 cm from a plaster board wall 13 cm thick. The end radar is at a diagonal to the corner of the wall. In the first test, the 6 in tube is placed at (2.5 m, 2.7 m) and the 8 in diameter tube is placed at (4.1 m, 2.8 m). In the second test, the 6 in diameter metal tube is placed at (2.5 m, 2.7 m) and a human target is at (4.1 m, 2.8 m). In the third test, the radars are in different locations and the scene is different. Due to facility construction and personnel availability at the time of experimentation, the room previously used was unavailable. So, for this test the antennas are located in a row and looking into an open area of the room. Although the radars were designed for through-the-wall applications they work the same without walls with very little difference in the results. The only observable difference is that targets' detection ranges increase due to less attenuation from the wall. The first human target is at (2 m, 1.3 m) and the second human is at (3.9 m, 3.1 m). Fig. 6.7 shows diagrams of each test scene. Fig. 6.8 shows pictures of the equipment setup and postings of the targets.

Fig. 6.9 shows the resulting two-dimensional plots locating each target's position. In the first scene, the 6 in diameter tube is at (2.5 m, 2.7 m) and the 8 in diameter tube is at (4.1 m, 2.8 m). It is expected that high intensity spots, red and orange, would be shown at these locations. The results show two clusters of spots. A thick red spot appears at (3.8 m, 2.8 m) with various yellow spots around it and two yellow-orange spots appear to be centered about (2.8 m, 2.9 m). The red spot would be the the 8 in diameter tube and the yellow-orange spots would be the 6 in diameter tube. The slight error in the location is within the range resolution limits.

There a few items interest in these results. These items are the greater intensity of the 8 in diameter tube response and the two similar strength yellow-orange spots indicating the 6 in diameter tube. The 8 in tube showing a higher intensity correlation
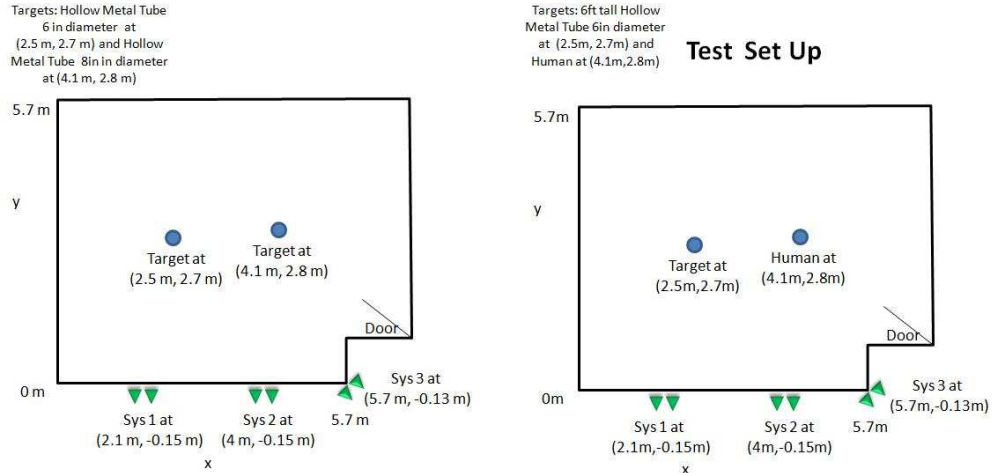
(a) Targets: 6 in Diameter Tube at (2.5 m, 2.7 m) and 8 in Diameter Tube at (4.1 m, 2.8m

(b) Targets: 6 in Diameter Metal Tube at (2.5 m, 2.7 m) and Human at (4.1 m, 2.8 m)
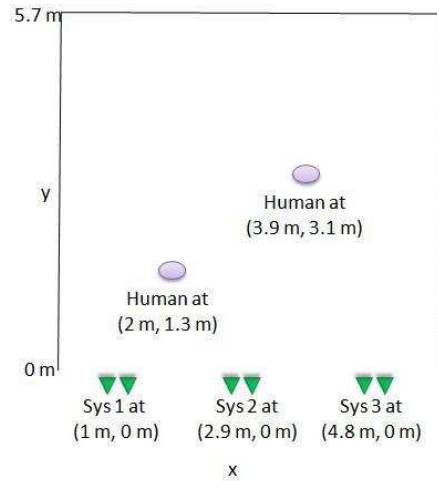


(c) Targets: Human 1 at (2 m, 1.3 m) and Human 2 at (3.9 m, 3.1 m)

Figure 6.7:    Diagrams of Networked Radar Systems Test Scenes with Multiple Targets

(a) Radar Systems Setup 1

(b) Targets: 6 in Diameter Tube at (2.5 m, 2.7 m) and 8 in Diameter Tube at (4.1 m, 2.8 m)
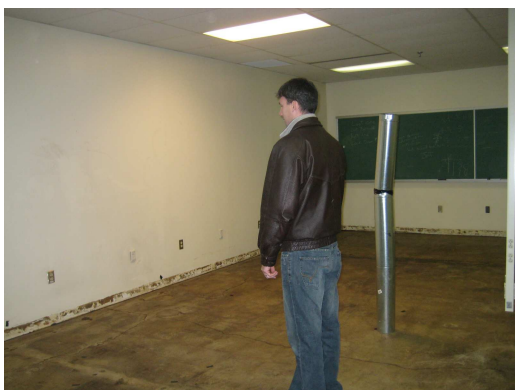
(c) Targets: 6 in Diameter Metal Tube at (2.5 m, 2.7 m) and Human at (4.1 m, 2.8 m)

(d) Radar Systems Setup 2

(e) Targets: Human 1 at (2 m, 1.3 m) and Human 2 at (3.9 m, 3.1 m)

Figure 6.8: Pictures of Networked Radar Systems Setup and Test Scenes with Multiple Targets

is not unexpected. The 8 in diameter tube generally had a higher correlation strength in the rotation testing. (See Section 5.3 for these results) This makes the 8 in tube a more visible target and the results show this.

The two yellow-orange spots of similar intensity could exist for several reasons. The peaks that can exist on either side of the main correlation peak could be strong which can create a false target. In situations where two similar intensity spots exist the center point of these spots, in this case (2.8 m, 2.9 m), most likely marks the target location. Another reason for the dual spots could be due to multipath effects between the targets. When the target is hit by the transmit signal the direction of the reflected electromagnetic waves depends upon the incident angle. Some of the reflected waves may have been reflected towards the other target. If the signal strength of these reflected waves are strong enough they could strike the other target and then be reflected towards the receive antenna of the radar system. The returned signal would be correlated with the transmit signal and create a correlation peak. This peak would occur later in time than the original correlation peak of the target and possibly seen as another target.

In the second scene, the 6 in diameter tube is at (2.5 m, 2.7m) and the human target is at (4.1 m, 2.8 m). It is expected that high intensity spots, red and orange, would be shown at these locations. The results show a red spot (the tube) at (2.5 m, 2.7 m) and some yellow areas around (4.1 m, 2.8 m), possibly the human. The 6 in diameter tube's location is clearly identified, while the human's location is less certain. In the target characterization the 6 in diameter tube generally had a much higher correlation strength than the human target. Also, the human target is at the edges of where he can be detected. Since the image color scheme works on a relative intensity scale, the much higher tube correlation strength mostly likely overshadows the human correlation intensity. A different imaging method might bring out the human target's location.

In the third scene, human 1 is at (2 m, 1.3 m) and human 2 is at (3.9 m, 3.1 m). High intensity, red or orange, spots are expected at these points. The results show two clusters of red, orange, and yellow spots. The first is centered around (2 m, 1.5 m), the location of human 1, and the second is centered at approximately (3.7 m, 3 m), the location of human 2. These results correspond well to the actual locations of the targets. These results clearly show the clusters of similar strength spots very near each other. These clusters appear more frequently for human targets than for the tubes. This is most likely due to the way the human target scatters the signal. When characterizing the human target at various angles the results show that a human target can have one main peak, but at some angles he has two peaks of similar strength. This offers a degree of error in identifying the exact location of the target and possibly contribute to the cluster effect. To adjust for this affect, the assumption is that the target's location is in the center of the cluster. This assumption seems to work consistently. As a note, in this scene the human target is located at over 3 m and that is expected because without the wall attenuating the signal a human target can be detected at a further range. Further detection range of targets is the only observable difference in through-the-wall and through-air usage.

## 6.4 Results of Networked Radar Systems and Multiple Targets with Clutter In Area

This section covers the setup, results, and analysis of the networked radar systems and multiple targets with clutter in in the area. For this test the antennas are located in a row and looking into an open area of the room. The first human target is at (2 m, 1.3 m), the second human is at (3.9 m, 3.1 m), a chair (clutter) is located at (3.3 m, 1.3 m). Fig. 6.10 shows diagrams of each test scene. Fig. 6.11 shows pictures of the equipment setup, positions of the targets, and clutter location.

Fig. 6.12 shows the resulting two-dimensional plot locating each target position in the scene. In the third scene, human 1 is at (2 m, 1.3 m), human 2 is at (3.9 m, 3.1 m), and a chair is at (3.3 m, 1.3 m). High intensity, red or orange, spots are
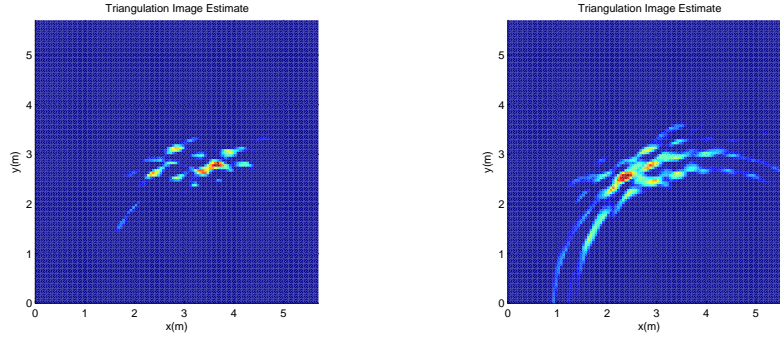
(a) Targets: 6 in Diameter Tube at (2.5 m, 2.7 m) and 8 in Diameter Tube at (4.1m, 2.8m)

(b) Targets: 6 in Diameter Metal Tube at (2.5 m, 2.7 m) and Human at (4.1 m, 2.8 m)
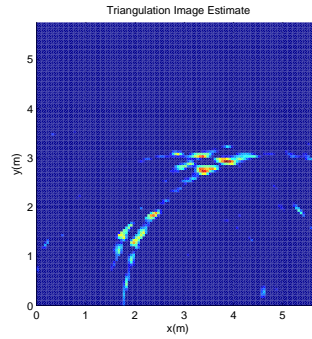


(c) Targets: Human 1 at (2 m, 1.3 m) and Human 2 at (3.9 m, 3.1 m)

Figure 6.9: Location Results of Networked Radar Systems with Multiple Targets

Figure 6.10:     Diagram of Radar Systems Setup and Test Scene with Multiple Targets and Clutter Targets: Human 1 at (2 m, 1.3 m) and Human 2 at (3.9 m, 3.1 m) Clutter: Chair at (3.3 m, 1.3 m)



(a) Radar Systems Setup

(b) Targets: Human 1 at (2 m, 1.3 m) and Human 2 at (3.9 m, 3.1 m) Clutter: Chair at (3.3 m, 1.3 m)

Figure 6.11:     Pictures of Radar Systems Setup and Test Scenes with Multiple Targets and Clutter

96

expected at these points. The results show three clusters of red, orange, and yellow hot spots. The first is at approximately (2 m, 1.1 m) corresponding the the location of human 1. The second is at approximately (3.6 m, 2.9 m), the location of human 2. The third spot is a spot at approximately (4.2 m, 1.4 m). This location has the approximately y value of the chair but not the correct x value. The location error of the humans is within the range resolution, but the chair's location is not within limits.

In fact, this third spot may or may not be the chair. A dotted ring from radar system 3's location is visible in this area. It appears that radar system 3 detected the range of the chair, but that none of the other radar were large amplitude contributors to its location. The spot at (4.2 m, 1.4 m) is a false target most likely created by radar system 1's detection of human 2. A faint dotted ring can be seen crossing the human 2 target and the false target. This combination creates a false target. This type of false target problem can likely be solved by adding more radar systems.

In all the previously shown results, the overall background scene of the empty area is subtracted out. In the case above, clutter in the form of a chair, is included in the target scene. It does not appear to interfere with identifying the location of the targets, but it introduces a false target. During experimentation a background shot of the chair within the area was taken. It is assumed that if this background is subtracted out the false target will disappear. To prove this assumption the chair background was subtracted out and Fig. 6.13 shows the two-dimensional plot results. Without the chair background, it is expected that there will be high intensity spots where human 1 is at, (2 m, 1.3 m) and where human 2 is at, (3.9 m, 3.1 m). The results show two spots located at approximately (1.9 m, 1.1 m) and (3.5 m, 3 m), the approximate location of the humans. The results also show, as expected, that the false target and the chair are no longer visible.

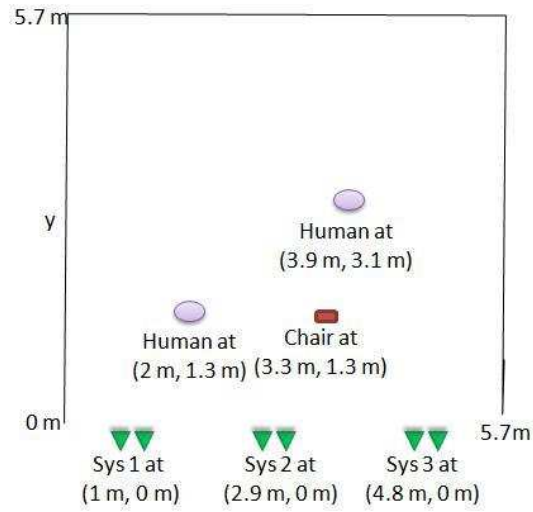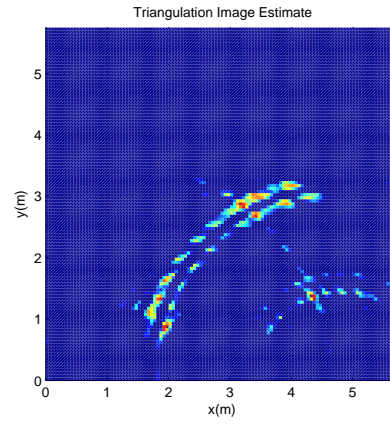Figure 6.12:    Location Results of Radar Systems Setup and Test Scene with Multiple Targets and Clutter Targets: Human 1 at (2 m, 1.3 m) and Human 2 at (3.9 m, 3.1 m) Clutter: Chair at (3.3 m, 1.3 m)
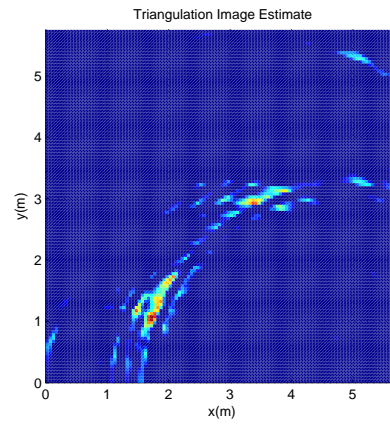


Figure 6.13:    Location Results of Radar Systems Setup and Test Scene with Multiple Targets and with the Background Clutter Subtracted Out Targets: Human 1 at (2 m, 1.3 m) and Human 2 at (3.9 m, 3.1 m)

## 6.5    Results of Networked Radar Systems and Moving Target

This section covers the setup, results, and analysis of the networked radar systems and moving targets. For these tests, the radars are placed in a row 1.3 cm from a plaster board wall 13 cm thick. The end radar is at a diagonal to the corner of the wall. A human walked through the room diagonally and took 10 seconds to cross the room. He started in the bottom right of the room at (5.8 m, 1.2 m) and moved to the top left of the room at (0 m, 3.66 m). The walk is timed, and an attempt is made to keep a constant speed, but small variations in speed is possible during each test and between tests. Also, the exact path between tests is only approximately the same. In the first test, the human walks diagonally through an empty room. In the second test, clutter in the form of three chairs are located at (1.8 m, 1.8 m), (3.78 m, 0.9 m), and (5.8 m, 2.74 m) and the human walks approximately the same diagonal path as in the empty room. Fig. 6.14 shows diagrams of these test scenes. Fig. 6.15 shows pictures of the equipment setup for both tests and movement path of the human.

A arbitrary waveform generator (AWG) is connected to each of the external trigger ports of each digitizer. It synchronizes the radar systems and assures that each digitizer is capturing data from the scene at the same time. The AWG sends out 1000 square pulses of 10 ns duration at a rate of 100 Hz. This means that 10 seconds of data is captured. Each of the digitizer's data recorder programs are set to acquire 1000 acquisitions each being triggered by the 1000 pulses sent out. If for some reason not all of the pulses were sent or not received by the digitizer an error would occur when the digitizer wrote to file. This function acted as a check to assure a clean data capture.

Fig. 6.16 shows the resulting two-dimensional plots locating of the human walking through the empty room at 0, 1, 2, 3, 4, 5, and 6 seconds. The duration of the test was 10 seconds, but after 6 seconds the target moved out of range. The results also produced 50 plots, but only 1 second increments are shown to summarize the human's progress across the room. High intensity spots are expected to move in a diagonal

(a) Test Scenario of a Human Moving through an Empty Room

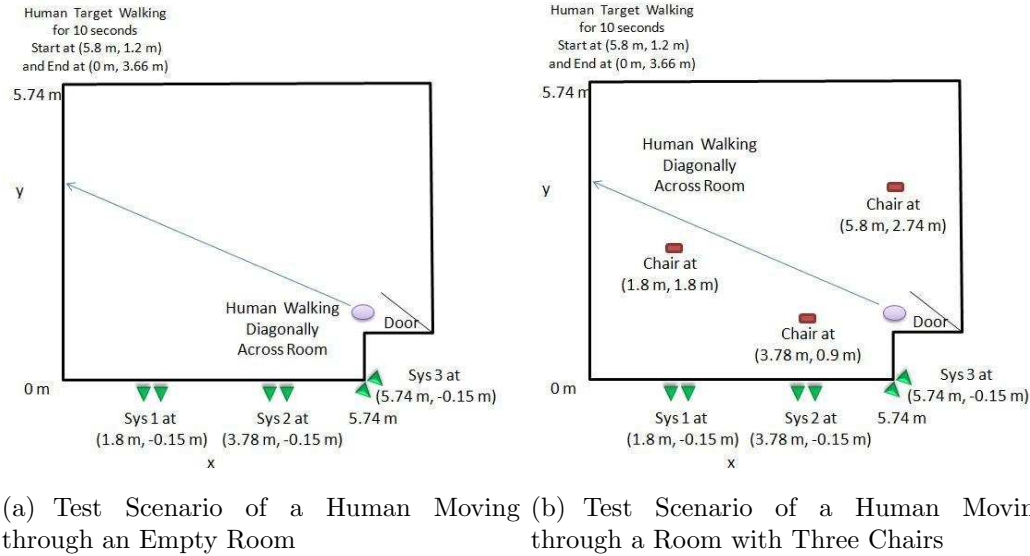(b) Test Scenario of a Human Moving through a Room with Three Chairs

Figure 6.14: Diagrams of Networked Radar Systems with a Human Moving through a Room

line starting from (5.8 m, 1.2 m) and heading to (0 m, 3.66 m) as time passes. The results only detect a target up until 6 seconds. After that time, no detection is made. This is expected since the human is out of the possible detection range. The results from 0 to 6 seconds do show results that indicate the human's location. At 0 seconds a red spot exists at approximately (5.8 m, 1.1 m). After that high intensity spots or clusters can be seen moving diagonally towards (0 m, 3.66 m). At 6 seconds the final spot is at (1.5 m, 2.9 m). This is the approximate location expected for the target at that time period.

The results do have several false targets obscuring the actual target. There are possible reasons including the dual correlation peaks that can indicate the detection of a human. Another possibility that enters here is the effect of movement. Until now none of the targets were moving and timing of when the samples were taken becomes an issue. The AWG synchronizes the digitizers' data capture, but there are possible sources of error. Also, the cable length from the AWG to each digitizer is supposed to be the same, but some amount of error is possible. Any difference in cable length would lead to a small amount of timing error. Small errors in timing could easily lead

100

(a) Radar Systems Setup
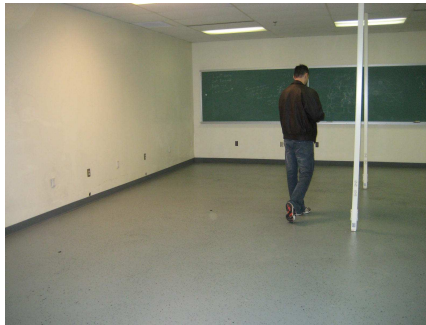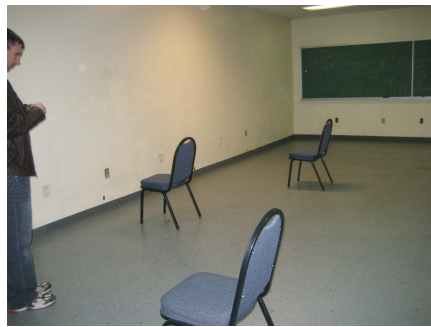


(b) Human Walking Through Empty Room (Start)



(c) Human Walking Through Empty Room (Middle)



(d) Human Walking Through Empty Room (End)



(e) Human Walking Through Room with Chairs (Start)



(f) Human Walking Through Room with Chairs (Middle)



(g) Human Walking Through Room with Chairs (End)

Figure 6.15:    Pictures of Networked Radar Systems Setup and Test Scenes with Human Moving

to false targets or a variation in location. Another possibility for error is that over time, small environmental factors may have changed. The same background scene was subtracted from all of the test scenes. Over time and the course of the test the background could have slightly changed inducing error.

Another possibility is due to the fact that a moving target changes the frequency of the signal. This effect is known as the Doppler effect. The Doppler frequency of the signal, $f_d$, can be calculated by [37]:

$$f_d = \frac{-2\dot{R}f}{c} \tag{6.1}$$

where $\dot{R}$ is the range rate, $f$ is the frequency, and $c$ is the speed of light. The range rate depends on the velocities of the radar and the target. For a target moving away from the radar, the range rate is equal to the numerical difference of the magnitudes of the target and radar's velocities, given by [37]:

$$\dot{R} = -(V_r - V_t) \tag{6.2}$$

where $V_r$ is the magnitude of the radar's velocity and $V_t$ is the magnitude of the target's velocity. For a target moving towards the radar, the range rate is equal to the numerical sum of the magnitudes of the two velocities. Knowing the time, 10 s, and the distance that the human traveled, 6.3 m, the human's rate of speed can be calculated. The human's speed was approximately 0.63 m/s. The target's velocity depends on direction relative to each radar, but to make a simplification the velocity will be 0.63 m/s, traveling directly away from the radars. The radar's velocity is zero since it is stationary. This makes the range rate equal to 0.63 m/s. If the center frequency of the noise signal, 600 MHz, is used and the range rate is 0.63 m/s, then Eq. 6.1 yields -2.52 Hz. Though a simplification was made on the velocity of the target, it is apparent that the frequency change is small. The change may be small, but it will still alter the reflected signal from its original. When correlated with the original transmitted signal there will be differences lowering the correlation values.

102

This change may not be large, but how Doppler affects the correlation results can be considered for a future study.

Fig. 6.17 shows the resulting two-dimensional plots locating the human walking through the cluttered room at 0, 1, 2, 3, 4, 5, and 6 seconds. The duration of the test was 10 seconds but after 6 seconds the target moved out of range. The results produced 50 plots, but only 1 second increments are shown to summarize the human's progress across the room. High intensity spots are expected to move in a diagonal line starting from (5.8 m, 1.2 m) and heading towards (0 m, 3.66 m) as time passes. In this test, clutter in the form of chairs was present. It is expected that high intensity spots indicating the chairs will be at (1.8 m, 1.8 m), (3.78 m, 0.9 m), and (5.8 m, 2.74 m). The results do show the human's movement across the room, but not as clearly as with the room empty. The chairs effect location results, most likely due to multipath effects. Also, only one chair is located at approximately (3.9 m, 1.2 m). The other two chairs do not appear, but they were at much further distances and their reflected signal strength may be below detection range.

The results show that at 0 seconds a red spot exists at approximately (5.8 m, 1.1 m). The high intensity spots or clusters can be seen moving diagonally across the room, and a spot indicating one of the chairs remains at about (3.9 m, 1.2 m). This is true except for at 2 and 3 seconds. At 2 seconds there are two high intensity spots one at approximately (4.4 m, 2 m) and the other at about (4 m, 1.7 m). The human target is mostly likely between these at (4.2 m, 1.8 m), which is approximately where the human should be at that time. The chair has disappeared in this scene. There are two possible explanations. The first is that the human is a better reflector with a much higher correlation strength than the chair. This theory is supported by the inability to see the other two chairs in the scene, while the human can be seen up to at least 3 m. Another possibility is that the imaging algorithm assigns color by relative strength. The human approaching the chair might be masking the chair's lower correlation strength. The second possible explanation is multipath effects between the chair and the human.
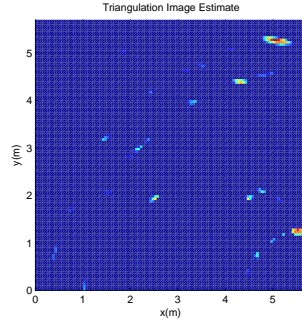
(a) Human Walking Through Empty Room at 0 seconds
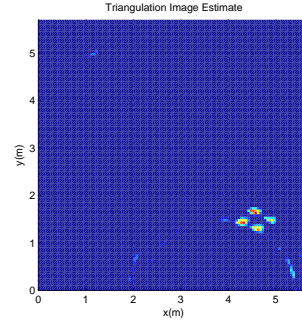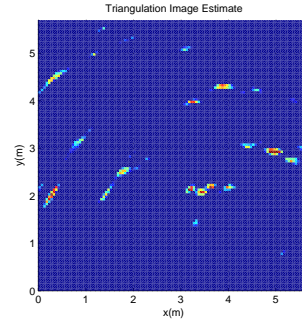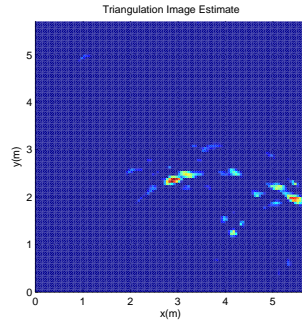
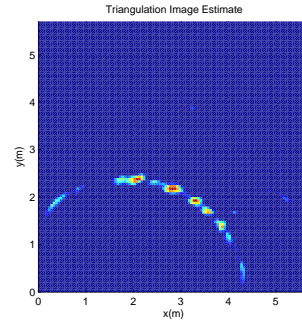(b) Human Walking Through Empty Room at 1 seconds
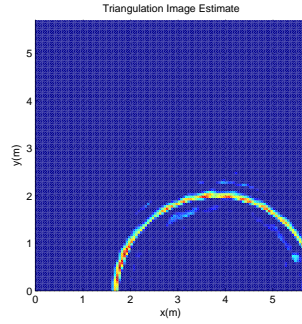
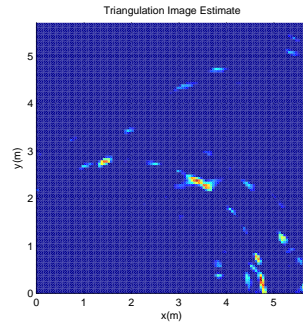(c) Human Walking Through Empty Room at 2 seconds

(d) Human Walking Through Empty Room at 3 seconds

(e) Human Walking Through Empty Room at 4 seconds

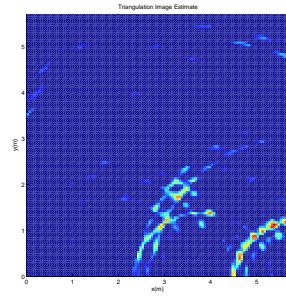(f) Human Walking Through Empty Room at 5 seconds

(g) Human Walking Through Empty Room at 6 seconds

Figure 6.16:    Location Results of Human Walking Through Empty Room

104

Another anomaly is at 3 seconds. In this scene, a red spot is at (3.6 m, 1.5 m). While the x direction value might be within limits the y value is clearly too low. The best possible explanation is some sort of interaction between the chair and the human. This effect mislocates the human target. After 3 seconds the human can be seen tracking towards (0 m, 3.66 m) until 6 seconds at which point the human's location is out of range.

Also, the results show several false targets or high intensity areas that are not the human or the chairs. Possible reasons such as the dual correlation peaks and effects due to the movement of the human have already been discussed. Another reason could include the human's correlation strength at farther distances. On Fig. 17(g), at 6 seconds, dotted rings are very visible in the results image. The human is nearing its detection limit, but with the relative color intensity settings, seeing the target means more false targets. The rings create and X-like effect near the target's location. These ring could possibly help locate the actual target and eliminate false targets.

To test if the chairs and human are affecting each other at close distances the background of the chairs can be subtracted from the same data set and compared. If the oddities seen in the results of the human walking through the cluttered room disappear, then the most likely possibility is the chairs. Fig. 6.18 shows the resulting two-dimensional plots locating the human walking through the cluttered room with background subtraction of the chair at 0, 1, 2, 3, 4, 5, and 6 seconds. In this set of results, it is expected that the chair's location and its effects on the location of the human target will disappear. The human is expected to move in a diagonal line starting from (5.8 m, 1.2 m) and heading towards (0 m, 3.66 m). The results from 0 to 6 seconds show positive location results at 2 and 3 seconds and the chair is not visible. At 0 seconds the results show a red spot at approximately (5.8 m, 1.2 m). After that, high intensity spots or clusters can be seen moving diagonally towards (0 m, 3.66 m). At 6 seconds the target has made it to (1 m, 3 m). The location results in these graphs very closely resemble the results from the human walking through the empty room. The chair background subtraction results are slightly different at 4 and 5 seconds from

(a) Human Walking Through Cluttered Room at 0 seconds
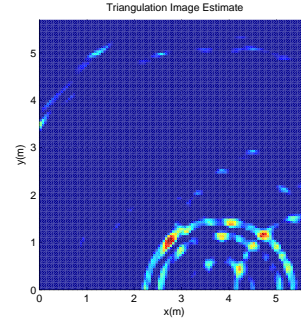


(b) Human Walking Through Cluttered Room at 1 seconds
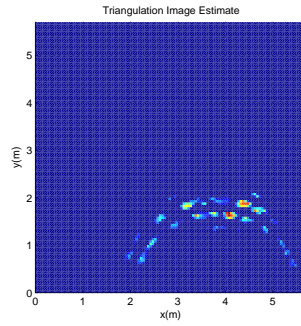


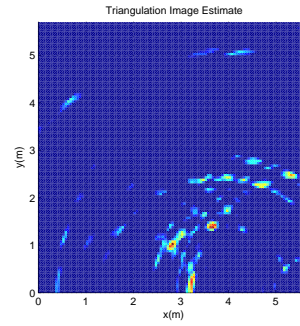(c) Human Walking Through Cluttered Room at 2 seconds



(d) Human Walking Through Cluttered Room at 3 seconds



(e) Human Walking Through Cluttered Room at 4 seconds



(f) Human Walking Through Cluttered Room at 5 seconds



(g) Human Walking Through Cluttered Room at 6 seconds

Figure 6.17:    Location Results of Human Walking Through Cluttered Room

the clutter room results. These are the same data sets only with different background subtractions, so the differences at 4 and 5 seconds suggest that the chair at (1.8 m, 1.8 m), though not seen, could be affecting the human's location results. This chair would have been near the human at this point in time. An assumption can be made that objects in the room though not located by the noise radar, may interact with the target of interest and slightly alter its location. The solution to this problem would be to take a background shot of the area in question and subtract it out.

## 6.6 Data Length

The digital correlation statistics developed in Chapter 3 shows that the signal-to-noise (SNR) ratio is proportional to the square root of the number of samples. This means that an increase in the data length of the correlation signals will increase the SNR. For example, an increase from a data length of 200 to 400 will increase the SNR by 2.5 dB. An increase in SNR means weaker return signals are more likely to be detected. The drawback to increasing the data length is an increase in processing time, but for a target that needs to be tracked that is further in range this may be beneficial. The human target from Fig. 6.6 is located at (4.1 m, 2.8 m) and just barely detectable because he is near the range detection limit. The results shown were correlated with a data length of 1200. A lower data length would decrease the SNR and the target would be more difficult to detect. Fig. 6.19 shows the comparison of the 1200 data length to the 400 data length results. The results of the 1200 data length show red spot at approximately (3.7 m, 2.9 m) close to the actual location of the human target. The results of the 400 data length show two orange spots centered at approximately (3.2 m, 2.8 m). The 400 data length results show much more error in location than the 1200 data length results. This is expected since the target's SNR decreased. These results show that the optimal data length needs to be determined by balancing an acceptable SNR for target identification and if there are limits on processing time. In this thesis, processing time was not a limiting factor.

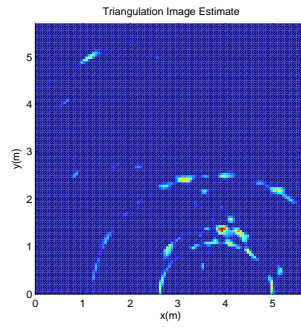(a) Human Walking Through Cluttered Room at 0 seconds
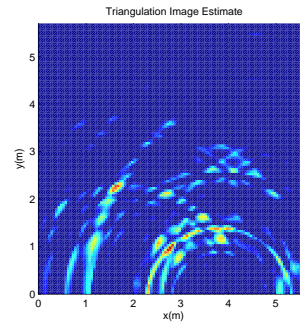
(b) Human Walking Through Cluttered Room at 1 seconds

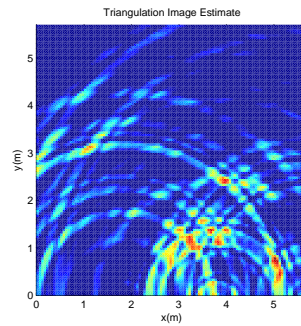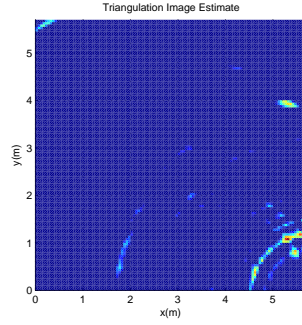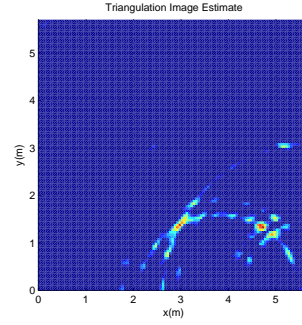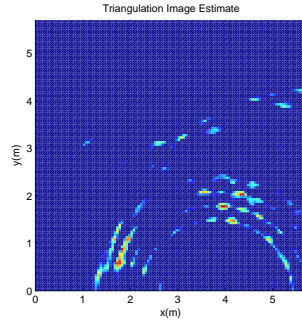(c) Human Walking Through Cluttered Room at 2 seconds

(d) Human Walking Through Cluttered Room at 3 seconds
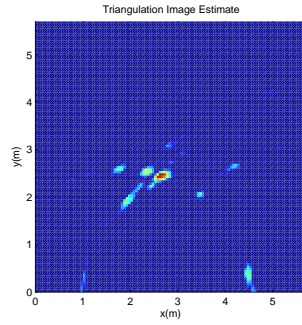
(e) Human Walking Through Cluttered Room at 4 seconds
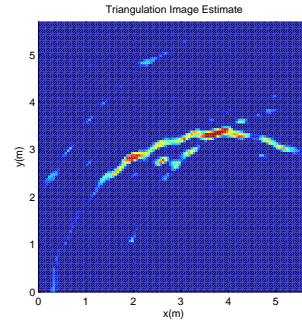
(f) Human Walking Through Cluttered Room at 5 seconds
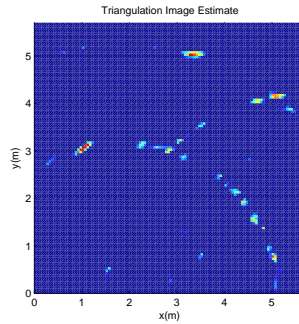
(g) Human Walking Through Cluttered Room at 6 seconds

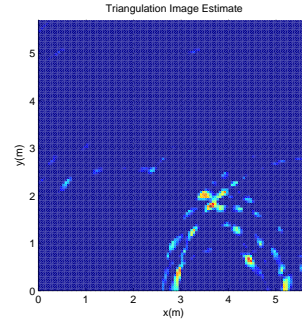Figure 6.18:    Location Results of Human Walking Through Room with Chair Background Subtracted Out
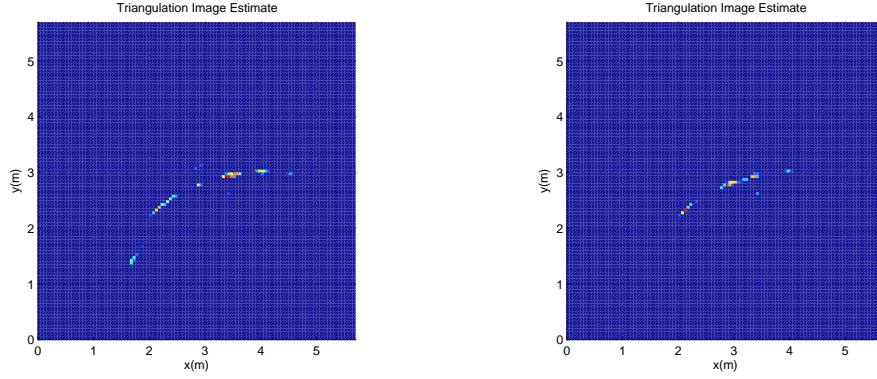
(a) Target: Human at (4.1 m, 2.8 m) with Data Length of 1200

(b) Target: Human at (4.1 m, 2.8 m) with Data Length of 400

Figure 6.19:     Comparison of Location Results Generated with Data Lengths of 1200 and 400

## 6.7   Summary of Results

This chapter reported and analyzed the results of tests accomplished with the noise radar system, and detailed the effects data length had on the results. Tests accomplished included single radar with a single target, networked radar systems with single and multiple targets, networked radar systems with target(s) and clutter in the area, and networked radar systems with moving targets. In nine out of ten cases the stationary targets were clearly identified. In eight out of ten cases the stationary targets were located within the range solution of the system, 0.375 cm. In the one miss case, the results image indicated the presence of the human target, but the detection was faint and possible to miss. Tests were also accomplished with moving human targets. In these tests the network of radar systems tracked the human target in an empty and cluttered room until the target was out of range. The test results prove that a network of simultaneously operating noise radars can locate and track multiple human and non-human targets, some in motion. For a complete list of tests conducted during the course of this research and more test scenarios with results see Appendix B and Appendix C.

# VII. Conclusion

Due to the threat of terrorism, today's enemy can be anyone and can exist anywhere from barren wastelands to populated cities. Monitoring human activities in an urban environment is a difficult problem due to walls, clutter, and other obstructions. In an effort to solve this problem, the focus of this research was to build a network of noise radar systems that could track human and non-human targets inside rooms and through walls. This chapter discusses the implications of this research from its goals to its contributions and offers suggestions for future research.

## 7.1  Research Goals

The overall goal of this research is to build a network of noise radar systems that can operate simultaneously without interference, locate multiple human or non-human targets, and track human movement through a room. Another goal is to design this network of sensors in a manner that will allow for integration with the QUEST processing kernel.

## 7.2  Results

The results presented in this thesis show that a network of noise radars can locate and track human and non-human objects in rooms and through walls. In nine out of ten cases the stationary targets were clearly identified. In eight out of ten cases the stationary targets were located within the range solution of the system, 0.375 m. In the one miss case, the results image indicated the presence of the human target, but the detection was faint and possible to miss. Tests were also accomplished with moving human targets. In these tests the network of radar systems tracked the human target in an empty and cluttered room until the target was out of range. The test results prove that a network of simultaneously operating noise radars can locate and track multiple human and non-human targets,some in motion. Also, this network of noise radar systems proved that real world noise radars can operate simultaneously in the same area without interfering with each other.

110

## 7.3  Research Contributions

Individuals, governments, and researchers have become interested in discovering methods to monitor suspicious human activities through walls. Monitoring human activities through walls is also of interest to rescue workers and fire fighters. Discovering the location of humans within a crumbling or on-fire building would allow lifesaving activities to be directed appropriately. Noise radars with ultra-wideband (UWB) signals have shown great promise at locating human and non-human targets through walls. Recently, Dr. Narayanan from Pennsylvania State University developed a digital noise radar system that located humans through-the-wall within 0.375 m [25]. This thesis used Dr. Narayanan's digital radar concept as a basis and built upon that foundation.

This research established the initial digital noise radar test bed at the Air Force Institute of Technology (AFIT). This research went beyond what Dr. Narayanan accomplished by developing three separate digital noise radar systems and networking them together. The three systems operated simultaneously, consolidated received data, and two-dimensionally located human (stationary and mobile) and non-human targets. Simultaneous operation of noise radars has been proven in simulation, but real world demonstration of this was not apparent in any literature on noise radars [38]. This thesis proved that digital noise radars can be networked and operated simultaneously to locate and track multiple human or non-human targets within a room.

## 7.4  Future Research

This thesis creates the initial noise radar test bed at AFIT, paving the way for future research. Some future possibilities are refinement of the current system, creation of a new imaging program, construction of addition sensors, making use of macro and micro Doppler information, and possible extraction of voice information. Sections 7.4.1- 7.4.5 discuss each of these future possibilities.

*7.4.1 Refinement of Current Noise Radar System.* Several refinements and upgrades can be made to the current system to improve performance. These refinements include increasing the speed of the processing algorithm, creation of an overall software program that will interact with each digitizer card, an increase of the digitizer's input range, and an upgrade to the amplifiers. First, the speed of the processing algorithm is fairly slow due to the loop structure. A new method to correlate the transmit and receive signals might speed up results. Currently, operation of each each radar system must be accomplished individually and manually. Second, an overarching software program could access each digitizer and automate the data collection process. Third, the current limiting factor in a target's range detection is the -2V to 2V digitizer input range. The weak received signal is flowed through two amplifiers which pushes the signal strength outside the -2V to 2V limits. Attenuation before the amplifiers is necessary to insure that the amplified received signal is within -2V to 2V. A range of -5V to 5V would offer more levels of digitation which would better characterize the fluctuations of the noise. It would also allow for more amplification of the return signal increasing the target detection range. Last, an increase to the digitizer's input would allow for the purchase of larger gain amplifiers which would further increase the detection range.

*7.4.2 Creation of a New Imaging Program.* The current imaging program is basic and relies on correlation amplitude strength. Use of correlation amplitude strength has its limitations. In its current form, the coloring of the two-dimensional plots are based on the lowest and the highest strength points in the matrix. It is possible that targets with excellent reflectivity, like the metal tubes, skew the relative color pattern and effectively hide less reflective targets like the human target. A different approach to imaging might offer clearer pictures of the target area.

*7.4.3 Construction of Additional Sensors.* Construction of additional sensors will more accurately locate targets. One target located near all three radars offers a low possibility of false targets. But as more targets are introduced and/or are

moving there exists a larger possibility of false targets. More sensors placed around a room are more likely to "see" the target since they can view more area of the room. The more sensors that pick up a target the more accurately the target's location can be triangulated.

*7.4.4  Macro and Micro Doppler Information.*    There exists a possibility to extract macro and micro Doppler information from the targets. Macro doppler might be captured by correlating a known set of time-dilated transmit signals to a received signal. A high correlation between a time dilation of the transmit signal and the receive signal will reveal the target's speed. Another possibility is extraction of the micro Doppler. Dr. Narayanan of Pennsylvania State University was able to extract human breathing rate from a 750 Hz sine wave mixed in with the noise signal [18] [19]. It might be possible to modify the current system to extract the micro Doppler information.

*7.4.5  Extraction of Voice Information.*    It may be possible to extract voice information from the received noise radar signal. The ability to see that voice had an effect on the received noise signal was an unexpected discovery during testing. When setting up some of the scenes it was necessary to call from outside the room to the person inside the room to see if he was in place. At the time, a display of the received signal was up on an oscilloscope. The operator noticed that when the individual in the room yelled or spoke loudly an observable effect occurred on the oscilloscope, even though the person in the room was not moving. An investigation is necessary to discover why this occurs and if the information can be extracted.

## Appendix A. Signal Processing Code

This appendix documents the signal processing code used in this thesis. The code is broken up into four files. The first is the Matlab® m-file Startnoiseradar.m. This file is considered the master file and is the only file that needs to be run. The file establishes the parameters used during testing and calls the other files necessary to process and graph the test data. The use of a master file provided the ability to easily change variables and offered programming flexibility. The other three Matlab® m-files are NoiseRadarCorrelationv2.m, Image.m, and triloc.m. NoiseRadarCorrelationv2.m pulls in the data file and provides the correlation routine. Image.m sets the variables necessary for creating a two-dimensional image and calls the function triloc. triloc.m is a function that consolidates each radar system's information into one matrix and plots the two-dimensional images. The Matlab® code examples shown are taken from human motion tests.

### A.1 Startnoiseradar.m

Listing A.1: Startnoiseradar.m Matlab® file(Appendix1/Startnoiseradar.m)

```
1 % Written/Modified by Capt Ashley Schmitt
  % Version 1 began 17 Dec 08 for Folder Human_motion_17Dec

  % Code Description:  This code is a Master script file for ...
      analyzing the
  % noise radar data that calls all the working script file.  It ...
      also defines
6 % several global varibles.
  %Note:  All these script files are dependant on one another.  This...
      file
  %must be run to make them work correctly.

  % There are 8 Test Setups and 2 Backgrounds
11 %Test 1: Human moving from (5.8m, 1.2m) to (0m, 3.66m) in 10 ...
      Seconds
  %Test 2: Human moving from (5.8m, 1.2m) to (0m, 3.66m) in 10 ...
      Seconds
  %Test 3: Human moving from (0m, 0m) to (5.8m, 3.66m) in 10 Seconds
  %Test 4: Human moving from (0m, 0m) to (5.8m, 3.66m) in 10 Seconds
  %Test 5: Human moving from (5.8m, 1.2m) to (0m, 3.66m) in 10 ...
      Seconds with
16     %chairs at (1.8m, 1.8m), (3.78m, 0.9m), and (5.8m, 1.2m).
  %Test 6: Human moving from (5.8m, 1.2m) to (0m, 3.66m) in 10 ...
      Seconds with
```

114

```
        %chairs at (1.8m, 1.8m), (3.78m, 0.9m), and (5.8m, 1.2m).
    %Test 7: Human moving from (0m, 0m) to (5.8m, 3.66m) in 10 Seconds...
        with
        %chairs at (1.8m, 1.8m), (3.78m, 0.9m), and (5.8m, 1.2m).
21  %Test 8: Human moving from (0m, 0m) to (5.8m, 3.66m) in 10 Seconds...
        with
        %chairs at (1.8m, 1.8m), (3.78m, 0.9m), and (5.8m, 1.2m).
    %Test 9: Background shot of  chairs at (1.8m, 1.8m), (3.78m, 0.9m)...
        ,
        %and (5.8m, 1.2m).
    %Test 10: Background shot of empty room
26
    clc
    close all
    clear all

31  %Defintion of Global Varibles
    sys=3;            %# of Radar Systems
    max_test=10;       %Sets the number of test cases
    acquisitions=1000; %# of acquistions that is inputed into ...
        Digitizer board
    samples=5000;      %# of samples pts aquired for each CH in each data...
        file
36  data_runs=20;     %# of data runs in each set (used for averaging ...
        purposes)
    data_length=1200;      %Data Length
    start_pt=404;    %Correlation start point
    shift_num=1200;  %# of times data is shifted for correlation
    sample_rate=1.5e9;  % Sample rate on each channel of the digitizer
41  c=3e8;                 %Speed of light (m/s)
    %This file pulls in each data file created by the three noise ...
        radar
    %systems and correlates it
    run Noise_Radar_Correlationv2

46  save Human_motion_17Dec  % saves the workspace from ...
        Noise_Radar_Correlationv2
    %as a mat file

    %This file creates 2D Images of results
    run Image
```

### A.2  NoiseRadarCorrelationv2.m

Listing A.2:    NoiseRadarCorrelationv2.m Matlab® file
(Appendix1/NoiseRadarCorrelationv2.m)

```
% Written/Modified by Capt Ashley Schmitt
% Version 2 began 3 Oct 08
%Recently Modified 17 Dec 08 for Folder Human_motion_17Dec
% This version has the data acquistions in one long file rather ...
    than in
5 % separate files
```

115

```matlab
   % Code Description:  This code calls up the saved data sets that ...
      were
   % acquired by three Noise Radar Systems. The call up an ...
      correlation is
   % identical for each system. Binary data file contains a mix of
10 % transmitted(odd numbered) and recieved data(even).  These ...
      signals are
   % split apart and renamed.  The program then applies a software ...
      filter
   % and then correlates the signal.  The correlation shifts the RX ...
      signal
   % across the TX signal. The data is then saved into .mat files and...
       plotted.

15 % Acknowledgements:  This code, though greatly modified from the
   % orginal code, was based on the work of PhD students from ...
      Pennslyvania
   % State University


20

   %Local Varible Definition
   ACC=data_length+1;    %Location of Autocorrelation value in the ...
      vector
25 max_set=acquisitions/data_runs; %# of sets within a test (time ...
      snapshots)


   %Initalize looped varibles
   all_cor_signal=[];
30 max_pt_list=[];
   set_cor_signal=zeros(max_set, shift_num);
   peak=zeros(1,shift_num);
   tx_signal=zeros(samples,1);
   rx_signal=zeros(samples,1);
35 tx_signal_wfilter=zeros(samples,1);
   rx_signal_wfilter=zeros(samples,1);

   %========= bandpass filter =================
               wp=[263   730]/750;
40             ws=[10    749]/750;
               Rp = 1; Rs =40;
               [n Wn] = buttord(wp,ws,Rp,Rs);
               [b,a] = butter(n,Wn);
               %freqz(b,a,128,1.5E9);
45 %===========================================
   %Software filter used because it improves results
   %===========================================
```

```matlab
    %Test for loop pulls in each test case's data files
50  for system=1:sys;


        for test=1:max_test
            distance=zeros(data_runs,shift_num);
55

            % Opens CH1 data files gathered from Noise Radar sample
            fid=fopen(['Sys' num2str(system) '_' num2str(test) '_CH1'...
                ],'r');
        %Reads the data that is in binary form and saves to variable
60          tx_signal=fread(fid,2*samples*acquisitions,'int8');
            fclose(fid);

        % Opens CH2 data files gathered from Noise Radar sample
            fid=fopen(['Sys' num2str(system) '_' num2str(test) '_CH2'...
                ],'r');
65      %Reads the data that is in binary form and saves to variable
            rx_signal=fread(fid,2*samples*acquisitions,'int8');
            fclose(fid);


70
            tx_signal_wfilter=filter(b,a,tx_signal); %filters Tx ...
                signal
            rx_signal_wfilter=filter(b,a,rx_signal); %filters Rx ...
                signal

            %Reshapes Tx and Rx matrices to separate the different ...
                sets of
75          %acquisitions
            tx_signal_wfilter=reshape(tx_signal_wfilter, samples, ...
                acquisitions).';
            rx_signal_wfilter=reshape(rx_signal_wfilter, samples, ...
                acquisitions).';


80  %Set for loop(along with the data_run loop) pulls out and ...
        correlates each of the data runs that was done
    %on a particular set.  Example if set 1 had 20 separate data ...
        acquisitions
    %then this loop this pulls each of those 20 acquisitions out, ...
        correlates them,
    %and then averages the peak returns to acheive a better SNR and ...
        put them
    % the max_set number of sets.
85          counter=1;


            for set=1:max_set
```

```matlab
90
            for data_loop=1:data_runs

        %Pulls out portion of the Tx signal that will be used for
        %correlation
95          tx=tx_signal_wfilter(counter, start_pt:start_pt+...
                data_length);

        %Shift for loop correlates the Tx and Rx signal.  The loop...
            shift
        %the Rx signal over by 1 each loop and then after each ...
            correlation
        %the value at the center location of the correlation ...
            varible is
100     %saved into a matrix.

            for shift=1:shift_num

            rx=rx_signal_wfilter(counter, start_pt+shift:start_pt+...
                data_length+shift);
105         xx=xcorr(rx,tx);
            peak(shift)=xx(ACC);

            end

110         counter=counter+1;
            distance(data_loop,:)=peak;

            end

115     distance_sum=sum(distance)/data_runs;
        set_cor_signal(set,:)=distance_sum;

        % Finds and creates matrix for the maximum peak in each ...
            correlation.
        % This peak corresponds to the location of the wall within...
            the
120     % signal length.  Since the location of the wall is known ...
            this peak
        % is used as a reference to set range for the signal.

        [value,column]=max(set_cor_signal(set,:));
        max_pt_list=[max_pt_list; column];
125
         end

        all_cor_signal=[all_cor_signal; set_cor_signal];

130 end
```

```
    end

    cor_length=length(all_cor_signal);   %Find length of correlation ...
        vector
```

### A.3  Image.m

Listing A.3:    Image.m `Matlab`® file(Appendix1/Image.m)

```
  %Written by Capt Ashley Schmitt on 21 Nov 2008
2 %Updated 7 Jan 2009
  % This m-file plots the 2D Image results that were compiled and ...
      correlated
  % from Noise_Radar_Correlationv2.m

  close all  %closes any open figures to avoid confusion
7
  %This filter is included, though it usually does not improve
  %results.  It is included as a feature and is currently set to not...
      offer
  %any additional filtering.
  %========== lowpass filter =================
12
                wp=[748]/750;
                ws=[749]/750;
                Rp = 1; Rs =40;
                [n Wn] = buttord(wp,ws,Rp,Rs);
17              [b,a] = butter(n,Wn);
                %freqz(b,a,128,1.5E9);
  %=============================================
  %Software filter used after correlation
  %=============================================
22
  all_cor_signal_filter=[];
  for filter_loop=1:max_test*sys*acquisitions/data_runs
  all_cor_signal_filter(filter_loop,:)=filter(b,a,all_cor_signal(...
      filter_loop,:));
  end
27
  r1=137;  %Sets Radar System 1's 0 sec position in the correlated ...
      signal
  r2=129;  %Sets Radar System 2's 0 sec position in the correlated ...
      signal
  r3=143;  %Sets Radar System 3's 0 sec position in the correlated ...
      signal
  t_samples=100;  %sets the number of samples that are used from the
32 %correlated signal.
  t = linspace(0,2*((t_samples+1)/10/3e8),t_samples+1);   %Gives a ...
      vector
  %of seconds for the number of t-samples
```

119

```matlab
   radar = [72,-6; 149, -6; 229,-6]./39.37;   % Defines radar (x,y)
   %locations in meters (39.37inches to a meter)
37 adj1=1/1.006e5; %Normalizes the differences in gain for radar ...
      system 1
   adj2=1/6.302e4; %Normalizes the differences in gain for radar ...
      system 2
   adj3=1/6.292e4; %Normalizes the differences in gain for radar ...
      system 3

   %frame1-8 are used as counters to get movie shots
42  frame1=1;
    frame2=1;
    frame3=1;
    frame4=1;
    frame5=1;
47  frame6=1;
    frame7=1;
    frame8=1;

   % This loop graphs each test case.  First it defines the varible ...
      rcvd for
52 % the triloc function. The rcvd vector contains the correlated ...
      signal minus the
   % background signal multipled by the normalization factor for each...
       of the 3
   % systems. The triloc function is then called. It takes in the ...
      varibles
   % rcvd,t,radar,and graph window size(in meters) and displays a ...
      graph for
   % each point in time.  In the case below each test has 50 points ...
      in time or
57 % 50 scenes.  There are 5 scenes per second accounting for the ...
      full 10 second
   % capture time.  There are 8 tests in this folder so that accounts...
       for graphs=1:400.

   for graphs=1:400
   rcvd=[adj1*abs(all_cor_signal_filter(graphs,r1:r1+t_samples)-...
      all_cor_signal_filter((max_test)*acquisitions/data_runs,r1:r1+...
      t_samples));...
62 adj2*abs(all_cor_signal_filter(graphs+max_test*acquisitions/...
      data_runs,r2:r2+t_samples)-all_cor_signal_filter(2*(max_test)*...
      acquisitions/data_runs,r2:r2+t_samples));...
   adj3*abs(all_cor_signal_filter(graphs+2*max_test*acquisitions/...
      data_runs,r3:r3+t_samples)-all_cor_signal_filter(3*(max_test)*...
      acquisitions/data_runs,r3:r3+t_samples))];
   [img,ximg,yimg] = triloc(rcvd,t,radar,[0 226/39.37]);
   %caxis([1.95 2.2])

67 % This if statement is used to capture each scene and place it in ...
      the
```

```matlab
    % appropriate varible for a movie.  Ex. Type in Matlab command ...
        line
    %movie(front_back1,1,5) it will play front_back1 1 time at 5 ...
        frames per
    %second. Close all is used to save memory due to the large
    %amount of graphs created.
72
        if (graphs>=1) && (graphs<=50)
            front_back1(frame1)=getframe;
            frame1=frame1+1;
            close all
77          elseif (graphs>=51) && (graphs<=100)
            front_back2(frame2)=getframe;
            frame2=frame2+1;
             close all
            elseif (graphs>=101) && (graphs<=150)
82          back_front1(frame3)=getframe;
            frame3=frame3+1;
             close all
            elseif (graphs>=151) && (graphs<=200)
            back_front2(frame4)=getframe;
87          frame4=frame4+1;
             close all
            elseif (graphs>=201) && (graphs<=250)
            front_back_wchairs_subout1(frame5)=getframe;
            frame5=frame5+1;
92           close all
            elseif (graphs>=251) && (graphs<=300)
            front_back_wchairs_subout2(frame6)=getframe;
            frame6=frame6+1;
             close all
97          elseif (graphs>=301) && (graphs<=350)
            back_front_wchairs_subout1(frame7)=getframe;
            frame7=frame7+1;
             close all
            elseif (graphs>=351) && (graphs<=400)
102         back_front_wchairs_subout2(frame8)=getframe;
            frame8=frame8+1;
             close all
        end

107


    end
112

    %Extra code used to create 1D plots for trouble shooting purposes.
    % close all
    % x=1:t_samples+1;
117 % p=3;
```

```matlab
% figure(max_test)
% subplot(p,1,1);
% plot(x,abs(all_cor_signal_filter(3,r1:r1+t_samples)-...
%     all_cor_signal_filter(max_test,r1:r1+t_samples)))
% %xlabel('Distance (meters)', 'FontSize', 12);
% ylabel('Correlation', 'FontSize', 12);
% title('Radar 1 Scene 1', 'FontSize', 12);
%
%
% subplot(p,1,2);
% plot(x,abs(all_cor_signal_filter(3+max_test,r2:r2+t_samples)-...
%     all_cor_signal_filter(max_test*2,r2:r2+t_samples)))
% %xlabel('Distance (meters)', 'FontSize', 12);
% ylabel('Correlation', 'FontSize', 12);
% title('Radar 2 Scene 1', 'FontSize', 12);
%
% subplot(p,1,3);
% plot(x,abs(all_cor_signal_filter(3+max_test*2,r3:r3+t_samples)-...
%     all_cor_signal_filter(max_test*3,r3:r3+t_samples)))
% %xlabel('Distance (meters)', 'FontSize', 12);
% ylabel('Correlation', 'FontSize', 12);
% title('Radar 3 Scene 1', 'FontSize', 12);
```

### *A.4 triloc.m*

Listing A.4:    triloc.m `Matlab`® file(Appendix1/triloc.m)

```matlab
function [img,ximg,yimg] = triloc(rcvd,t,radar,windowMinMax)
%This function was orginally created Nov 2008 by Professor Peter ...
    Collins.
%The code has been slightly modified since its orginal creation.
%% Form image from arbitrary number of radar units
% [img,ximg,yimg] = triloc(rcvd,t,radar,windowMinMax);

warning off
% Load measured receiver response in standard format (radar x time...
    )
if ~exist('rcvd','var'); rcvd = load(uigetfile('','Load radar data...
    ...')); end
% Load time vector
if ~exist('t','var'); t = load(uigetfile('','Load time vector...')...
    ); end
% Load radar locations (radar x coordinate)
if ~exist('radar','var'); radar = inputdlg('Input (x,y) for each ...
    radar','Radar Locations'); end
% Define rectangular and polar image sampling
imagRes = 0.05;  % image resolution (m)
angSam = 1;  % polar angle sampling (degrees)
if ~exist('windowMinMax')

    ximg = min(radar(:,1)):imagRes:max(radar(:,1));
```

```matlab
        yimg = min(radar(:,2)):imagRes:max(radar(:,2));
    else
24      ximg = windowMinMax(1):imagRes:windowMinMax(2);
        yimg = ximg;

    end
    phi = -pi:angSam*pi/180:pi;
29 % Calculate some useful constants
    c = 299.792458e6;                % meters/second
    rng = (c*t/2);                      % 2-way distance to range bin
    numX = length(ximg);
    numY = length(yimg);
34 numPhi = length(phi);
    numRadar = size(radar,1);
    % Create the image data cube
    img = zeros(numX,numY,numRadar);
    [ximg,yimg] = meshgrid(ximg,yimg);
39 for idx = 1:numRadar  % for each radar...
        x = rng'*cos(phi)+radar(idx,1);  % converts polar to ...
            rectangular
        y = rng'*sin(phi)+radar(idx,2);
        %normResponse = repmat((rng).*rcvd(idx,:),numPhi,1).';  % ...
            normalized radar response
        normResponse = repmat(rcvd(idx,:),numPhi,1).';  % normalized ...
            radar response
44      % Interpolate rectangular data to the desired image window
        img(:,:,idx) = griddata(x,y,normResponse,ximg,yimg).';
    end
    img = sum(img,3);  % sum response from each radar - highest ...
        overlaps are targets
    img(isnan(img))= 0*find(isnan(img));  % replace NaN with zeros for...
        plotting
49 ximg = ximg(1,:);
    yimg = yimg(:,1)';

    %% Generate plots

54 figure
    surf(ximg(:),yimg(:),img.','LineStyle','none','EraseMode','none');
    axis equal
    %caxis([max(caxis/numRadar) max(caxis)])
    view(0,90)
59 xlabel('x(m)')
    ylabel('y(m)')
    title('Triangulation Image Estimate')
```

*Appendix B.   List of All Experiments Accomplished and Additional*

*One and Two-Dimensional Images*

### B.1   List of All Experiments Accomplished

Over the course of working on this thesis many more experiments were conducted that were not included in the results. An attempt was made to present results in a logic manner, but without overwhelming the reader. Tables B.1, B.2, B.3, B.4 and B.5 list all tests conducted while accomplishing this thesis, including those presented in the methodology and results section. In addition to the tests listed, the 6 in diameter tube, 8 in diameter tube, and the human were each placed 0.9 m from the radar and rotated to 0°, 45°, 90°, 135°, 180°, 225°, 270°, and 315°.

Notes: Background is the room without any targets. Clutter like desks and other objects may exist around the edges of the room, but the center area is clear. This symbol (*) notes that the test was accomplished with a particular system's radar box. The radar boxes include the noise source, amps, and BPFs. These tests were done to see if each box performed in a similar manner. There are four radar boxes even though there are only three total systems. This symbol (**) notes an experiment where Sys 1's radar was behind a wall and Sys 2's radar was in open air. This test was accomplished to compare through wall results and through air results.

Table B.1:     Complete List of All Tests Conducted: Tests 1-9

| Test | Thru wall /Thru air | Target(s) Location (in meters) | Antenna Placement (in meters) | 1D /2D Image(s) |
|------|---------------------|-------------------------------|-------------------------------|-----------------|
| 1 | Thru wall | 8 sqft Metal board at (0, 1), (0, 2), (0, 2.9), (0, 3.8) | (0, 0) | 1D |
| 2 | Thru wall | 8 sqft Metal board at (0, 1), (0, 2), (0, 2.9), (0, 3.8) | (0, 0) | 1D with radar box 1* |
| 3 | Thru wall | 8 sqft Metal board at (0, 1), (0, 2), (0, 2.9), (0, 3.8) | (0, 0) | 1D with radar box 2* |
| 4 | Thru wall | 8 sqft Metal board at (0, 1), (0, 2), (0, 2.9), (0, 3.8) | (0, 0) | 1D with radar box 3* |
| 5 | Thru wall | 8 sqft Metal board at (0, 1), (0, 2), (0, 2.9), (0, 3.8) | (0, 0) | 1D with radar box 4* |
| 6 | Thru wall | Human at (0, 1), (0, 2), (0, 2.9), (0, 3.8) | (0, 0) | 1D |
| 7 | Thru wall | Background | (0, 0) | 1D |
| 8 | Thru wall | 8 sqft Metal board at (0, 1), (0, 2), (0, 2.9), (0, 3.8) | (0, -1) | 1D |
| 9 | Thru wall | Background | (0, -1) | 1D |

Table B.2:    Complete List of All Tests Conducted: Tests 10-20

| Test | Thru wall /Thru air | Target(s) Location (in meters) | Antenna Placement (in meters) | 1D /2D Image(s) |
|------|------|------|------|------|
| 10 | Thru wall/air** | 8 sqft metal board at (0, 1), (0, 2), (0, 2.9), (0, 3.8) | Sys 1 (-1, 0), Sys 2 (1, 0) | 1D |
| 11 | Thru wall/air** | Background | Sys 1 (-1, 0), Sys 2 (1, 0) | 1D |
| 12 | Thru wall | 8 sqft Metal board at (3.8, 1), (3.8, 2), (3.8, 2.9), (3.8, 3.8), (3.8, 4.7), (3.8, 5.6), (3.8, 6.5) | Sys 3 (1.9, -0.15), Sys 2 (3.8, -0.15), Sys 3 (5.7, -0.15) | 1D |
| 13 | Thru wall | 8 sqft Metal board at (3.8, 1), (3.8, 2), (3.8, 2.9), (3.8, 3.8) | Sys 3 (1.9, -0.9), Sys 2 (3.8, -0.9), Sys 1(5.7, -0.9) | 1D |
| 14 | Thru wall | 8 sqft Metal board at (6.7, 1), (5.7, 1), (4.8, 1), (3.8, 1), (2.8, 1), (1.9, 1), (1, 1), (0 ,1) | Sys 3 (1.9, -0.15), Sys 2 (3.8, -0.15), Sys 1 (5.7, -0.15) | 1D |
| 15 | Thru wall | 8 sqft Metal board at (6.7, 2), (5.7, 2), (4.8, 2), (3.8, 2), (2.8, 2), (1.9, 2), (1, 2), (0 ,2) | Sys 3 (1.9, -0.15), Sys 2 (3.8, -0.15), Sys 1 (5.7, -0.15) | 1D |
| 16 | Thru wall | Background | Sys 3 (1.9, -0.15), Sys 2 (3.8, -0.15), Sys 1 (5.7, -0.15) | 1D |
| 17 | Thru air | 6 in Tube at (4.5, 2.7) | Sys 1 (1.8, 3), Sys 2 (3.9, 0.6), Sys 3 (6.4, 2.1) | 2D |
| 18 | Thru air | 6 in Tube at (3.8, 3.5) | Sys 1 (1.8, 3), Sys 2 (3.9, 0.6), Sys 3 (6.4, 2.1) | 2D |
| 19 | Thru air | Human at (4.5, 2.7) facing Sys 2 | Sys 1 (1.8, 3), Sys 2 (3.9, 0.6), Sys 3 (6.4, 2.1) | 2D |
| 20 | Thru air | Human at (4.5, 2.7) facing Sys 3 | Sys 1 (1.8, 3), Sys 2 (3.9, 0.6), Sys 3 (6.4, 2.1) | 2D |

Table B.3:     Complete List of All Tests Conducted: Tests 21-32

| Test | Thru wall /Thru air | Target(s) Location (in meters) | Antenna Placement (in meters) | 1D /2D Image(s) |
|---|---|---|---|---|
| 21 | Thru air | Human at (2.1, 0.7) | Sys 1 (1.8, 3), Sys 2 (3.9, 0.6), Sys 3 (6.4, 2.1) | 2D |
| 22 | Thru air | Human at (2.6, 1.3) | Sys 1 (1.8, 3), Sys 2 (3.9, 0.6), Sys 3 (6.4, 2.1) | 2D |
| 23 | Thru air | Human at (3.2, 2.1) | Sys 1 (1.8, 3), Sys 2 (3.9, 0.6), Sys 3 (6.4, 2.1) | 2D |
| 24 | Thru air | Human at (3.8, 2.7) | Sys 1 (1.8, 3), Sys 2 (3.9, 0.6), Sys 3 (6.4, 2.1) | 2D |
| 25 | Thru air | Human at (4.4, 3.3) | Sys 1 (1.8, 3), Sys 2 (3.9, 0.6), Sys 3 (6.4, 2.1) | 2D |
| 26 | Thru air | 6 in Tube at (3.6, 2.7) | Sys 1 (1.8, 3), Sys 2 (3.9, 0.6), Sys 3 (6.4, 2.1) | 2D |
| 27 | Thru air | 6 in Tube at (3.6, 2.7) Human at (4.5, 2.7) | Sys 1 (1.8, 3), Sys 2 (3.9, 0.6), Sys 3 (6.4, 2.1) | 2D |
| 28 | Thru air | Background | Sys 1 (1.8, 3), Sys 2 (3.9, 0.6), Sys 3 (6.4, 2.1) | 2D |
| 29 | Thru wall | 6 in Tube at (2.5, 2.7) | Sys1 (2.1, -0.15) Sys2 (4, -0.15) Sys3 (5.7, -0.13) | 2D |
| 30 | Thru wall | 8 in Tube at (4.1, 2.8) | Sys1 (2.1, -0.15) Sys2 (4, -0.15) Sys3 (5.7, -0.13) | 2D |
| 31 | Thru wall | Human at (4.1, 2.8) | Sys1 (2.1, -0.15) Sys2 (4, -0.15) Sys3 (5.7, -0.13) | 2D |
| 32 | Thru wall | 6 in Tube at (2.5, 2.7) 8 in Tube at (4.1, 2.8) | Sys1 (2.1, -0.15) Sys2 (4, -0.15) Sys3 (5.7, -0.13) | 2D |

127

Table B.4:    Complete List of All Tests Conducted: Tests 33-41

| Test | Thru wall /Thru air | Target(s) Location (in meters) | Antenna Placement (in meters) | 1D /2D Image(s) |
|------|---------------------|--------------------------------|-------------------------------|-----------------|
| 33 | Thru wall | 6 in Tube at (2.5, 2.7) Human at (4.1, 2.8) | Sys1 (2.1, -0.15) Sys2 (4, -0.15) Sys3 (5.7, -0.13) | 2D |
| 34 | Thru wall | Background | Sys1 (2.1, -0.15) Sys2 (4, -0.15) Sys3 (5.7, -0.13) | 2D |
| 35 | Thru wall | Human facing Sys 1 at (0, 1), (0, 2), (0, 2.9) | Sys1 (2.1, -0.15) | 1D |
| 36 | Thru wall | Human's profile at (0, 1), (0, 2), (0, 2.9) | Sys1 (2.1, -0.15) | 1D |
| 37 | Thru wall | Background | Sys1 (2.1, -0.15) | 1D |
| 38 | Thru air | Human 1 (2, 1.3) Human 2 (3.9, 3.1) | Sys1 (1, 0) Sys2 (2.9, 0) Sys3 (4.8, 0) | 2D |
| 39 | Thru air | Human 1 (2, 1.3) Human 2 (3.9, 3.1) Chair (3.3, 1.3) | Sys1 (1, 0) Sys2 (2.9, 0) Sys3 (4.8, 0) | 2D |
| 40 | Thru air | Chair (3.3, 1.3) | Sys1 (1, 0) Sys2 (2.9, 0) Sys3 (4.8, 0) | 2D |
| 41 | Thru air | Background | Sys1 (1, 0) Sys2 (2.9, 0) Sys3 (4.8, 0) | 2D |

Table B.5:    Complete List of All Tests Conducted: Tests 42-47

| Test | Thru wall /Thru air | Target(s) Location (in meters) | Antenna Placement (in meters) | 1D /2D Image(s) |
|------|------|------|------|------|
| 42 | Thru wall | Human Motion Start (5.8, 1.2) End (0, 3.66) | Sys1 (2.1, -0.15) Sys2 (4, -0.15) Sys3 (5.7, -0.13) | 2D |
| 43 | Thru wall | Human Motion Start (5.8, 3.66) End (0, 0) | Sys1 (2.1, -0.15) Sys2 (4, -0.15) Sys3 (5.7, -0.13) | 2D |
| 44 | Thru wall | Human Motion Start (5.8, 1.2) End (0, 3.66) Chairs (1.8, 1.8), (3.78, 0.9), (5.8, 2.74) | Sys1 (2.1, -0.15) Sys2 (4, -0.15) Sys3 (5.7, -0.13) | 2D |
| 45 | Thru wall | Human Motion Start (5.8, 3.66) End (0, 0) Chairs (1.8, 1.8), (3.78, 0.9), (5.8, 2.74) | Sys1 (2.1, -0.15) Sys2 (4, -0.15) Sys3 (5.7, -0.13) | 2D |
| 46 | Thru wall | Chairs (1.8, 1.8), (3.78, 0.9), (5.8, 2.74) | Sys1 (2.1, -0.15) Sys2 (4, -0.15) Sys3 (5.7, -0.13) | 2D |
| 47 | Thru wall | Background | Sys1 (2.1, -0.15) Sys2 (4, -0.15) Sys3 (5.7, -0.13) | 2D |

## Appendix C. Additional Test Scenarios with One and Two-Dimensional Results Images

Many more test scenarios were accomplished than were presented and analyzed in the main body of the document. This section presents additional test scenarios, some pictures, and the resulting one or two-dimensional images.

### C.1 One-Dimensional Images of 8 sqft Metal Board

The first test scenario had one radar system looking through the air at a 8 sqft metal board. Four test shots were taken with the metal board moved 0.9 m, 1.8 m, 2.7 m, and 3.7 m from the radar. Fig. C.1 shows a diagram of this test scenario, and the resulting one-dimensional plots. The results of the background shot are also included in the plot.

The second test scenario had one radar system looking through a plaster board wall at a 8 sqft metal board. The wall is approximately 5 in or 13 cm thick and the radar's antennas are 0.5 in or 1.3 cm from the wall. Four test shots were taken with the metal board moved 1 m, 2 m, 2.9 m, and 3.8 m from the radar. Fig. C.2 shows a diagram of this test scenario, and the resulting one-dimensional plots. The results of the background shot are also included in the plot.

### C.2 Two-Dimensional Images of 6 in Diameter Metal Tube and Human Target Through the Air

The first test scenario had the network of radar systems looking through air at a 6 in diameter metal tube located at (4.5 m, 2.7 m). Fig. C.3 shows a diagram of this test scenario, a photo, and the resulting two-dimensional plot.

The second test scenario had the network of radar systems looking through air at a 6 in metal tube located at (3.6 m, 2.7 m). Fig. C.4 shows a diagram of this test scenario, a photo, and the resulting two-dimensional plot.
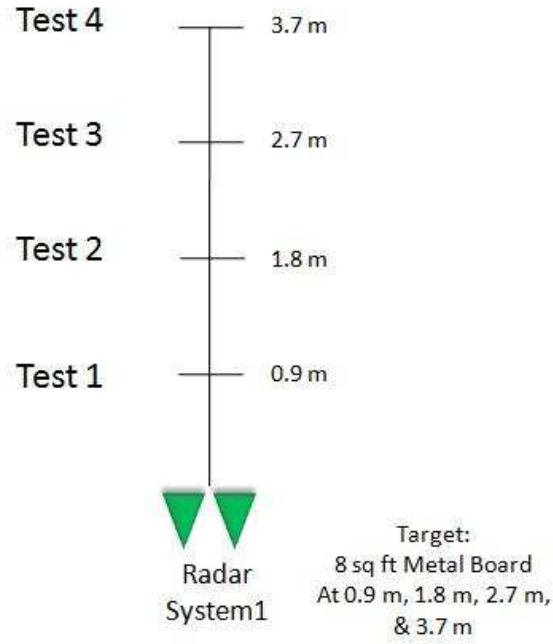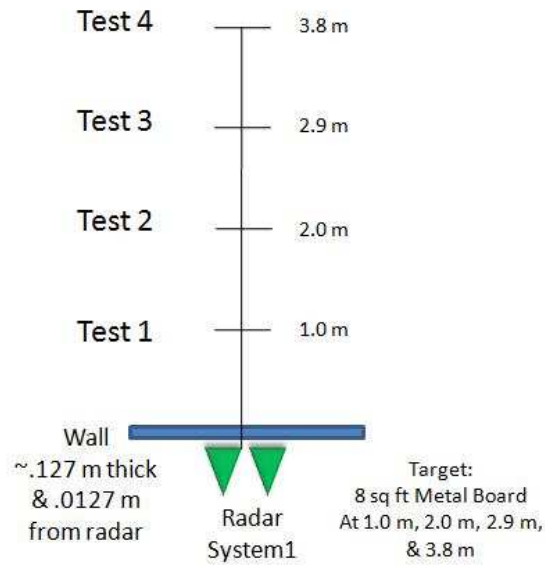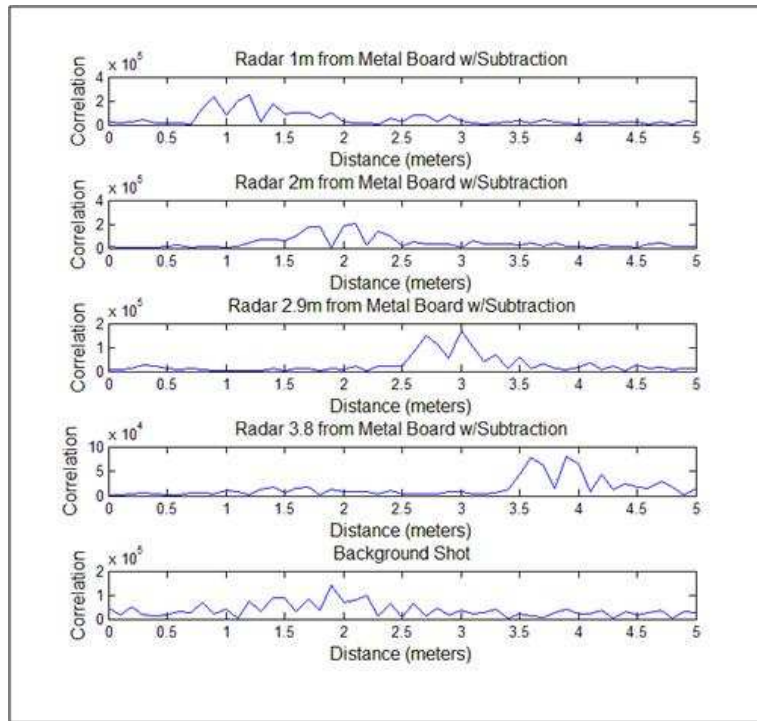
(a) Diagram of Test Scenario
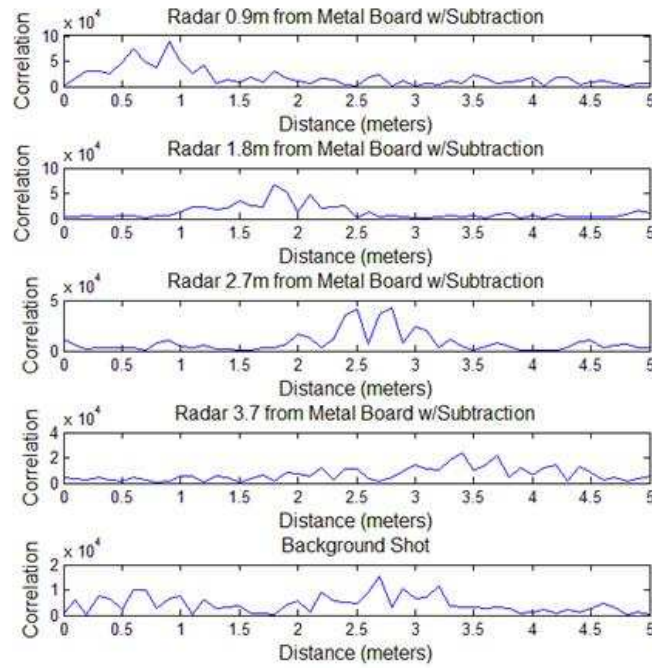


(b) Results Image

Figure C.1:    Diagram of Test Scenario with Radar Looking Through Air at a Metal Board and Results
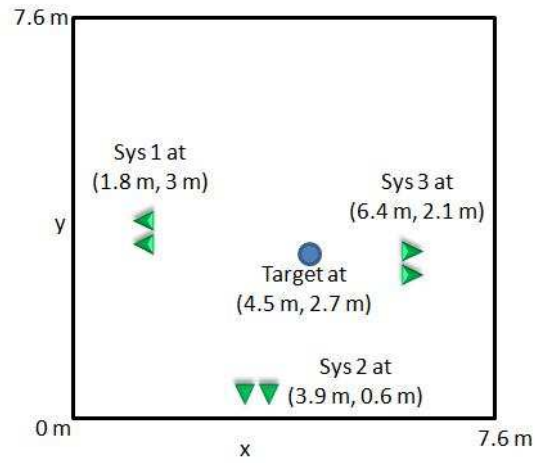
(a) Diagram of Test Scenario
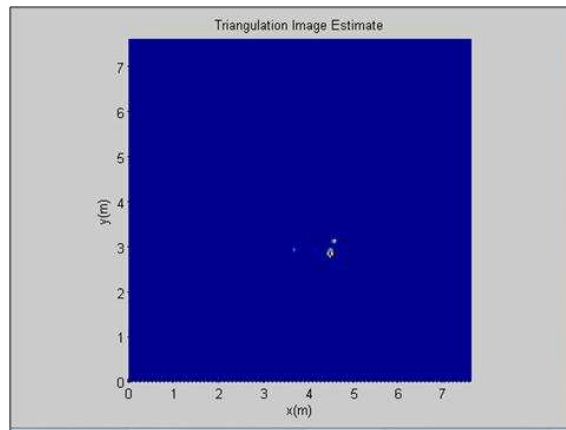


(b) Results Image

Figure C.2:    Diagram of Test Scenario with Radar Looking Through a Wall at a Metal Board and Results
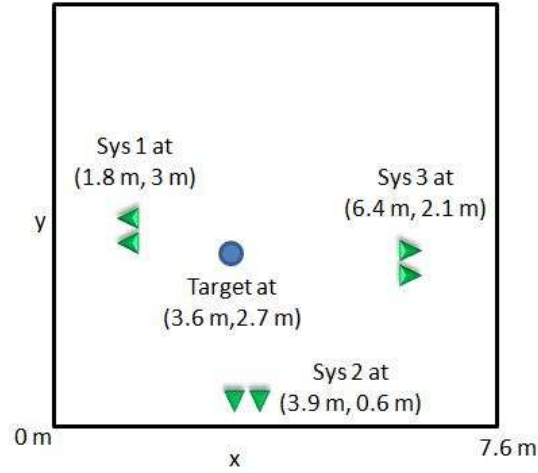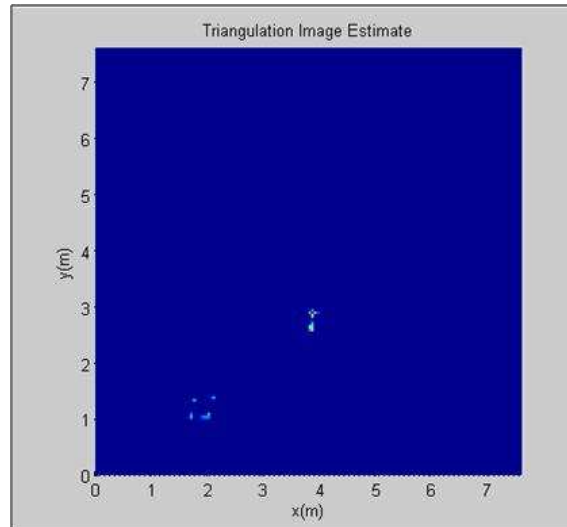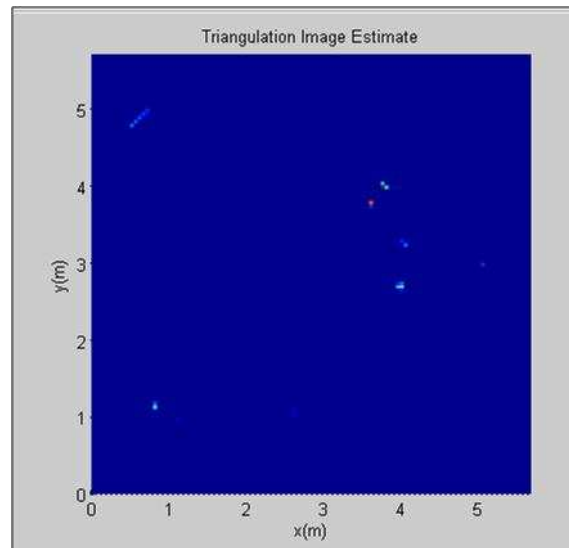
(a) Diagram of Test Scenario



(b) Photo of Test Setup



(c) Results Image

Figure C.3: Network of Radar Systems Looking Through Air at a Metal Tube Located at (4.5 m, 2.7 m)

(a) Diagram of Test Scenario



(b) Photo of Test Setup



(c) Results Image

Figure C.4: Network of Radar Systems Looking Through Air at a Metal Tube Located at (3.6 m, 2.7 m)

The third test scenario had the network of radar systems looking through air at a 6 in metal tube located at (3.8 m, 3.5 m). Fig. C.5 shows a diagram of this test scenario, a photo, and the resulting two-dimensional plot.

The fourth test scenario had the network of radar systems looking through air at a human target located at (4.5 m, 2.7 m). Fig. C.6 shows a diagram of this test scenario, a photo, and the resulting two-dimensional plot.
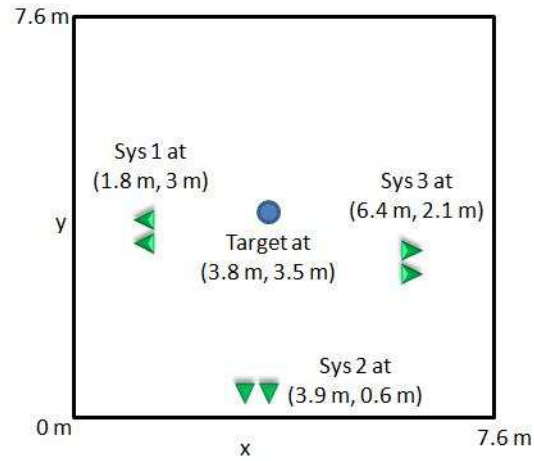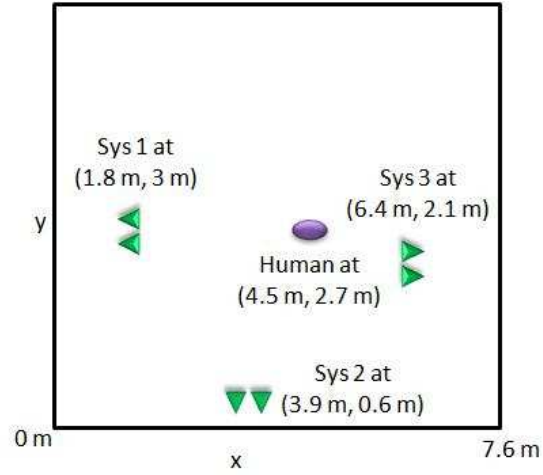
(a) Diagram of Test Scenario
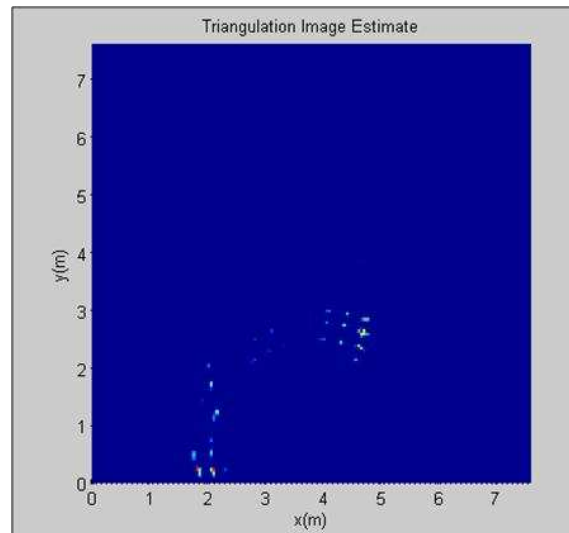


(b) Photo of Test Setup



(c) Results Image

Figure C.5:    Network of Radar Systems Looking Through Air at a Metal Tube Located at (3.8 m, 3.5 m)

(a) Diagram of Test Scenario



(b) Photo of Test Setup



(c) Results Image

Figure C.6:    Network of Radar Systems Looking Through Air at a Human Located at (4.5 m, 2.7 m)

137

## Appendix D.  Noise Radar Simulation Project

### D.1    Introduction

The types of waveforms used by radars has evolved and expanded over the years. One of the waveforms recently employed is the noise waveform. The use of a noise waveform holds many advantages [25]. Much research has been accomplished in recent years with noise radars. The newest noise radars have been implemented with Field Programable Gate Array (FPGA) boards, basic hardware components, and a digital correlator. The noise radar was designed using a software defined radio concept. This design opens new possibilities and flexibility for noise radars.

To more fully explore this design concept an accurate simulation needed to be created. The objective of this project was to create a realistic simulation model of a noise radar in `Matlab`® Simulink application that detects a human target through a concrete wall. The simulation model was validated with data obtained by a actual noise radar measuring human targets through a concrete wall. A block diagram of the Simulink model with only the wall and no targets is shown in Fig. D.1. The Simulink model has the same performance perimeters as the noise radar that the produced the real world data. This real world system was designed and built by Pennsylvania State University faculty and students [30] [31]. Fig. D.3 shows a detailed block diagram of the noise radar and Fig. D.2 several shows photos. All results from a real world noise radar used actual data files created by Pennsylvania State University PhD students [17].

### D.2    Simulation Model

The basic working premise of the noise radar is straight forward. A noise signal is produced by a noise source. The signal is split and one part is sent out into the environment. The other part is an exact duplicate and is stored digitally. The return signal is then compared to a time delayed version of the saved original signal. This process is implemented completely digitally in the simulation model.
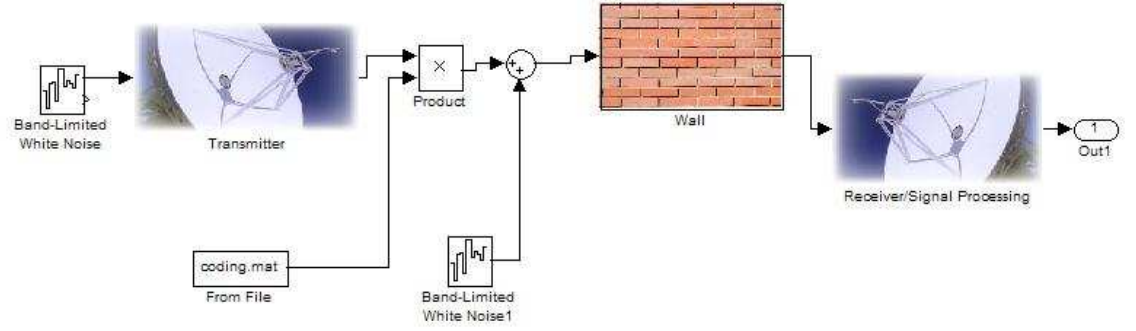
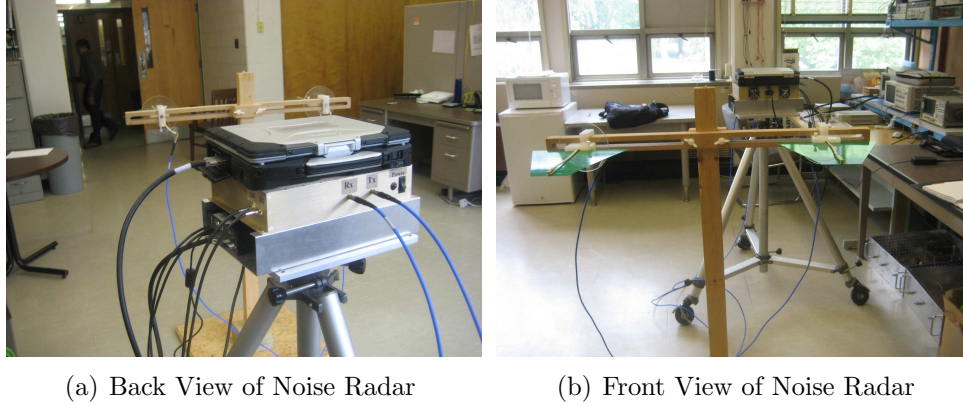Figure D.1:    Block Diagram of Simulink Noise Radar



(a) Back View of Noise Radar         (b) Front View of Noise Radar

Figure D.2:    Photos of Noise Radar System [31]

The simulation model is a combination of `Matlab`® code written in an .m file and Simulink blocks in .mdl files. To start the simulation, the .m file needs to be run. Then the .m file defines the variables, calls/runs the Simulink simulation files, digitally filters the data, correlates the data, and plots the results. The variable definitions pertaining to hardware performance parameters (i.e. antenna gain, output power, etc.) were set to recreate as closely as possible the same conditions as the of the Pennsylvania State University experiments. Four scenarios from their experiments were used to compare results. Fig. D.4 shows pictures from Pennsylvania State University's experiments of the antenna placement, wall background scene, and the locations of the humans. These experiments were accomplished in a controlled indoor
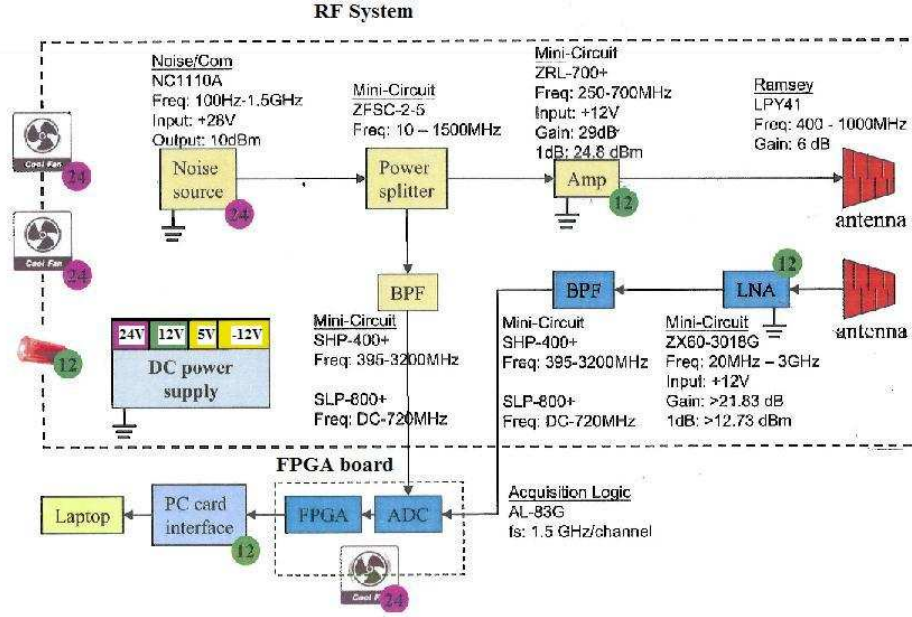
Figure D.3:     Block Diagram of University's Noise Radar System [31]

environment with a fabricated concrete wall. Each test scenario is with the radar 1.3 cm from a 14 cm thick concrete wall.

The first scene is a background scene used for background subtraction. No targets are present, only the wall. The second scene is with one human target at approximately 1.2 m from the wall. The third scene is with one human target at approximately 2 m. The fourth scene is with two human targets. The first target is 1.2 m from the radar. The second target is 2 m from the radar. Due to the simulation environment and the mathematic models applied, the closest the wall could be placed in the simulation was at 0.5 m. Though the location of the wall differs slightly, this is not a major deviation as far as the results are concerned. The software algorithm that calculates the results subtracts out the wall background scene. So, the location of the wall does not show up in the result graphs. Future work with the simulation may be able to fix this problem and move the wall closer to the radar.

Table D.1 shows the testing parameters for the simulation and the University's real world experiments [30]. Each simulation occurred over $1.6667 \times 10^{-6}$ seconds. In

140
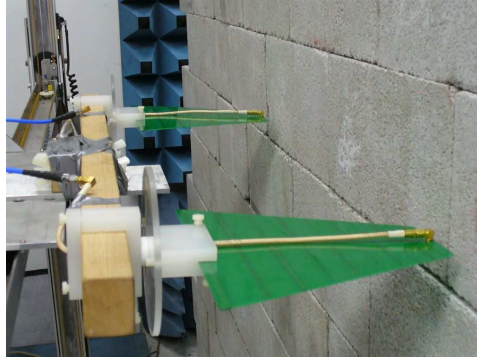
(a) Antenna Placement
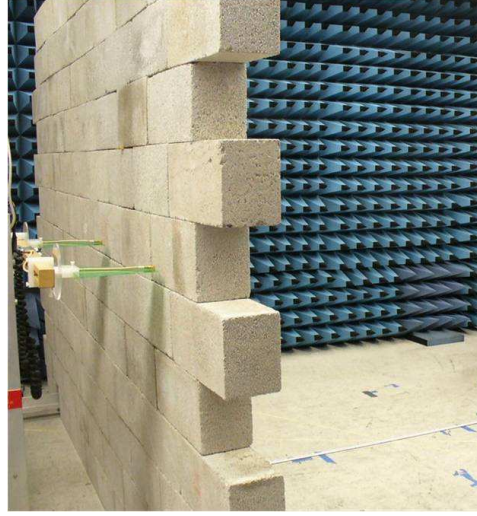


(b) Wall Background Scene



(c) Human Targets at 1.2 m and 2 m

Figure D.4:    Photos of Pennsylvania State University's Noise Radar Experiments [30]

the actual data, 20 samples were taken, each for $1.6667\text{x}10^{-6}$ seconds. These 20 sample results were averaged to achieve better results. Twenty data samples was determined by Pennsylvania State University students to be optimal [18].

Three Simulink models were necessary for these scenarios. The first Simulink model contains only the background scene which consists only of the wall. The second Simulink model has one human target. The target distance variable is 1.2 m on the first run and then changed on the second run to 2 m. The third model is with two human targets. Fig. D.5 shows the three Simulink models.

Table D.1:    Specifications of Components in Simulation

| Scenario | Source | Parameter |
|---|---|---|
| Scenario 1 | Simulation | Wall .5 m |
| Scenario 1 | Experiment | Wall 1.3 cm |
| Scenario 2 | Simulation | Wall .5 m, Human Target at 1.2 m |
| Scenario 2 | Experiment | Wall 1.3 cm, Human Targetat 1.2 m |
| Scenario 3 | Simulation | Wall .5 m, Human Target at 2 m |
| Scenario 3 | Experiment | Wall 1.3 cm, Human Target at 2 m |
| Scenario 4 | Simulation | Wall .5 m, 2 Human Targets at 1.2 m and 2 m |
| Scenario 4 | Experiment | Wall 1.3 cm, Targets at 1.2 m and 2 m |

There are several layers of components underneath the main blocks (Transmitter, Wall, Target and Receiver) that are shown in Fig. D.5. These components reflect the actual hardware pieces used in the University's noise radar. Some of the simulation components are different because it is a software simulation. For example, fans, power supplies, and a FPGA board would not be appropriate because they are not necessary for the operation of the simulation in the Simulink environment. Table D.2 show the specifications of the components in the Simulink simulation noise radar. These are the same component specifications as Pennsylvania State University's real world noise radar system shown in Fig. 4.3 [31].

Table D.2:    Specifications of Components in Simulation

| Component | Specifications |
|---|---|
| Noise Source | Output 10 dBm |
| Amp | Gain 29 dB |
| LNA | Gain 21.83 dB |
| 2 BPFs | 395 MHz to 720 MHz |
| Antenna (Tx and Rx) | Gain 6 dB |

The reflected energy from the wall and human targets are based on the attenuation equation [36]:

$$attenuation = \frac{\lambda^2 \sigma}{(4\pi)^3 R^4} \tag{D.1}$$
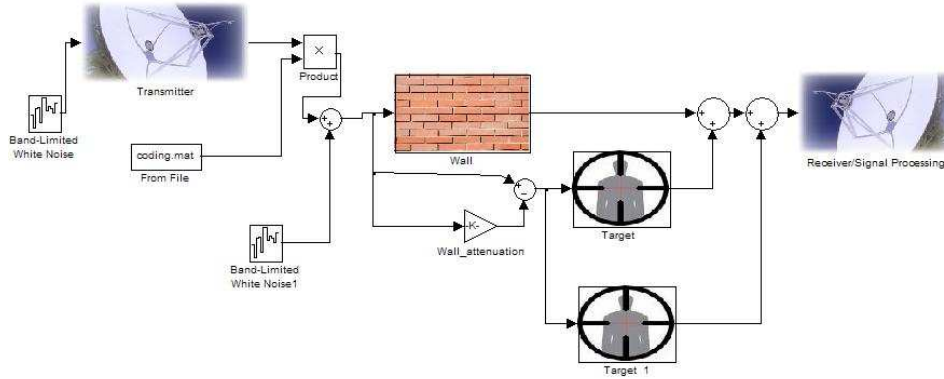
where $\lambda$ is the center frequency wavelength, $\sigma$ is the radar cross section (RCS) of the target, and $R$ is the distance from the radar to the target. The RCS of a human

142
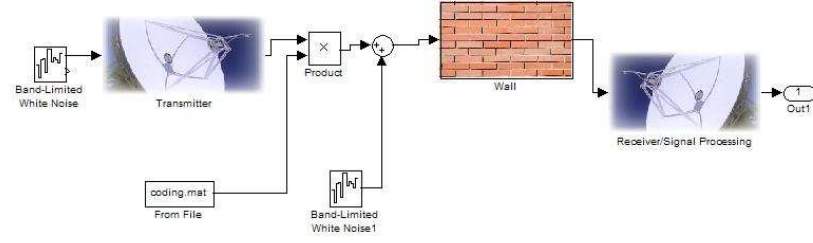
(a) Simulink Background Model
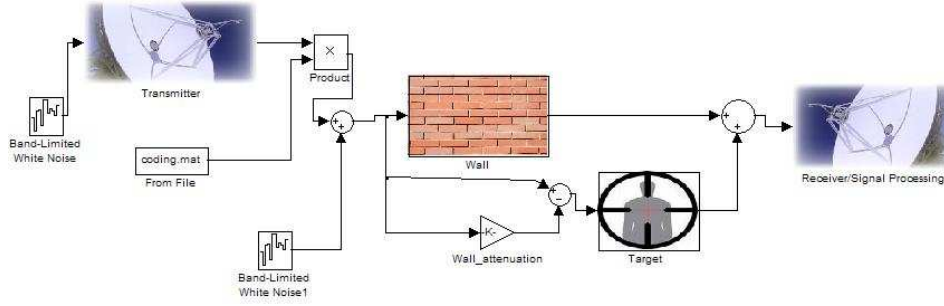


(b) Simulink Model with One Human Target



(c) Simulink Model with Two Human Targets

Figure D.5:     Three Simulink Models

was based on the research and findings of the Pennsylvania State University students, which is $\sigma = 0.55 * height$ [18]. The simulation sets the height of the human at 1.8m. The actual height of the human targets was unknown.

The correlation process that occurs within the .m file utilizes the xcorr `Matlab`®
function. This function basically creates the response of a matched filter. To find the
distance of the target, a loop applies the xcorr function to a portion of the received
signal and a portion of the time delayed transmit signal. The value from the center
of the resulting xcorr vector is then recorded. The loop then increases one increment
and the time delayed replica of the transmit signal shifts over by one. The the xcorr
function and recording of the center value is then accomplished again. This allows for
a plot of the matched filter responses at linearly spaced intervals in time. A tall peak
indicates a high response, like that from a target, at a specific point in time. This
time point can then be easily used to find at what range it occurs through the radar
range equation [36]:

$$R = \frac{cT}{2} \tag{D.2}$$

where $c$ is the speed of light, $T$ is the time it takes for the signal to travel to the target
and back, and $R$ is the range to the target.

Environmental noise is also included in this simulation. The noise floor level
was set at approximately -55 dB. Small adjustments to this number, however, did not
make any difference in the results. Only an adjustment that was much higher than
that of the transmitted signal made any difference. If the transmitting noise source
and the environmental noise sources had the same random noise generator seed, the
results were very skewed. This is because it took away the unique noise source signal
and combined it which the same exact environment signal and changed the results.
In a real world environment this is not the case because noise will always be unique.
To fix this problem, different random seeds were used. This worked much better and
restored some of the randomness that is seen in the real world.

`Matlab`® code was also created to take the raw data from the Pennsylvania
State University's noise radar and process the data in a similar fashion to that of the
model. The code pulls in the data, converts it from binary to numbers, applies a
digital filter, and performs the same correlation loop process.

Both the simulation and actual data m-files, use the radar range equation as is appropriate for each situation and plots the correlation peaks as a function of distance in meters.

### D.3  *Simulation Results and Comparison to Actual Data*

Overall, the simulation results and actual data results were similar. Fig. D.6 shows the simulation and actual data comparison results from the background scenario. The wall appears in the simulation results at approximately 0.5 m. In the actual data, one can see a peak very near 0.1 m. Both of these results were consistent with what was expected. The height of the correlation peak is of interest, however. For the simulation, it is at approximately $2.1x10^4$ and the actual data has a peak around $1.9x10^4$. These numbers are similar, however, in the other scenario results this is not the case.



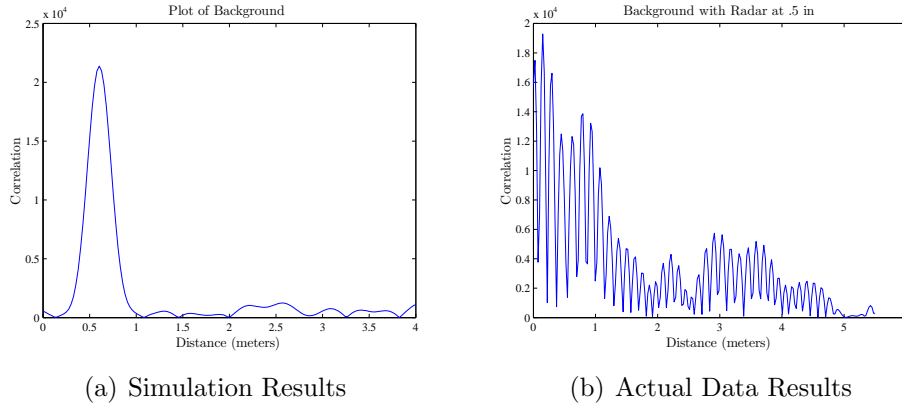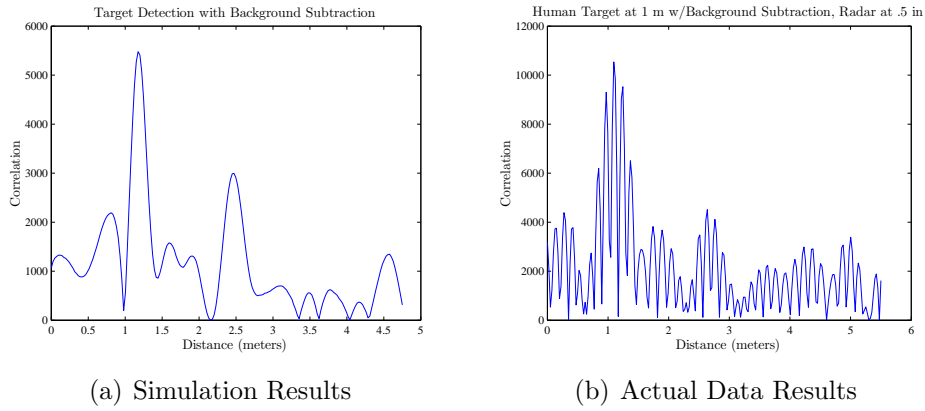(a) Simulation Results          (b) Actual Data Results

Figure D.6:    Simulation and Actual Data Results for Background

Fig. D.7 shows the simulation and actual data comparison results from the human target at 1.2 m. These results are also favorable with both the simulation and actual data results showing target detection at approximately 1.2 m. In this case, it is interesting to note that the correlation numbers at the peaks are different. The correlation peak of the simulation is almost half that of the actual data. Several simulation parameters variations were tested and only two parameters made much of a difference in the correlation number. These parameters were the distance of

the wall and the gain of the amplifiers. As the distance of the wall increased the correlation number decreases. The distance of the wall in the simulation is more than that of the actual data results. This might account for the difference in correlation numbers. The second parameter that affects correlation number is the amplifiers. the higher the amplifier's gain the higher the correlation number. This is to be expected since the this would raise the received signal's signal-to-noise (SNR) and increase the correlation. Another item to note is that both the simulation and actual data results have a similar noise pattern with secondary peaks at approximately 2.5 m.



(a) Simulation Results        (b) Actual Data Results

Figure D.7:     Simulation and Actual Data Results for One Human Target at 1.2m

Fig. D.8 shows the simulation and actual data comparison results from the human target at 2 m. The results for simulation and actual data both detect the human target at approximately 2 m. Again the correlation peaks are different with the simulation having a lower value, possibly due to the different wall location. Another interesting feature of these results is the second highest peak at approximately 2.5 m on my simulation and at 3 m on the actual data. While this is not a target, it is interesting to note that the simulation produces similar pattern results in this scenario and the pervious scenario.

Fig. D.9 shows the simulation and actual data comparison results from the two human targets at 1.2 m and 2 m. The simulation results detected both human targets. The peaks at 1.2 m and 2 m are distinct. The actual results show a definite peak at 2 m. There is a peak at 1.2 m as well, but its height is slightly less than that of

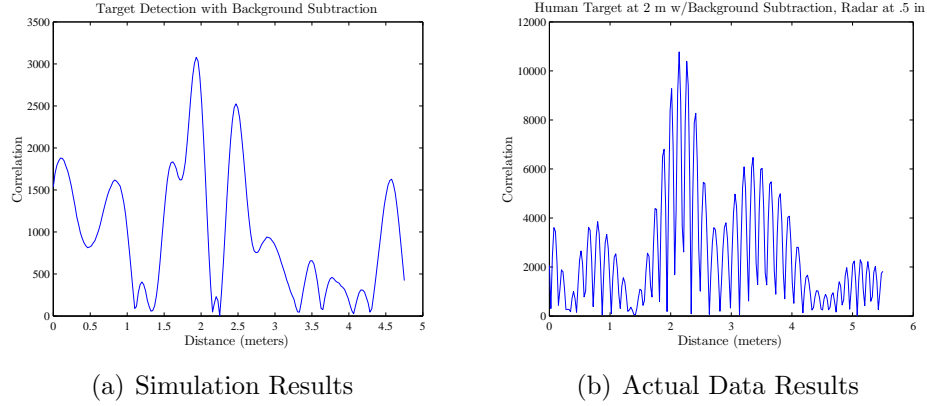(a) Simulation Results

(b) Actual Data Results

Figure D.8:    Simulation and Actual Data Results for One Human Target at 2m

another peak that is at approximately the range of the wall. After reviewing the data and results, it appears that there is some sort of interaction between the wall and the human. The simulation does not take multipath electromagnetic fields, reflections, and object interactions into account, so that may be a reason for the variation. Also, since this data and the test parameters were received from another source, a deviation might have occurred during the test that was not accounted for during the simulation. Again, there is a consistent pattern of the correlation peaks of the simulation being lower than that of the actual results.



(a) Simulation Results

(b) Actual Data Results
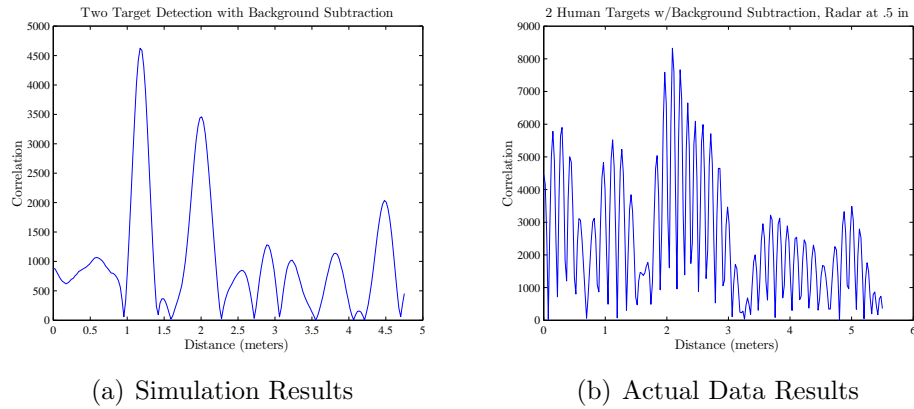
Figure D.9:    Simulation and Actual Data Results for Two Human Targets

147

### D.4   Conclusion

In conclusion, the simulation model was validated against data obtain by an actual noise radar measuring human targets through a concrete wall. The simulation model proved to perform in a similar manner to that of an actual noise radar with the same hardware components.

## *Bibliography*

1. Acquistion-Logic-Inc. *PCI Digitizer Board AL82xGT Manual.* Chantilly, VA, 2008.

2. Astanin, L. and A. A. Kostylev. *Ultrawideband Radar Measurements: Analysis and Processing.* The Institution of Electrical Engineers, London, UK, 1997. URL www.knovel.com/knovel2/Toc.jsp?

3. Axelsson, S. "Random Noise Radar/Sodar with Ultrawideband Waveforms". *IEEE Trans. on Geo. and Remote Sensing*, 45(5):1099–1114, May 2007.

4. Balanis, C. A. *Advanced Engineering Electromagnetics.* John Wiley and Sons, Hoboken, NJ, 1989.

5. Baum, C. E., G. P. Pochanin, and F. J. Yanovsky. "UWBUSIS 2006: The third international conference on a ultra-wideband and ultra-short impulse signals". *IEEE Antennas and Propgat. Mag*, 49:134–138, Feb 2007.

6. Brisken, W. "Cross Correlators", 9th Synthesis Imaging Summer School, New Mexico Tech, Socorro, NM, June 2004.

7. Collins, P., Course Notes, EENG 627, RCS Analysis, Measurement, and Reduction, School of Engineering, Air Force Institute of Technology , Wright Patterson AFB, OH, Fall 2008.

8. Dillinger, Madani, and Alonistioti. *Software Defined Radio.* Wiley, 2003.

9. Fontana, R. "A Brief History of UWB". *Pace*, June 2004. URL www.multispectral.com/history.html.

10. Gehrig, M. D., D. V. Morris, and J. T. Bryant. "Ground Penetrating Radar for Concrete Evaluation Studies". *Technical Presentation Paper for Performance Foundation Association*, 197–200. Mar 2004. URL www.foundationperformance.org/pastpresentations/gehrig_paper_march2004.pdf.

11. Griffith, C. M. *Unmanned Aerial Vehicle-Mounted High Sensitivity RF Reciever to Detect Improvised Explosive Devices.* MS. Thesis, Naval Post Graduate School, Monterey, CA.

12. Havrilla, M., Course Notes, EENG 622, Introduction to Electromagnetics, School of Engineering, Air Force Institute of Technology , Wright Patterson AFB, OH, Fall 2007.

13. Hawkins, D. W. "Digital Lag (XF) Correlator Theory". California Institute of Technology, Pasadena, CA, Jan 2002.

14. HD-Communications-Corp. *Low Noise Amplifer HD24395 Specifications.* Ronkonkoma, NY, Sep 2008. URL www.rfcomp.com/download/product_specs/low_noise/HD24395specs.pdf.

15. HD-Communications-Corp. "Low Power Amplifer HD24649 Specifications", Sept 2008. URL www.rfcomp.com/download/product_specs/HD24649specs.pdf.

16. Heuschel, E. R. *Time-Frequency, Bi-Frequency Dectection Analysis of Noise Technology Radar.*

17. Knott, E., J. F. Shaeffar, and M. T. Tuley. *Radar Cross Section, 2nd Ed.*

18. Lai, C. P. *Through Wall Surveillance Using Ultrawideband Random Noise Radar.* PhD dissertation. Pennsylvania State University, University Park, PA, Aug 2007.

19. Lai, C. P., R. M. Narayanan, Q. Ruan, and A. Davydov. "Hilbert-Huang Transform (HHT) Analysis of Human Activities Using Through-Wall Noise and Noise-Like Radar", 2008.

20. Leon-Garcia, A. *Probability and Random Processes for Electrical Engineering.* Addision-Wesley Publishing Company, Inc., 1994.

21. Meanwell-Inc. *Power Supply RQ-65D Specifications.* Fremont, CA, 2008. URL www.switching-powersupplies.com/upload/pdf/rd-65.pdf.

22. Mini-Circuit. "Low Pass Filter (LPF) SLP-800 Specifications".

23. Mini-Circuit. "High Pass Filter (HPF) SHP-400 Specifications", 2008. URL www.minicircuits.com/pdfs/SHP-400.pdf.

24. Mini-Circuit. "Power Splitter ZFSC-2-5 Specifications", 2008. URL www.minicircuits.com/pdfs/ZFSC-2-5.pdf.

25. Narayanan, R. M. "Through-wall radar imaging using UWB noise waveforms". *Science Direct, Journal of the Franklin Institute by ElSevier*, 659–678, 2008. URL www.sciencedirect.com;www.elsevier.com/locate/jfranklin.

26. Narayanan, R. M. and M. Dawood. "Doppler Estimation Using a Coherent Ultrawide-Band Random Noise Radar Systems". *IEEE Trans. on Antennas and Prop.*, 48(6):868–878, 2000.

27. Narayanan, R. M. and M. Dawood. "Doppler Estimation Using a Coherent Ultrawide-band Random Noise Radar." *IEEE Trans. on Antennas and Prop.*, 48(6):868–878, June 2000.

28. Narayanan, R. M. and C. Kumru. "Implementation of Fully Polarimetric Random Noise Radar". *IEEE Antennas and Wireless Prop. Letters*, 4:125–128, 2005.

29. Noise-Com-Inc. *Noise Source NC1110A Specification.* Parsippany, NJ, 2008. URL www.noisecom.com/Products/Components/Nc1000/nc1000.pdf.

30. Pin-Heng, P. and S. Mahesh. "Preliminary SAR Image from Data Collected in CAC, Villanova University", PhD Students, Pennsylvania State University, University Park PA. Aug 2008.

31. Pin-Heng, P. and S. Mahesh, PhD Students, Pennsylvania State University, University Park PA. Personal Interview. 10 Sep 2008.

32. Ramsey-Electronics. *Antenna LPY41 Specifications*. Victor, NY, 2008. URL www.ramseyelectronics.com/cgi-bin/commerce.exe?preadd=actionkey=LPY41.

33. Rogers, S. K. Class Notes, EENG 699, Basic Pattern Recognition, School of Engineering, Air Force Institute of Technology , Wright Patterson AFB, OH, Fall 2007.

34. Rogers, S. K., C. Sadowski, K. W. Bauer, M. E. Oxley, M. Kabrisky, A. S. Rogers, and S. D. Mott. "The Life and Death of ATR/Sensor Fusion and the Hope for Resurrection". *Proceedings of SPIE*, 6967, Mar 2008.

35. Rogers, S. K., C. Sadowski, K. W. Bauer, M. E. Oxley, M. Kabrisky, A. S. Rogers, and S. D. Mott. Meeting Handout, Weekly Meeting: QUEST Definition, Air Force Institute of Technology and Air Force Research Laboratories, Wright Patterson AFB, OH, 2008.

36. Skolnik, M. I. *Introduction to Radar Systems, 3rd Ed.* McGraw Hill, Boston, MA, 2001.

37. Stimson, D. W. *Introduction to Airborne Radar, 2nd Ed.* SciTech Publishing Inc., Raleigh, NC, 1998.

38. Thayaparan, T. and C. Wernik. *Noise Radar Technology Basics.* Technical Memorandum 2006-266, Defence R and D Canada, 2006.

39. Theron, I. P., E. K. Walton, and S. Gunawan. "Compact Range Radar Cross-Section Measurements Using a Noise Radar". *IEEE Trans. on Antennas and Prop.*, 46(9):1285–1288, 1998.

40. Theron, I. P., E. K. Walton, and S. Gunawan. "Compact Range Radar Cross-Section Measurements Using a Noise Radar". *IEEE Trans. on Antennas and Prop.*, 46(9):1285–1288, 1998.

41. Theron, I. P., E. K. Walton, S. Gunawan, and L. Cai. "Moving Vehicle Range Profiles Measured Using a Noise Radar". *1997 IEEE AP-S Symposium and URSI Meeting.* Montreal, Canada, 1997.

42. Theron, I. P., E. K. Walton, S. Gunawan, and L. Cai. "Ultrawide-band Noise Radar in VHF/UHF Band". *IEEE Trans. on Antennas and Prop.*, 47(9):1080–1084, 1999.

43. Tribble, A. C. "The Software Defined Radio: Fact or Fiction". *IEEE*, 1–8, 2008.

44. Ustun, T. E. *Design and Development of Stepped Frequency Continuous Wave and FIFO Noise Radar Sensors for Tracking Moving Ground Vehicles.* MS. Thesis, The Ohio State University, Columbus, OH, 2001.

45. Walton, E. K. "Radar System Using Random RF Noise", 2005.

46. Walton, E. K. *Signal To Noise Ratio Calculations for Noise Radar.* Power point presentation, Ohio State University, 25 Oct 2007.

47. Walton, E. K. and F. Paynter. "Comparision of Impulse and Noise-Based UWB Ground Penetrating Radars". *URSI Radio Science Meeting (Joint with AP-S)*. Seattle, Washington, 1994.

48. Youngblood, G. "A Software-Defined Radio for the Masses, Part 1". *QEX*, (Jul/Aug 2002), 2002.

# REPORT DOCUMENTATION PAGE

Form Approved
OMB No. 0704–0188

**1. REPORT DATE** *(DD–MM–YYYY)*
12–03–2009

**2. REPORT TYPE**
Master's Thesis

**3. DATES COVERED** *(From — To)*
Sept 2007 — Mar 2009

**4. TITLE AND SUBTITLE**

Radar Imaging with a Network of
Digital Noise Radar Systems

**5a. CONTRACT NUMBER**

**5b. GRANT NUMBER**

**5c. PROGRAM ELEMENT NUMBER**

**6. AUTHOR(S)**

Schmitt, Ashley L., Capt, USAF

**5d. PROJECT NUMBER**

08-251 and 08-275

**5e. TASK NUMBER**

**5f. WORK UNIT NUMBER**

**7. PERFORMING ORGANIZATION NAME(S) AND ADDRESS(ES)**

Air Force Institute of Technology
Graduate School of Engineering and Management (AFIT/EN)
2950 Hobson Way
WPAFB OH 45433-7765

**8. PERFORMING ORGANIZATION REPORT NUMBER**

AFIT/GE/ENG/09-39

**9. SPONSORING / MONITORING AGENCY NAME(S) AND ADDRESS(ES)**

Air Force Research Laboratories Sensors Directorate
Attn: Steven Rogers
2241 Avionics Cir
WPAFB, OH 45433
(937) 904-9891 steven.rogers@wpafb.af.mil

**10. SPONSOR/MONITOR'S ACRONYM(S)**

AFRL/RYA

**11. SPONSOR/MONITOR'S REPORT NUMBER(S)**

**12. DISTRIBUTION / AVAILABILITY STATEMENT**

Approval for public release; distribution is unlimited.

**13. SUPPLEMENTARY NOTES**

**14. ABSTRACT**

Due to the threat of terrorism, today's enemy can be anyone and they can exist anywhere even in populated cities. Monitoring human activities in an urban environment is a difficult problem due walls, clutter, and other obstructions. This thesis discusses the development of a network of digital noise radars that operate simultaneously to track humans and non-human targets inside rooms and through walls. Each individual noise radar works by cross correlating the received signal with a time delayed replica of the transmit signal. A high correlation indicates the range of the target. This design of noise radar makes use of digitization by converting the analog transmit and receive signals to digital signals. With the signals in digital form, the cross correlation and time delay process can be accomplished in software. The development of a network of three digital noise radars enabled triangulation of the (x, y) position of a target within a room. The results show that the network of radars was capable of locating stationary human and non-human targets through walls as well as tracking a human within a room.

**15. SUBJECT TERMS**

noise radar, simultaneous operation of radars, network of digital noise radars, radar

**16. SECURITY CLASSIFICATION OF:**

| a. REPORT | b. ABSTRACT | c. THIS PAGE |
|---|---|---|
| U | U | U |

**17. LIMITATION OF ABSTRACT**

UU

**18. NUMBER OF PAGES**

168

**19a. NAME OF RESPONSIBLE PERSON**
Dr. Peter J. Collins, PhD (ENG)

**19b. TELEPHONE NUMBER** *(include area code)*
(937) 255-3636, ext 7256; peter.collins@afit.edu

**Standard Form 298 (Rev. 8–98)**
Prescribed by ANSI Std. Z39.18